KAUNAS UNIVERSITY OF TECHNOLOGY

FACULTY OF ELECTRICAL AND ELECTRONICS ENGINEERING

Kireeti Maddela

DETERMINATION OF POSITION OF DEFECTS IN RAILS USING ULTRASONIC PHASED ARRAYS

Master's Degree Final Project

Supervisor

Assoc. prof. dr. Elena Jasiuniene

KAUNAS, 2017

KAUNAS UNIVERSITY OF TECHNOLOGY
FACULTY OF ELECTRICAL AND ELECTRONICS ENGINEERING

DETERMINATION OF POSITION OF DEFECTS IN RAILS USING ULTRASONIC PHASED ARRAYS

Master's Degree Final Project

Measurement Engineering (code 621H14001)

Supervisor
(signature) Assoc. prof. dr. Elena Jasiuniene
(date)

Reviewer
(signature) Assoc. prof. dr. Vytautas Dumbrava
(date)

Project made by
(signature) Kireeti Maddela
(date)

KAUNAS, 2017

KAUNAS UNIVERSITY OF TECHNOLOGY

Faculty of Electrical and Electronics Engineering

(Faculty)

Kireeti Maddela

(Student's name, surname)

Measurement Engineering (621H14001)

(Title and code of study programme)

"Determination of position of defects in rails using Ultrasonic Phased Arrays"

DECLARATION OF ACADEMIC INTEGRITY

___ _____ 20 ____

Kaunas

I confirm that the final project of mine, **Kireeti Maddela**, on the subject "Determination of position of defects in rails using Ultrasonic Phased Arrays" is written completely by myself; all the provided data and research results are correct and have been obtained honestly. None of the parts of this thesis have been plagiarized from any printed, Internet-based or otherwise recorded sources. All direct and indirect quotations from external resources are indicated in the list of references. No monetary funds (unless required by law) have been paid to anyone for any contribution to this thesis.

I fully and completely understand that any discovery of any manifestations/case/facts of dishonesty inevitably results in me incurring a penalty according to the procedure(s) effective at Kaunas University of Technology.

(name and surname filled in by hand) *(signature)*

Maddela, Kireeti. DETERMINATION OF POSITION OF DEFECTS IN RAILS USING ULTRASONIC PHASED ARRAYS: Final project of Measurement Engineering, *Master's degree* / supervisor Assoc. prof. dr. Elena Jasiuniene, Kaunas University of Technology, Faculty of Electrical and Electronics Engineering.

Kaunas, 2017. 87 p.

SUMMARY

In this work, positions of defects in the rail (test sample) were determined using Ultrasonic Phased Arrays. Several kinds of defects in rails and welds were studied along with the concept of Ultrasonic Phased Arrays. Using CIVA software, the test sample was designed and inspected virtually with two types of phased arrays. Beam profiles, interaction of ultrasonic waves with defects were mainly studied from the obtained results. Experimental analysis was also performed using OLYMPUS OMNISCAN^{MX} set-up. This helped to analyse the ultrasonic wave propagation in the test sample and interaction with the defects. An efficient phased array methodology was specified by comparing the results of different phased arrays. At last, uncertainties in the measurement results were evaluated.

CONTENTS

INTRODUCTION

In this work, we shall discuss “Determination of position of defects in rails using ultrasonic phased arrays.” Rail assessment is a vital task in railway maintenance and it is periodically required for avoiding risky mishaps. The speed and load of trains are observed increasing in recent decades, and these factors mainly raise the danger of producing rail defects. Crack detection in rails is quite tough and challenging and hence a huge amount of research effort is being spent on the development of reliable crack detection techniques. Many failed in-service rails are related to the internal defects in the web and head region that propagate easily. The annual damage to life and property due to rail accidents is vast. Rail failures and accidents can be even reduced through an increased reliability of flaw detection technologies. Thus, Ultrasonic Rail Flaw Detection Systems are broadly employed by railroads to identify rail defects. Typically, ultrasonic testing systems are implemented on a high-rail vehicle platform that is specifically dedicated to the ultrasonic inspection service. Present day’s ultrasonic rail testing methodologies can identify more than 90% of common rail defects.

The aim of this thesis is to determine the positions of defects in rails using Ultrasonic Phased Arrays. The main tasks are:

- To study different types of defects in rails and welds.
- To know the principle of testing with Ultrasonic Phased Arrays, their advantages over conventional testing; characteristics of different phased array probes and wedges; and the scanning patterns.
- To perform computer modelling using CIVA software which enables us to determine the position of defects in rails virtually by considering different parameters of the given phased arrays.
- To perform experimental analysis on a piece of rail (test sample) which has two defects in it in such a way that positions of these defects are determined efficiently by considering different positions of the given phased arrays.
- To determine uncertainties in the determination of position of each defect.
- To determine the influence of different sources of uncertainty in the determination of position of defects in rails.

1. Description of rail defects and brief study on Ultrasonic Phased Arrays

In this section, some of the common defects that occur in rails and welds are described which allows knowing how a defect initiates in the rail and the possible factors for its cause. It is important to know the principle of Ultrasonic Phased Arrays, their advantages over conventional testing. Also, studying fundamental characteristics of phased array probes and wedges help us to select the appropriate phased array probes and wedges as per the different inspections.

1.1.Nature of defects in rails and welds

It is necessary to study rail defects as they stand as a severe threat to railway safety since they could cause rail breaks [1]. Also, the nature of defects in welds plays an important role as the quality of weld depends on the careful welding operation [6].

1.1.1. Nature of defects in rails

The rail defects can be categorised into three main groups [1]:

- Defects due to manufacturing flaws
- Defects due to improper handling and usage
- RCF (Rolling Contact Fatigue) defects

Based on the mechanical loading conditions and the fatigue lifetime of the rails, flaws might grow into transverse cracks that end up in rail breaks [2]. Advanced manufacturing technologies have resulted in reduced amount of fatigue crack initiations within the rails. The most important factors like increase in average load, high train speeds, short inspection windows and high wear resistance have led to new issues [3]. New rail steels are of prime quality and are immune to abrasion such that material wear isn't any longer needed to avoid the expansion of cracks within the rail surface [4]. RCF is a serious future concern as the speed of the rails, their axle load, traffic density and tractive forces will certainly continue to increase. RCF defects are produced by high traditional and tangential stresses that cause severe shearing of the surface layer of the rail. From there, it develops branches that either turn upwards or produce spalling at the rail surface or turn downwards. The main reason for the formation of these branches could be the action of longitudinal stresses within the rail head [1]. The typical locations of defects in rails are shown in **Fig.1.1**.

RCF defects can be divided into two sub-categories namely, squats and head checks. Squats, generally seem like dark areas on the rail surface because of sub-surface cracking and can be found in straight or slightly curved tracks on the high-speed railway lines. Head checks and Gauge Corner Cracking (GCC) refers to a cluster of fine cracks between crown and gauge corner of the rail [2], [4].

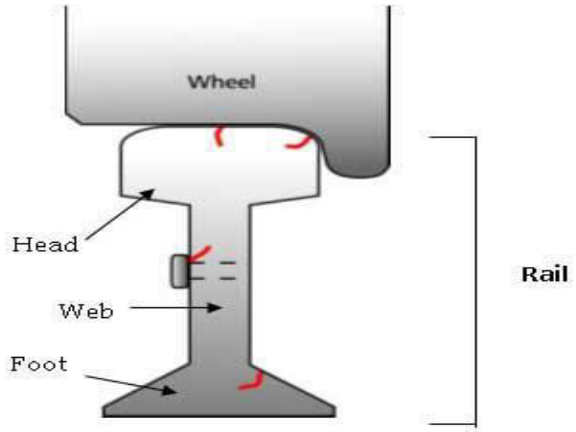

Fig.1.1. Typical locations of defects in rails [7]

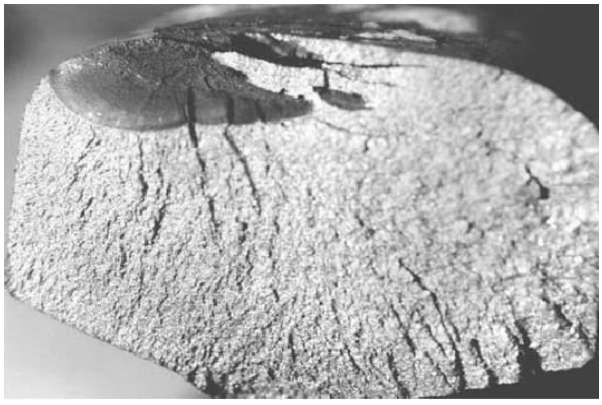

Fig.1.2. Rail failure resulting from GCC [5]

An example of a rail break caused by GCC is shown in **Fig.1.2**. Head checks are one of the main types of RCF defects in the British rail network [5]. General types of transverse defects that are usually seen within the rail head are:

- Detail fracture:

This type of fracture is progressive and usually initiates from a separation near the running surface of the railhead. This separation turns down and progresses transversally at right angles to the rail's running surface. The defect is typically related to a horizontal separation that grows parallel to the railhead running surface referred to as a shell [17]. It is shown in **Fig.1.3 (a)**.

- Compound fissure:

This type of fracture is progressive and usually originates at the horizontal separation which turns up or down and gives rise to transverse separation perpendicular to the running surface. Compound fissures include multiple horizontal or vertical planes [17]. It is shown in **Fig.1.3 (b)**.

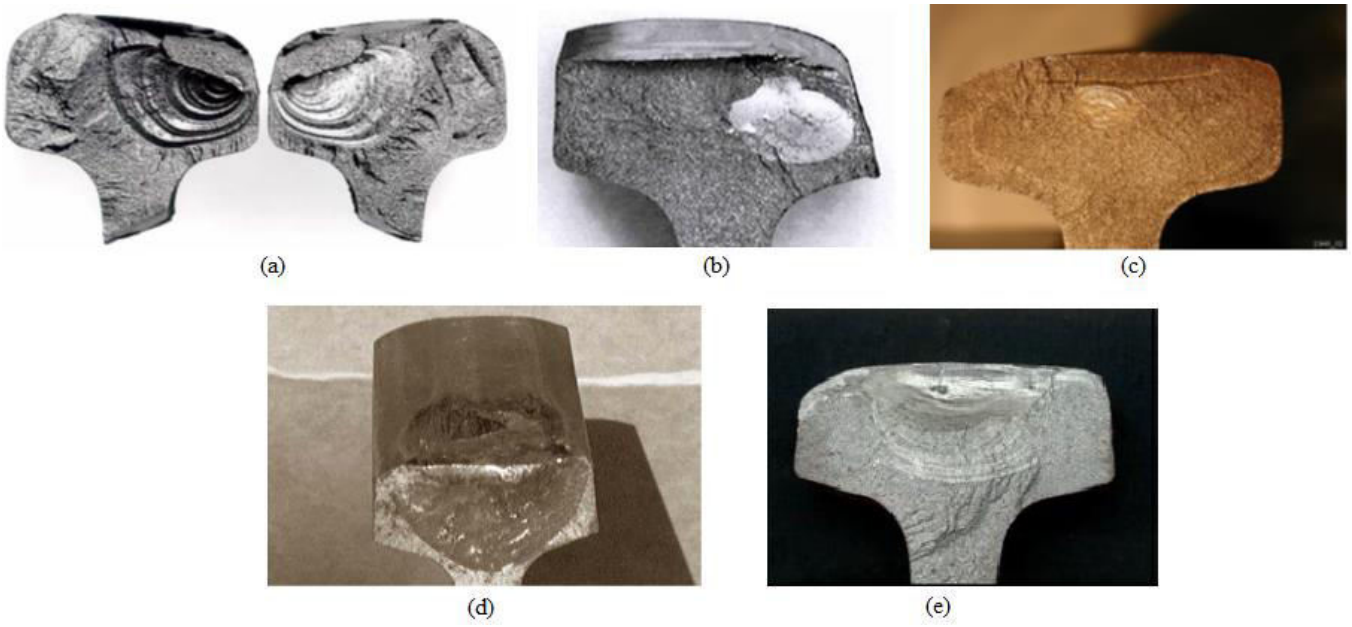

Fig.1.3. (a) Detail fracture **(b)** Compound fissure **(c)** Transverse Fissure **(d)** Engine burn fracture **(e)** Welded burn fracture [17]

- Transverse fissure:

This type of fracture is progressive and initiates from the center internally within the railhead and propagating outwards considerably at right angles to the rail's running surface [17]. It is shown in **Fig.1.3 (c)**.

- Engine burn fracture:

This type of fracture is progressive which occurs within the head of the rail that initiates from overheating generated by slippery locomotive wheels. Extreme cooling results in the formation of thermal cracks. Usually, the fatigue generated by the engine burn propagates perpendicularly to the running surface and might occur in many directions in the rail [17]. It is shown in **Fig.1.3 (d)**.

- Welded burn fracture:

This type of fracture occurs within the head of the rail that initiates from an inclusion due to weld repair or from a stress crack due to rail resurfacing. The defect generally initiates at the interface between the weld filler metal and parental material of the rail section. The flaw can progress transversally into the railhead and will not show any visible proof that it is present until the defect breaks out at the railhead surface [17]. It is shown in **Fig.1.3 (e)**.

1.1.2. Nature of defects in welds

Improper welding of rails could introduce a certain range of defects on the joints and within the Heat Affected Zone (HAZ) e.g. cracks, porosity, lack of fusion, structural variation, etc. [6]. Flash butt weld and Alumino-Thermic (AT) weld are shown in **Fig.1.4 (a)** and **Fig.1.4 (b)** respectively.

Fig.1.4. (a) Flash butt weld [8] **(b)** Alumino-Thermic (AT) Weld [9]

- Defects in Flash butt welds:

✓ Transverse cracks:

Because of various improper welding activities like lack of fusion, inclusions etc., transverse cracks are formed in the rails. These cracks are found within the head, web and foot regions of a rail [6].

✓ Horizontal cracks:

Horizontal cracks initiate in web region and propagate both in head and foot regions [6].

- Defects in Alumino-Thermic (AT) welds:

✓ Transverse cracks:

These cracks are caused by inclusions captured during welding that leads to crack initiation on the foot and its progress in the web region causing fracture [6].

✓ Horizontal cracks:

These cracks occur in AT welds at the ends having boltholes in the web that have not been removed. The presence of holes leads to uneven stress distribution because of non-uniform cooling [6].

1.2.Ultrasonic Phased Arrays

An ultrasonic phased array is a single transducer that contains many individually connected elements [10]. An ultrasonic phased array probe consists of multiple elements, typically between 16 and 256. The sequence in which these elements are arranged offers a range of options. By pulsing the

elements individually or as a group, the ultrasonic wavefronts could be excited. The beam profile is formed by the combination of these wavefronts and it can be changed by varying the amplitude and excitation time of each element. Amplitude and time delay for each element are controlled using the focal laws [11]. Ultrasonic phased arrays have two key benefits over standard transducers. Firstly, a phased array can perform a variety of different inspections from one location which shows its flexibility over single element transducer. Secondly, most of the phased arrays can be used to produce images at every test location which ends up in the sensible visualisation of the interior structure of the test object [10]. Frequencies of the transducer are most commonly in the range of 2 MHz to 10 MHz. Phased array probes could be used directly on the test object as well as immersion testing [13]. Ultrasonic Phased Arrays can be used for the following industrial purposes [12]:

- ✓ Weld inspection
- ✓ Thickness measurements
- ✓ Corrosion inspection
- ✓ Flaw detection

1.3.Conventional Testing Vs. Phased Array Testing

Ultrasonic phased array testing can be implemented in almost any test where conventional testing is used. The two major applications are inspection of welds and detection of cracks and these tests are performed in a wide range of industries that include aerospace, power generation, petrochemical, pipeline construction and maintenance, etc. The advantages of ultrasonic phased arrays over conventional ultrasonic transducers originate from its capability to use multiple elements to steer, focus and scan with a single probe construction. Beam steering which is commonly referred to as S-scan (Sectorial scan) is used for mapping components at suitable angles. This greatly simplifies the inspection of components that have complex geometry. Sectorial scanning is also used for inspection of welds. The capacity to test welds using various angles from a single probe greatly increases the probability of detection of irregularities. Electronic focusing allows improvising the shape and size of the beam at the expected defect locations and further improves the probability of detection. The capacity to focus the beam at several depths also improves the capability for sizing critical defects during volumetric inspections. Focusing also improves the signal-to-noise ratio in various challenging applications, whereas electronic scanning allows rapid formation of C-scan images. The capacity to test using multiple angles and/or to perform scanning of a large area of the test sample through linear scanning increases the speed of inspection. The major disadvantages of Ultrasonic Phased Array systems are high cost and requirement for well-trained operator [16].

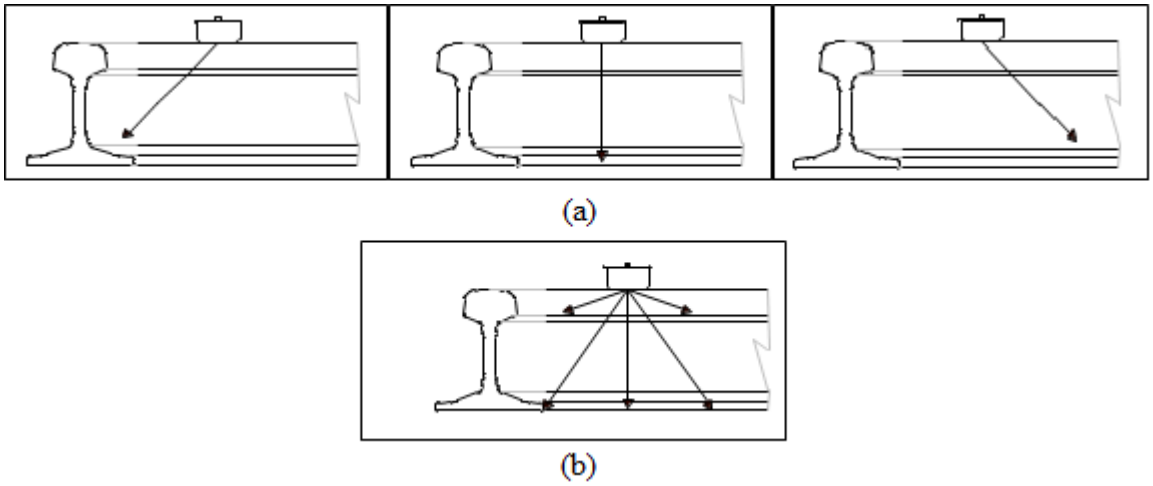

Fig.1.5. (a) Conventional Ultrasonic Testing **(b)** Phased Array Ultrasonic Testing [18]

The schematic representation of conventional ultrasonic testing with different transducers for each angle and phased array ultrasonic testing with single transducer for different angles are shown in **Fig.1.5 (a) and Fig.1.5 (b)** respectively. Inspection speed of Ultrasonic Phased Arrays is 10 times faster than conventional ultrasonic transducers and hence stands as a major advantage [16].

1.4.Principle of testing rails using Ultrasonic Phased Arrays

The main principle of ultrasonic phased arrays is to excite all or some of the transducer elements for each shot which results in beam formation by the means of adapted delay laws [19].

- Electronic focusing:

By applying balanced delay laws to the different elements of a phased array system, the beam can be focused electronically. This acts as an alternative method for using several transducers to focus at different depths. Electronic focusing is shown in **Fig.1.6 (a)**. Main advantages are listed below [19]:

✓ A single probe is required to focus at each depth.
✓ Inspection of thick samples can be done quickly using dynamic focusing.
✓ Focusing abnormalities due to refraction at interfaces can be compensated using electronic focusing.

- Electronic steering:

By applying delay laws to different elements of a phased array system, the beam can be deflected electronically. 2D beam steering can be obtained in linear and circular arrays, while 3D steering can be obtained in matrix arrays. This acts as an alternative method for using numerous transducers at different angles. Electronic steering is shown in **Fig.1.6 (b)**. Main advantages are listed below [19]:

✓ A single transducer is sufficient to perform inspection at various angles.
✓ Samples with complex geometry can be inspected faster.
✓ This method can be implemented along with electronic focusing.

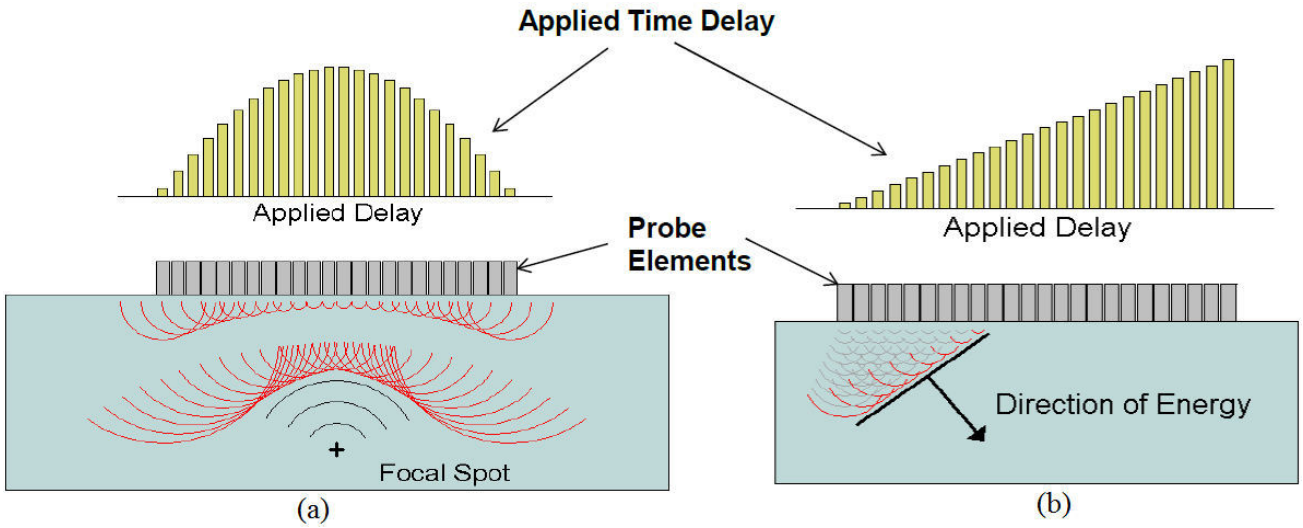

Fig.1.6. (a) Electronic focusing **(b)** Electronic steering [20]

1.4.1. Characteristics of Phased Array Probes

In simple words, an ultrasonic phased array probe is a combination of individual elements in a single unit. It is shown in **Fig.1.7**. These elements are much smaller compared to conventional transducers and they can be excited as a group to generate directionally controllable wavefronts. This results in electronic beam forming which allows multiple inspection areas to be analysed at very high speeds without any movement of the probe [16].

Fig.1.7. Ultrasonic Phased Array probe [16]

These probes are available in a wide range of sizes, shapes, frequencies, and number of elements. Although they vary as per the requirement, they all have a common piezoelectric element that contains several segments. Ultrasonic phased array probes used for industrial NDT applications are typically constructed around piezo-composite materials, which are made up of several tiny, thin rods of piezoelectric ceramic implanted in a polymer matrix. They are more challenging to manufacture and the composite probes offer 10 dB to 30 dB sensitivity range compared to piezo-ceramic probes of same design [16]. Phased array probes are categorized as per the following basic parameters:

- Type:

Most of the phased array probes operate with angle beam and they are intended to use either a delay line, plastic wedge or a straight plastic shoe (zero-degree wedge). They can be used for direct contact as well as immersion testing [16].

- Frequency:

Ultrasonic flaw detection operates in a frequency range between 2 MHz and 10 MHz and hence phased array probes also fall within this range. As in conventional transducers, lower frequency results in good penetration of ultrasonic waves, while higher frequency results in good resolution and focal sharpness. Lower frequencies are required for the test samples that have high attenuation or scattering. Usually, phased array probes for industrial purpose operates in the frequencies between 1 MHz and 15 MHz [16].

- Number of elements:

Ultrasonic phased array probes usually contain 16 to 256 elements. Focusing and steering ability increases with the use of large number of elements, which also results in large area coverage, but ends up in higher cost of probe and instrumentation as well. These elements are individually excited to create the required wavefront [16].

- Size of elements:

Beam steering ability increases with smaller element width, but large area coverage needs more elements at a higher cost. The practical size of an element is approximately 0.2 mm in case of commercial probes. Strong unwanted noise (side lobes) will be resulted if the size of element is less than one wavelength [16].

- Pitch and aperture:

The distance between individual elements is referred to as pitch and aperture refers to effective size of a pulsing element that usually contains a group of individual elements which are excited at the same time (virtual aperture). To enhance beam steering, small pitch must be used. To obtain optimal sensitivity and good beam focusing, large aperture must be used [16].

The dimensional parameters of a phased array probe are shown in **Fig.1.8.**

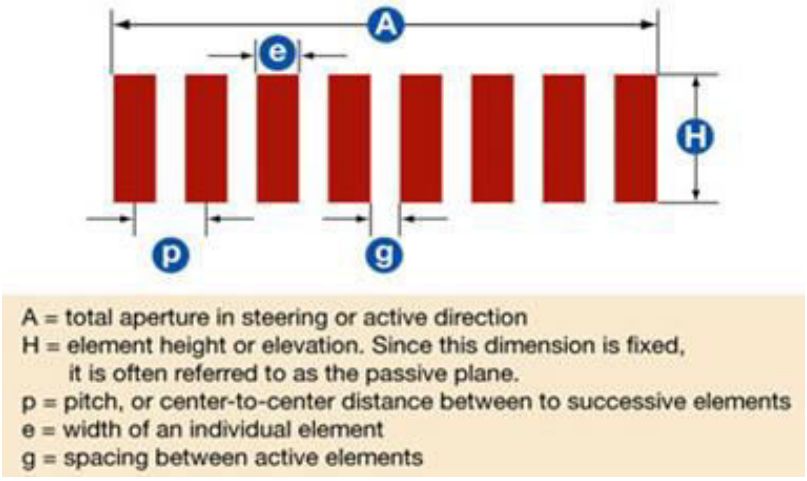

Fig.1.8. Dimensional parameters of a phased array probe [16]

1.4.2. Characteristics of Phased Array Wedges

Phased array probes generally comprise of a plastic wedge assembly. Wedges are employed in both shear wave and longitudinal wave applications. As in conventional testing, these wedges also involve the same function in Ultrasonic Phased Array systems by coupling sound energy from the probe to the test sample such that it does mode conversion and/or refracts at a required angle in correspondence to Snell's law [15]. Shear wave wedges look alike those used with conventional transducers, and like conventional wedges they come in various sizes and styles [16].

Wedge parameters are shown in **Fig.1.9** and listed below:

- ✓ Incident angle of the wedge
- ✓ Nominal velocity of the wedge
- ✓ Offset Z = height to centre of first element
- ✓ Index offset X = distance from front of wedge to first element
- ✓ Scan offset Y = distance from side of wedge to centre of elements

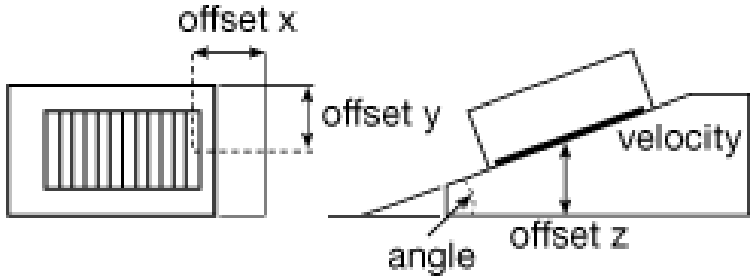

Fig.1.9. Schematic representation of wedge parameters [16]

1.4.3. Scanning Patterns

The main scanning patterns in the inspection of rails are sectorial scan and linear scan.

- ✓ Linear Scan:

Scanning is performed in a line along the railhead as the array does an electronic scan of the material. Linear scanning uses fixed angle with sequencing apertures [17]. It is shown in **Fig.1.10 (a)**.

- ✓ Sectorial scan:

Sectorial scan (S-Scan) which is also called azimuthal or angular scan involves beam steering mechanism to investigate material under test. The test sample is inspected as the beam is steered or moved using the same elements through a sweep range of a definite focal depth. This arrangement provides a good visualisation of internal structure of the rail. Sectorial scanning uses fixed apertures and the beam is steered through a sequence of angles [17]. It is shown in **Fig.1.10 (b)**.

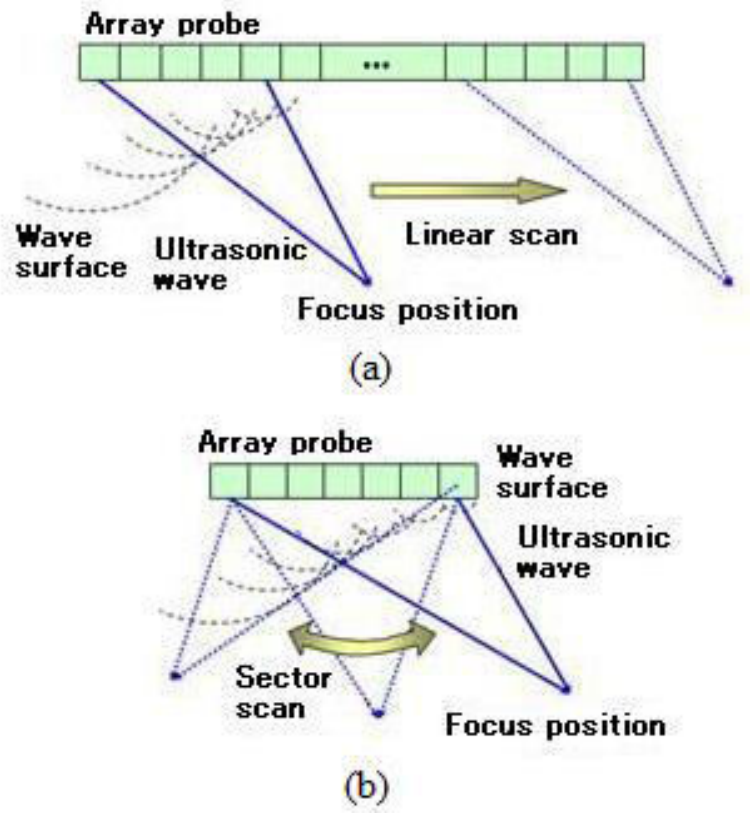

Fig.1.10. (a) Linear scan **(b)** Sectorial scan [21]

1.5.Conclusions

From studying the rail defects, I conclude that RCF defects are a major concern as they purely initiate by the action of locomotive wheels. All the defects start with micro-cracks which progresses due to various factors like applied load, environmental conditions, etc. Hence, the rails must be inspected at regular intervals to prevent dangers to both life and property. The conventional ultrasonic testing uses a single ultrasonic transducer which transmits and receives ultrasonic waves. This process is time consuming. Evolution of Ultrasonic Phased Arrays has provided a variety of inspections in different conditions. The major advantage of the phased arrays was the inspection speed which is approximately 10 times faster compared to conventional ultrasonic testing. Hence, it is an efficient and effective way that can be used for detection of defects in the rails.

2. Description of the test sample and parameters of phased array transducers

In this section, the test sample with two defects is described along with the dimensions of both the test sample and each defect. Also, the parameters of two different phased array probes and corresponding wedges used in this work are described in detail.

2.1.Dimensions of the test sample and location of the defects

Here, a piece of rail is considered as the test sample. The length of the sample is 155 mm. Other dimensions such as height of the rail, width of the head, web & foot, the radius of arcs at the curves are given in **Fig.2.1** which gives front view of the test sample.

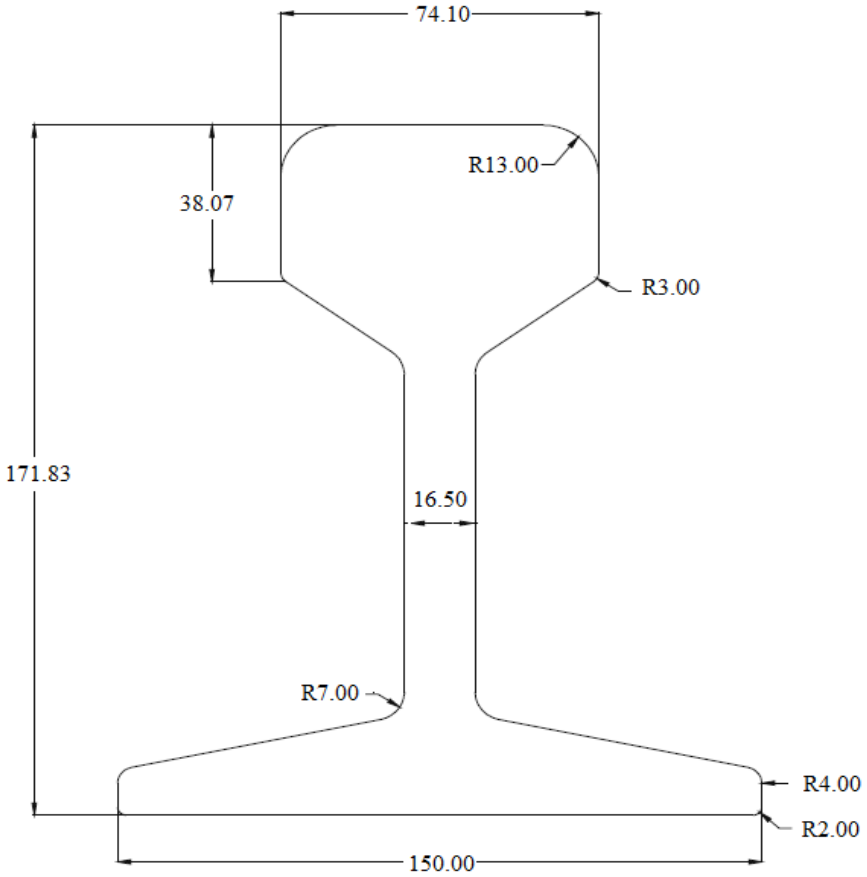

Fig.2.1. Dimensions of the test sample

The basic material properties of the test sample are given below in **Table 2.1**.

Table.2.1. Material properties of the test sample

Name	Steel
Density	7.8 g/cm^3
Longitudinal Wave (LW) velocity	5900 m/s
Shear Wave (SW) velocity	3230 m/s

The test sample contains two defects which are side drilled holes. The dimensions of these two defects are: diameter- 5 mm; length of defect-1- 23 mm and length of defect-2- 26 mm. **Fig.2.2** shows the location of defects in the test sample. Defect-1 can be seen in the head region where as defect-2 can be seen in the interface of head and web region. Both the defects are side drilled holes which are present on the opposite sides to each other.

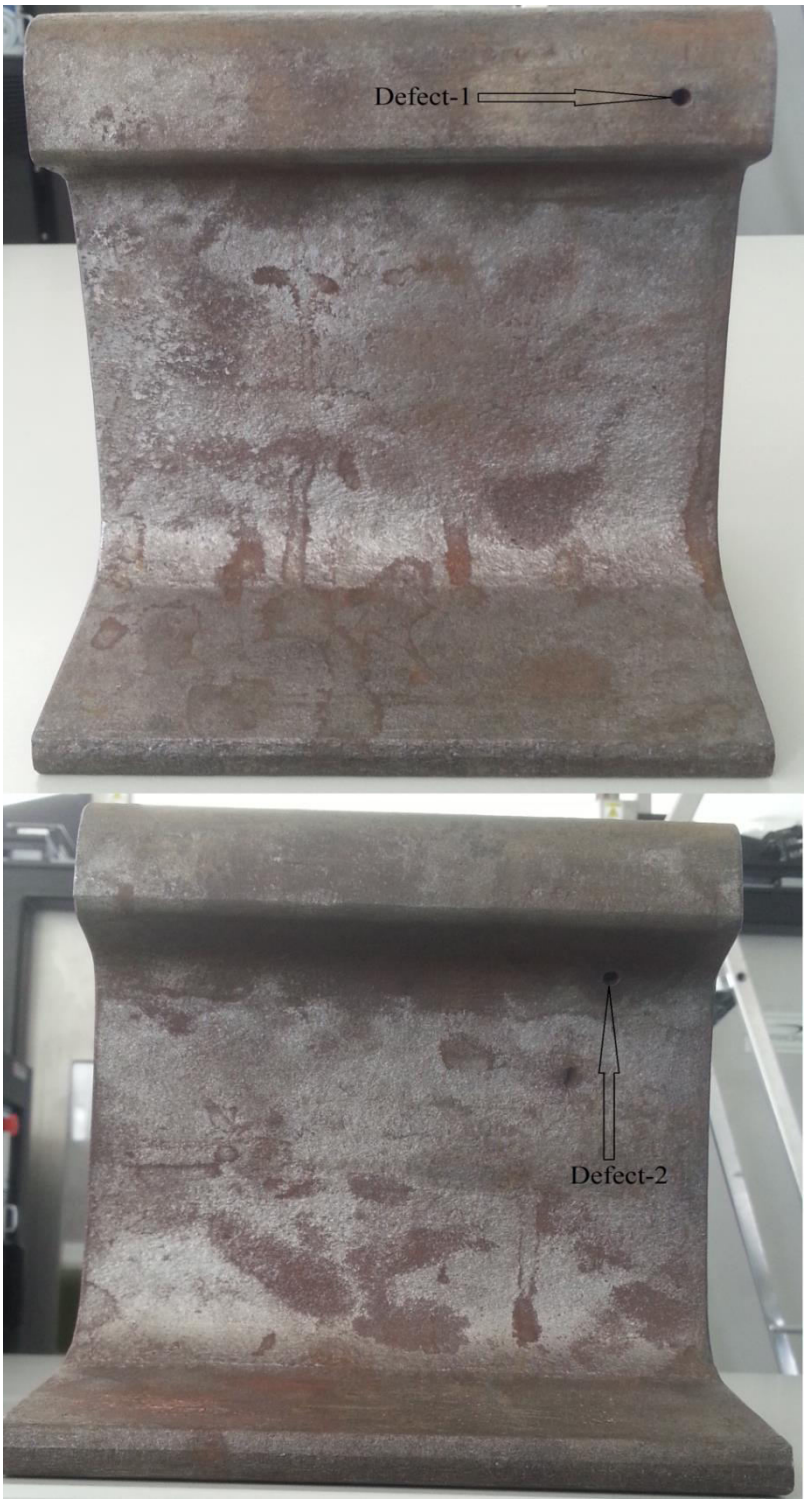

Fig.2.2. Location of defects in the test sample

2.2.Fundamental parameters of the phased array transducers

The table below gives an overview of the parameters of phased array probes.

Table.2.2. Parameters of the phased array probes

PARAMETER	Phased Array-1 (PA1)	Phased Array-2 (PA2)
Frequency	5 MHz	5 MHz
Number of elements	16	16
Active aperture	9.6 mm	9.6 mm
Virtual aperture	9.6 mm	9.6 mm
Passive aperture	10 mm	10 mm
Pitch	0.6 mm	0.6 mm
Width of one element	0.5 mm	0.5 mm
Inter-element spacing	0.1 mm	0.1 mm
Angle (in degrees)	45	LW- (-30° to +30°) SW- (30° to 70°) LW- (30° to 70°)
Matching medium	Wedge	Rexolite
Housing	45 SW	Angle beam

The table below gives the parameters of phased array wedges.

Table.2.3. Parameters of the phased array wedges

Phased Array	Front length, L_1 (mm)	Back length, L_2 (mm)	Width, L_3 (mm)	Height, L_4 (mm)	Refraction angle, R (degrees)	Incidence angle, I (degrees)
PA1	15	15	15	31	45	39.923
PA2 (Wedge-1)	12.5	12.5	23	20	0	0
PA2 (Wedge-1)	11.5	11.5	23	14	55	42.818
PA2 (Wedge-3)	13	13	23	30	60	23.165

3. Computer modelling using CIVA software

In this section, we shall model the ultrasonic beams from different phased array with different wedge configurations in order to know the volume covered by each of them. Based on the beam profiles of the two different phased arrays, the best one for the inspection of rail is determined. Also, inspection of the test sample using sectorial scanning and multi-point focusing is performed and best position of phased arrays for the defect detection in the different parts of rail is estimated.

3.1.Modelling the beams

The modelling of ultrasonic beams is performed under "Beam computation" module in CIVA software. To get a clear picture of the ultrasonic beams, the length of test sample is considered to be 500 mm. Here, we shall model the beams using the two types of phased arrays. Specimen, probe and wedge parameters can be referred from section 2. Other parameters for different phased arrays are given below:

- Inspection settings:

Inspection is done in positive orientation. Offset X and Offset Y have to be chosen carefully in order to maintain the wedge at the centre and to obtain the equal distribution of ultrasonic waves in the test sample. These are given in **Table.3.1**. Wedge centre is chosen as the reference point. Water is used as coupling medium and air is considered as bottom medium.

Table.3.1. Inspection settings of different phased arrays

Phased Array	Inspection plane	Positioning	
		Offset X (mm)	Offset Y (mm)
PA1	Normal to profile	76.3	150
PA2 (Wedge-1)	Along profile	76.3	150
PA2 (Wedge-1)	Normal to profile	76.3	150
PA2 (Wedge-3)	Normal to profile	76.3	150

- Array settings:

Unisequential function is used for initialization and sectorial scanning is chosen for all the phased arrays used. Other parameters are given in **Table.3.2**.

Table.3.2. Array settings of different phased arrays

Phased Array	Initial angle (degrees)	Final angle (degrees)	Number of steps
PA1	30	70	8
PA2 (Wedge-1)	-30	+30	12

PA2 (Wedge-1)	30	70	8
PA2 (Wedge-3)	30	70	8

- Simulation settings:

3D computation mode is chosen with direct mode for all the phased arrays used. Rectangular computation zone is chosen whose parameters are given in **Table.3.3**. The local Cartesian coordinates (X and Z) are used to adjust the scan area. "X" value is used to adjust the computation zone in horizontal direction and "Z" value is used to adjust the computation zone in vertical direction.

Table.3.3. Computation zone dimensions of different phased arrays

Phased Array	X-zone (mm)	No. of steps along X-zone	Z-zone (mm)	No. of steps along X-zone	Local Cartesian coordinates	
					X (mm)	Z (mm)
PA1	355	200	171.83	150	172.5	86
PA2 (Wedge-1)	74.1	200	171.83	150	0	85.9
PA2 (Wedge-1)	355	200	171.83	150	172.5	86
PA2 (Wedge-3)	355	200	171.83	150	172.5	86

3.1.1. Modelling the beams using Phased Array-1 (PA1)

Here, the beam is modelled in such a way that scanning is performed using Shear waves which covers 30° to 70° region. From **Fig.3.1**, we can observe several rays which indicate the initial angle as 30° and final angles as 70° respectively. The number of steps between these angles is 8 which mean scanning is done for each 5° region.

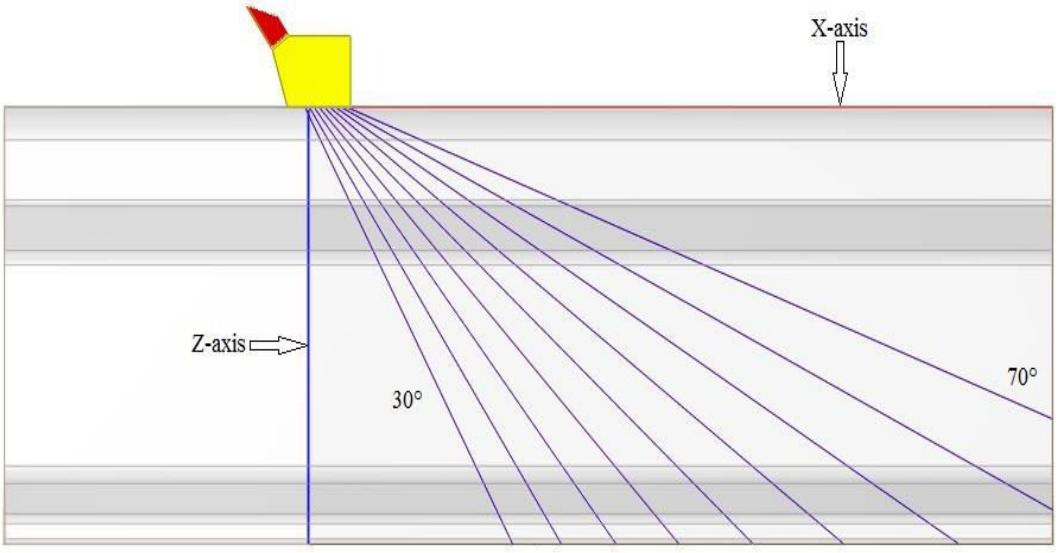

Fig.3.1. Arrangement of PA1

✓ Results:

From **Fig.3.2 (a)**, it can be known that 2D cumulated field shows several shots that were fired accordingly. Also, the beam intensity can be observed with a different colour pattern and an even beam spread is seen in the 2D cumulated field. **Fig.3.2 (b)** gives a clear view of ultrasonic beam entering the test sample from the wedge as per the given set of angles.

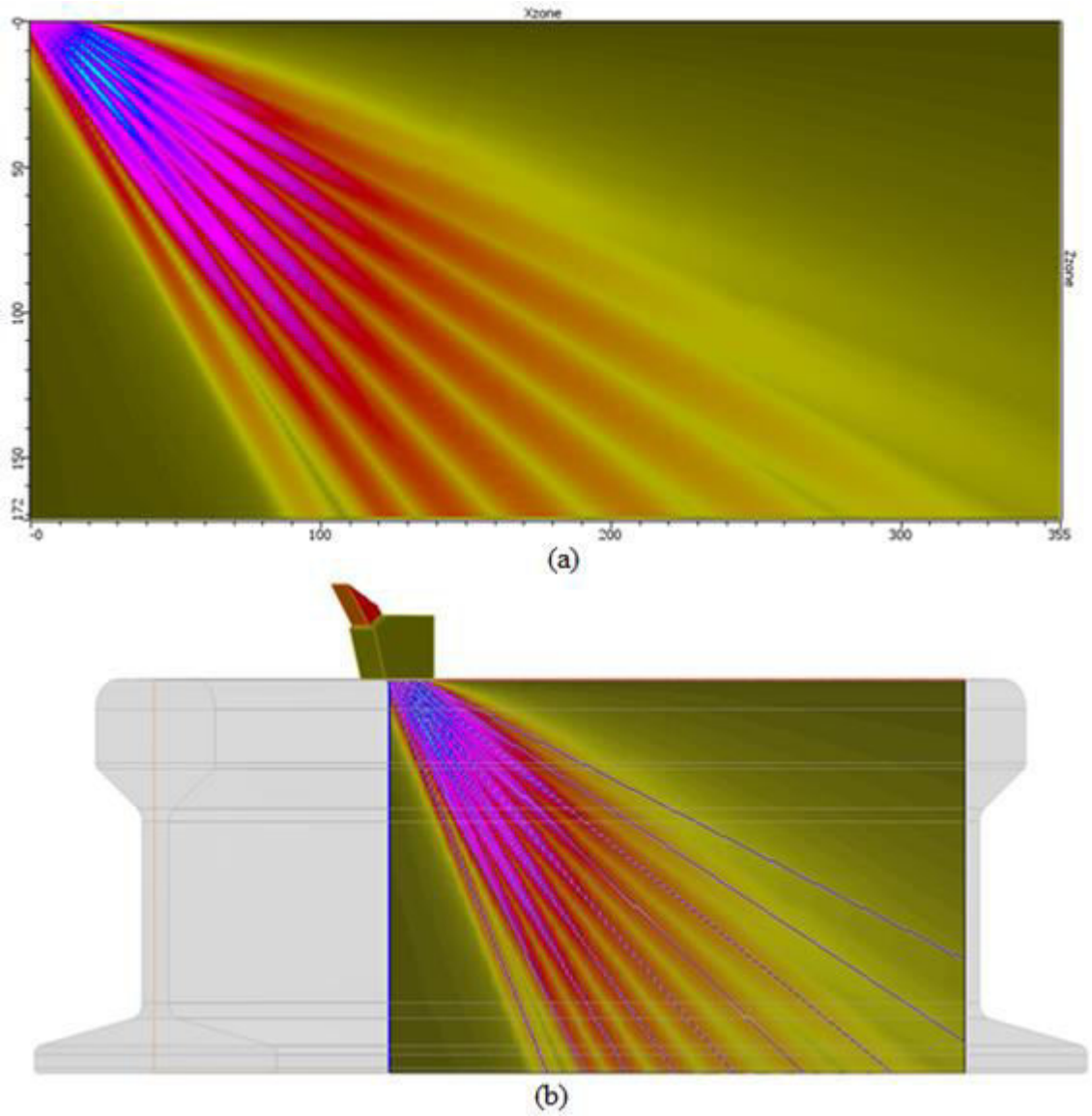

Fig.3.2. (a) 2D cumulated field of PA1; **(b)** 3D image view of PA1

From **Fig.3.3,** we have a clear representation of each shot that was triggered by PA1. As we observe it, the triggering starts with shot-1 at 30° and ends with shot-9 at 70° respectively. The beam intensity varies with each shot. At the shot-1, intensity of beam looks weak but from shot-2 to shot-6, the intensity of beams both in the near field and far field is quite stable which means that the echoes will have stronger amplitude in the A-scan. In shot-7 and shot-8, the intensity of beams in the near field looks stable but the intensity in the far field keeps on decaying. In shot-9, intensity in both the

near field and far field is very weak which results in weak echoes and hence amplification of the signal as well as the compensation techniques must be used.

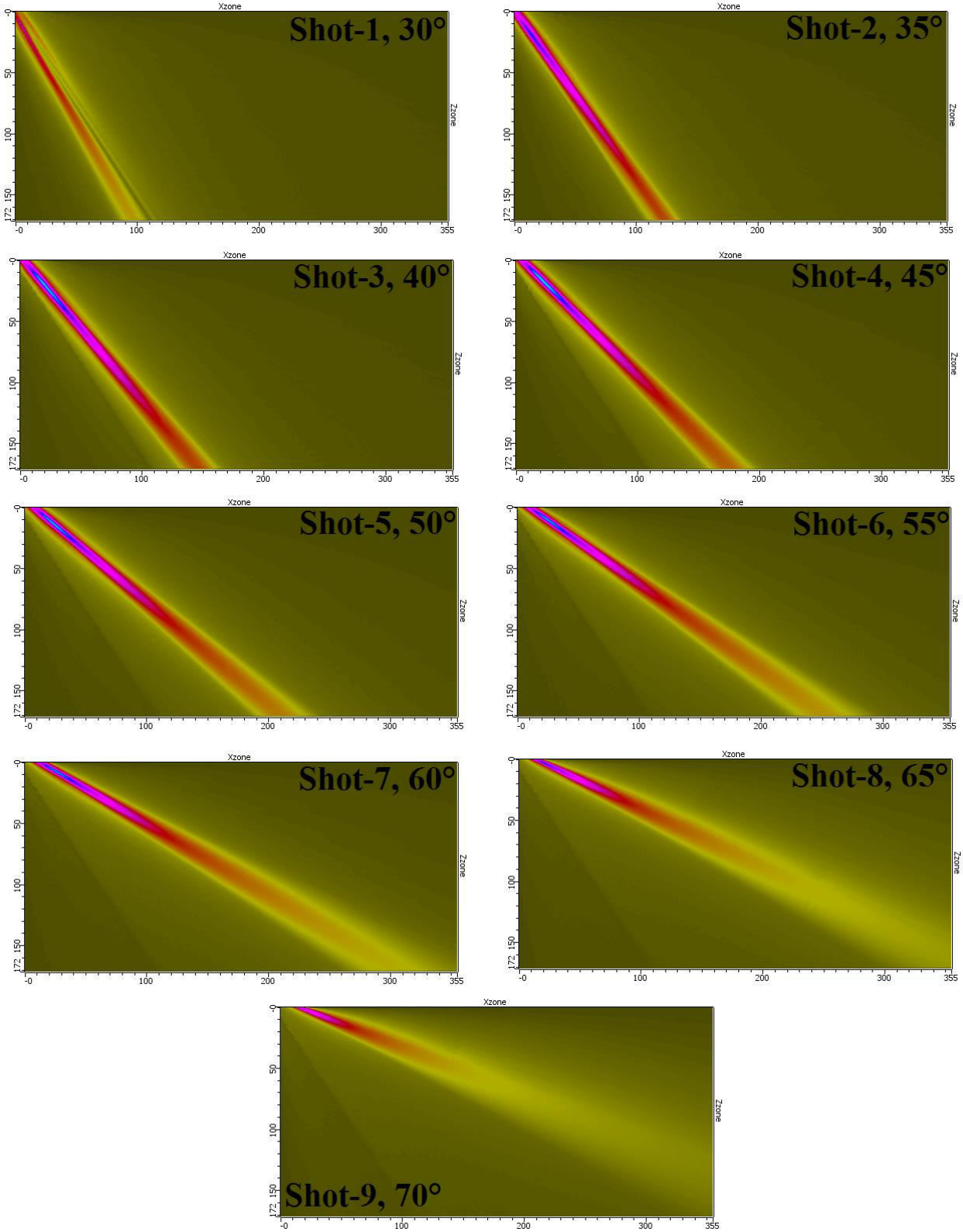

Fig.3.3. Several shots triggered by PA1

3.1.2. Modelling the beams using Phased Array-2 (PA2)

- Wedge-1:

Here, the beam is modelled in such a way that scanning is performed using longitudinal waves which covers -30° to +30° region. From **Fig.3.4**, we can observe several rays which indicate the initial angle as -30° and final angles as +30° respectively. The number of steps between these angles is 12 which states that scanning is done for each 5° regions.

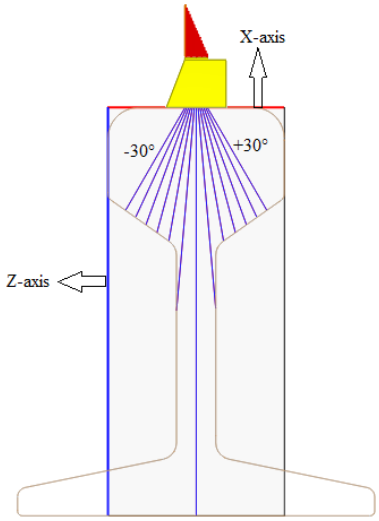

Fig.3.4. Arrangement of PA2 (Wedge-1)

✓ Results:

From **Fig.3.5 (a)**, it can be known that 2D cumulated field shows several shots that were fired accordingly. Also, the beam intensity can be observed with a different colour pattern and an even beam spread is seen in the 2D cumulated field. Fig.3.5 (b) gives a clear view of ultrasonic beam entering the test sample from the wedge as per the given set of angles.

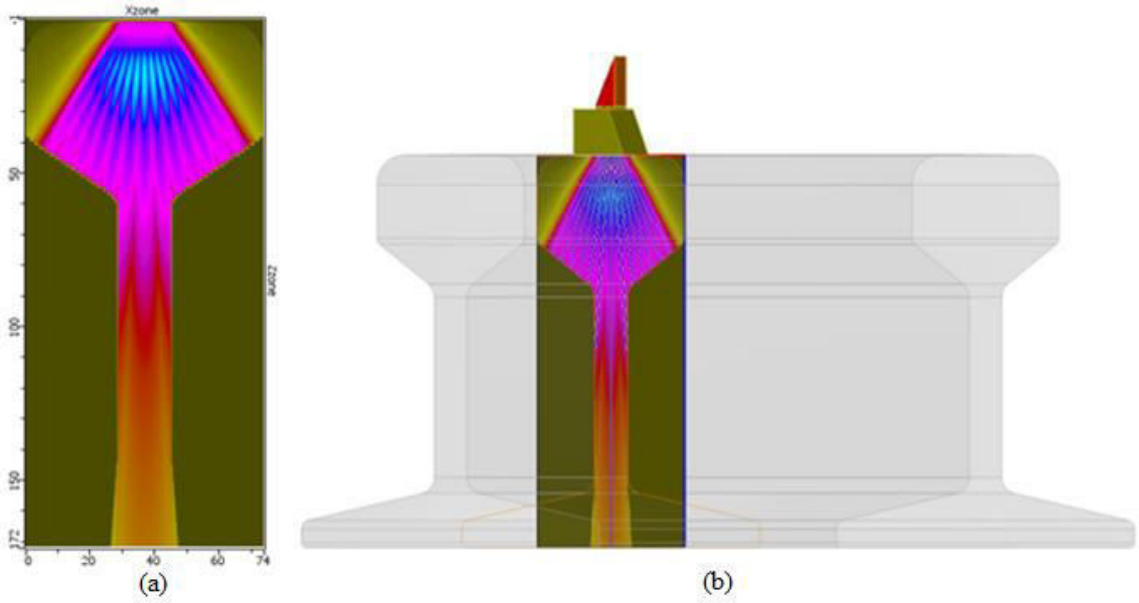

Fig.3.5. (a) 2D cumulated field of PA2 (Wedge-1); **(b)** 3D image view of PA2 (Wedge-1)

From **fig.3.6**, we have a clear representation of each shot that was triggered by PA2 (Wedge-1). As we observe, the triggering starts with shot-1 at -30° and ends with shot-13 at +30° respectively. The beam intensity also varies with each shot. In all the shots i.e. from shot-1 to shot-13, it can be seen that the intensity of beams both in the near field and far field is stable which means that we obtain good echoes from obstacles and will have stronger amplitude in the A-scan.

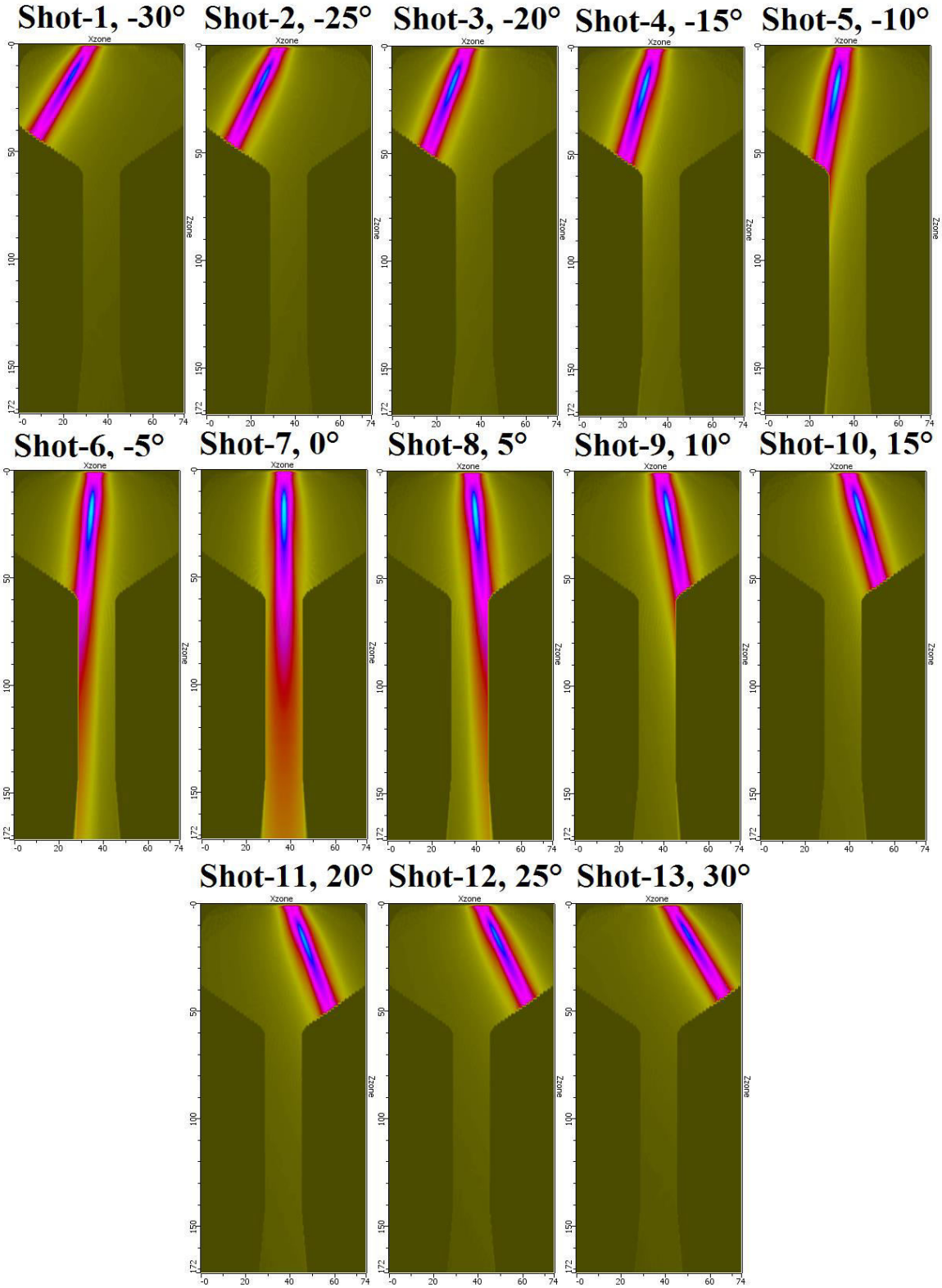

Fig.3.6. Several shots triggered by PA2 (Wedge-1)

- Wedge-2:

Here, the beam is modelled in such a way that scanning is performed using Shear waves which covers 30° to 70° region. From **Fig.3.7**, we can observe several rays which indicate the initial angle as 30° and final angles as 70° respectively. The number of steps between these angles is 8 which mean scanning is done for each 5° region. Also, computation zone can be viewed as a box.

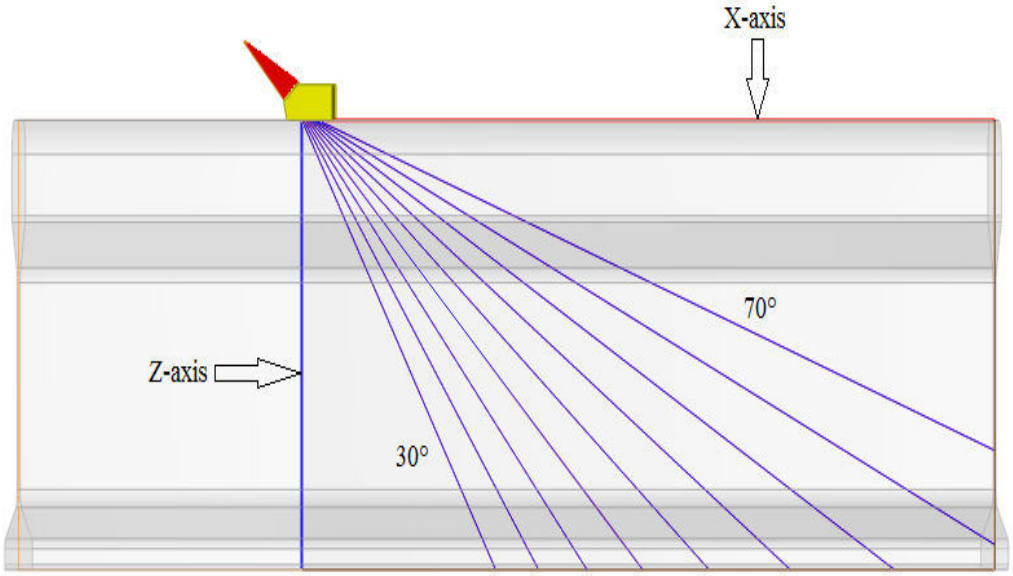

Fig.3.7. Arrangement of PA2 (Wedge-2)

✓ Results:

From **Fig.3.8 (a)**, it can be known that 2D cumulated field shows several shots that were fired accordingly. Also, the beam intensity can be observed with a different colour pattern and an even beam spread is seen in the 2D cumulated field. **Fig.3.8 (b)** gives a clear view of ultrasonic beam entering the test sample from the wedge as per the given set of angles.

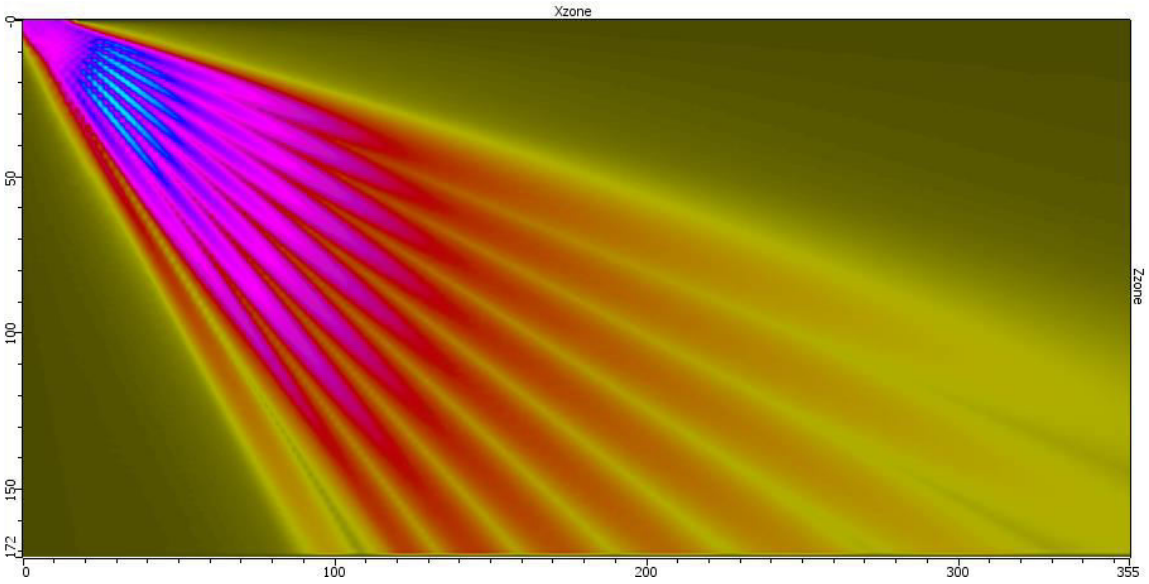

(a)

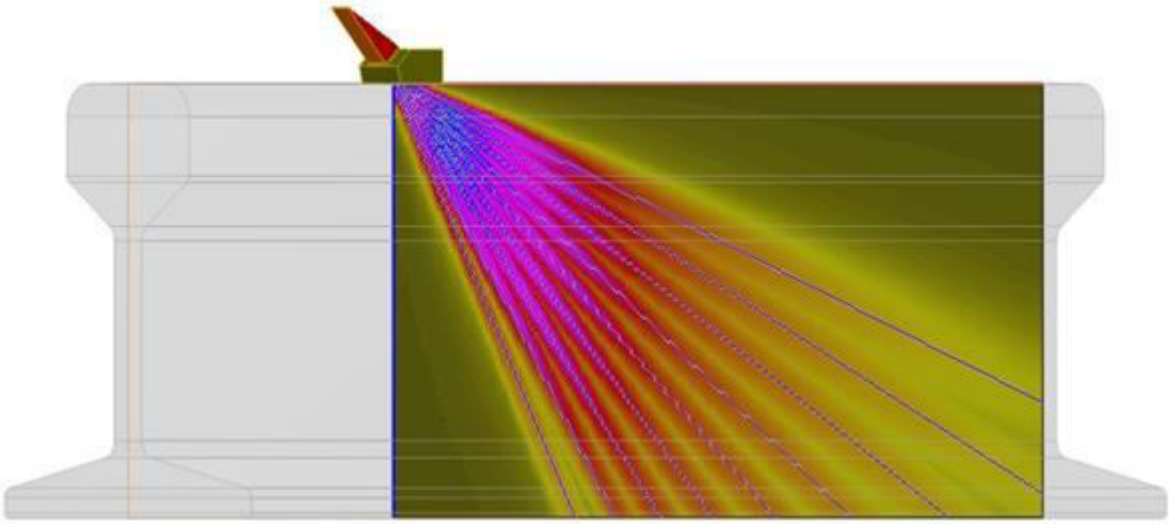

(b)

Fig.3.8. (a) 2D cumulated field of PA2 (Wedge-2); **(b)** 3D image view of PA2 (Wedge-2)

From **Fig.3.9**, we have a clear representation of each shot that was triggered by PA2 (Wedge-2). As we observe it, the triggering starts with shot-1 at 30° and ends with shot-9 at 70° respectively. The beam intensity also varies with each shot. In shot-1, the intensity of beam in the far field is very low and it leads to weak echoes. From shot-2 to shot-6, the intensity of beams both in the near field and far field is stable which means that we obtain good echoes and will have stronger amplitude in the A-scan. From shot-7 to shot-9, it can be observed that the intensity of beams in the near field is quite good but keeps on diminishing in the far field which leads to weak signals at the receiving end and hence amplification might be required.

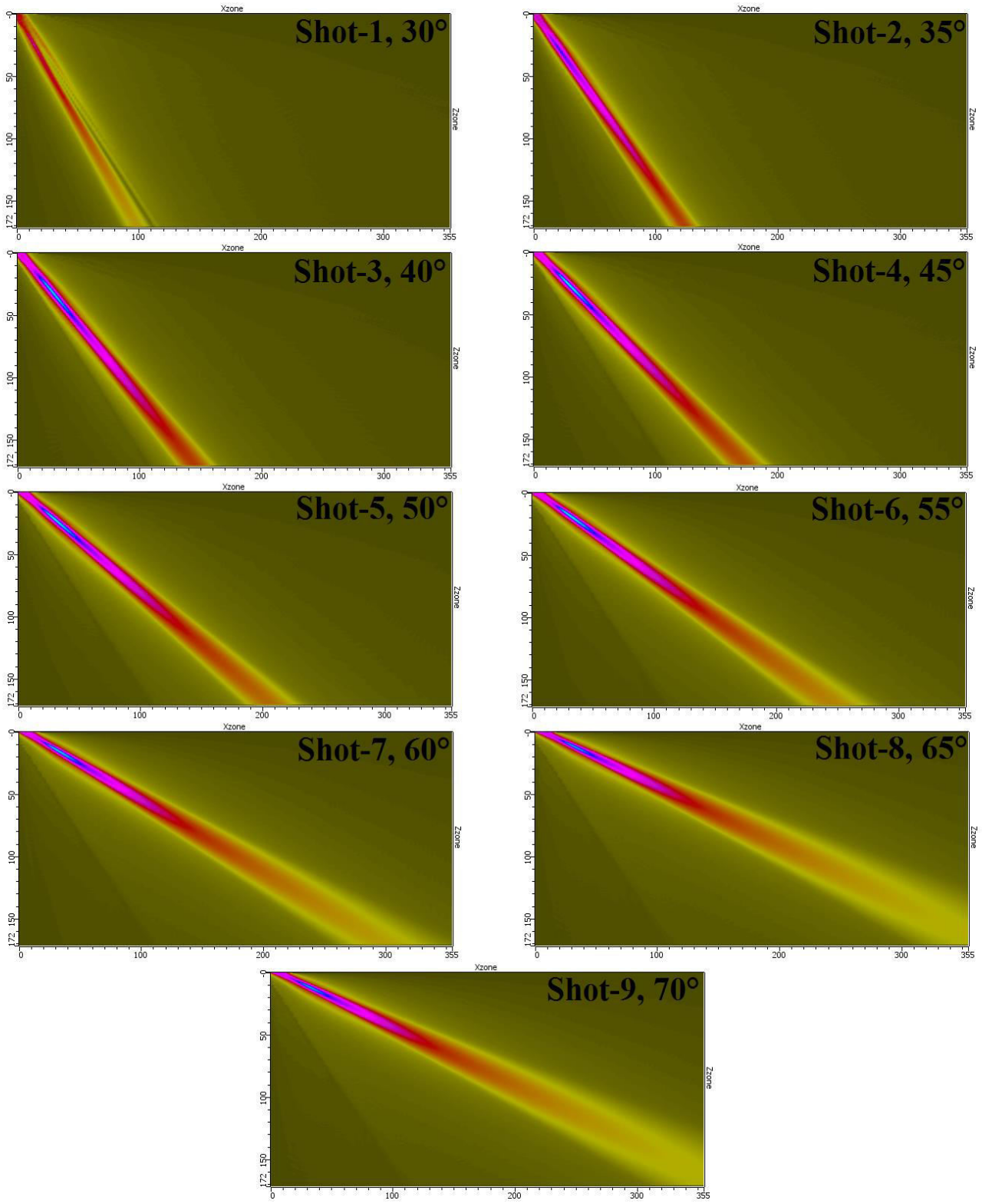

Fig.3.9. Several shots triggered by PA2 (Wedge-2)

- Wedge-3:

Here, the beam is modelled in such a way that scanning is performed using longitudinal waves which covers 30° to 70° region. From **Fig.3.10**, we can observe several rays which indicate the initial angle as 30° and final angles as 70° respectively. The number of steps between these angles is 8 which mean scanning is done for each 5° region. Also, computation zone can be viewed as a box.

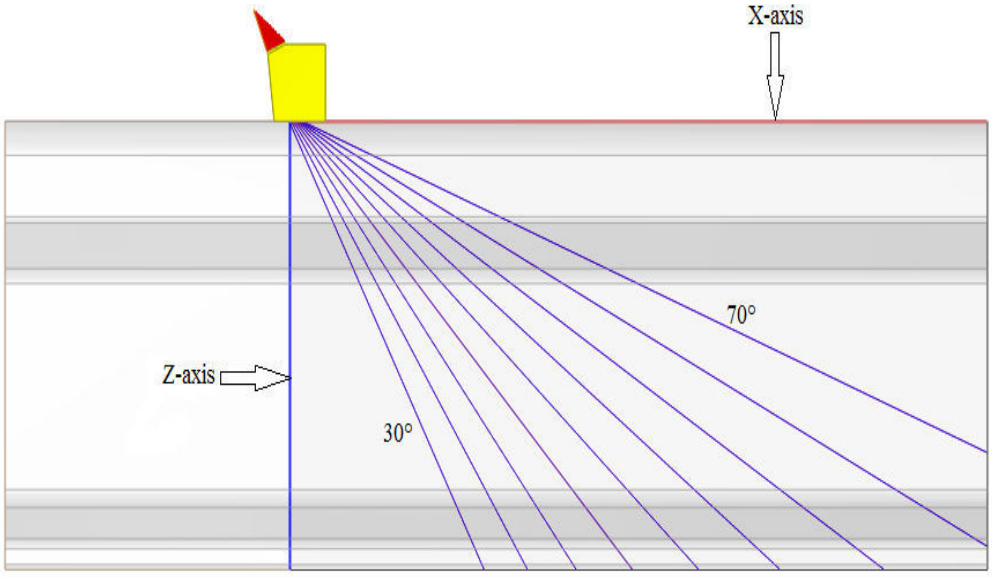

Fig.3.10. Arrangement of PA2 (Wedge-3)

✓ Results:

From **Fig.3.11 (a)**, it can be known that 2D cumulated field shows several shots that were fired accordingly. Also, the beam intensity can be observed with a different colour pattern and an even beam spread is seen in the 2D cumulated field. **Fig.3.11 (b)** gives a clear view of ultrasonic beam entering the test sample from the wedge as per the given set of angles.

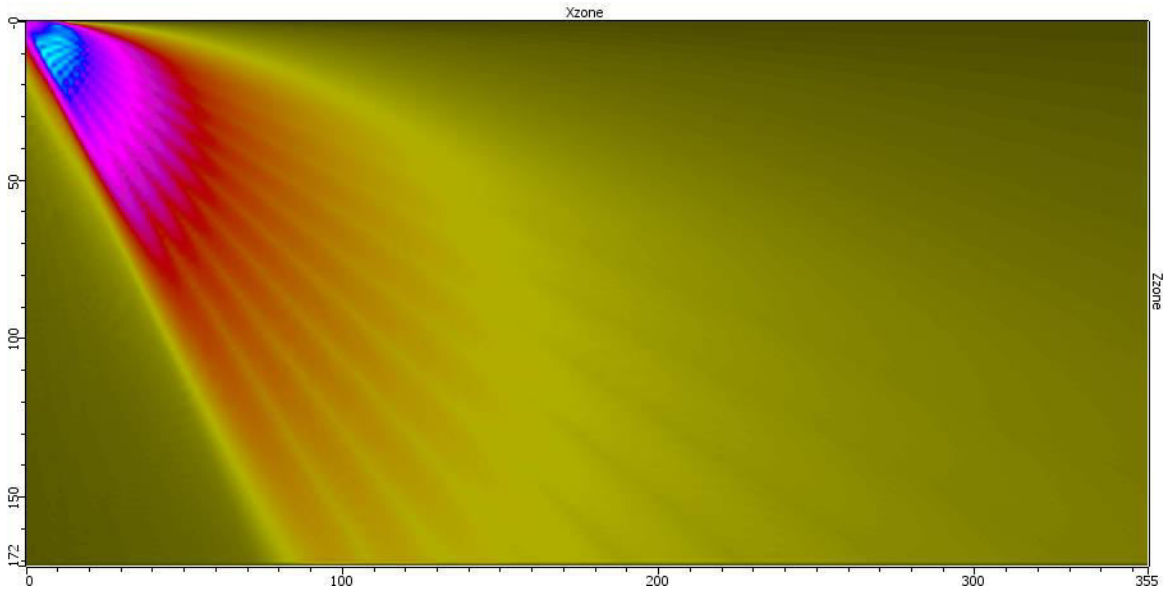

(a)

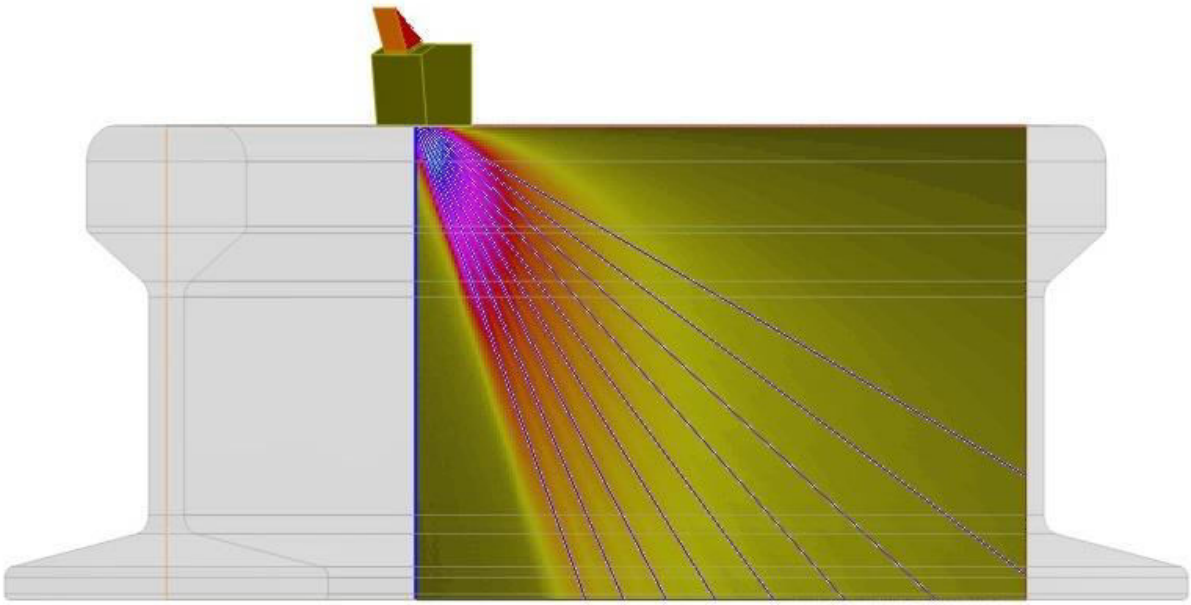

(b)

Fig.3.11. (a) 2D cumulated field of PA2 (Wedge-3); **(b)** 3D image view of PA2 (Wedge-3)

From **Fig.3.12**, we have a clear representation of each shot that was triggered by PA2 (Wedge-3). As we observe it, the triggering starts with shot-1 at 30° and ends with shot-9 at 70° respectively. The beam intensity also varies with each shot. In all the shots, the intensity of beam in the near field is quite strong but the intensity in the far field is low at first and keeps on diminishing with high scattering which means that we obtain weak echoes and hence amplification of the signal as well as the compensation techniques must be used.

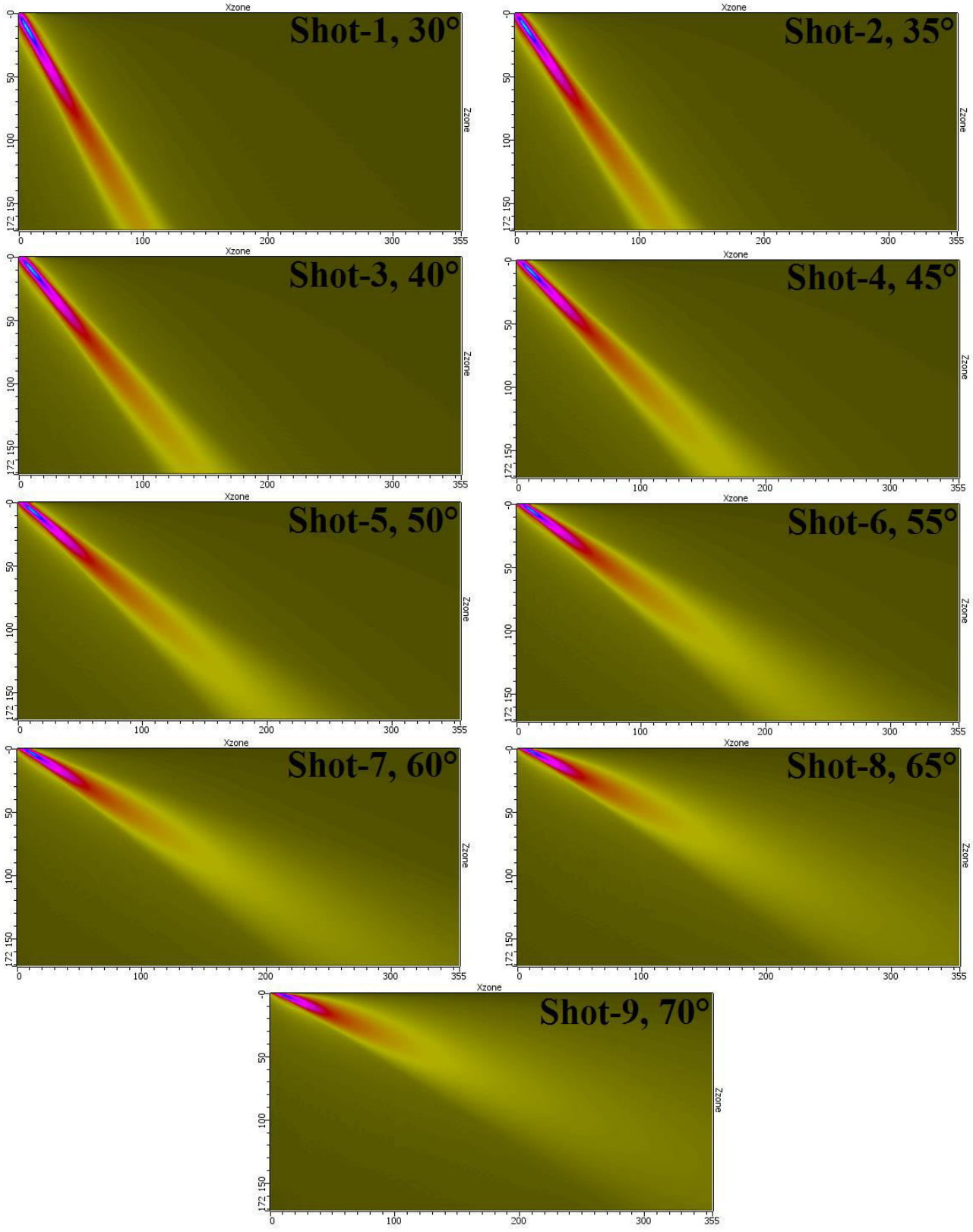

Fig.3.12. Several shots triggered by PA2 (Wedge-3)

3.2.Inspection of defects in the test sample using Sectorial scanning

The inspection of defects is performed under “Inspection simulation” module in CIVA software. Here, we shall consider original dimensions of the test sample which will be inspected practically. All the dimensions except the length are same. In this case, the length of test sample is 155 mm. Two side drilled holes are considered as the defects. The dimensions of these two side drilled holes are considered to be: diameter- 5 mm; length- 22 mm. The coordinates of defects in the test sample are given in **Table.3.4**.

Table.3.4. Coordinates of defects in CIVA

Defect	Distance in X-axis (mm)	Distance in Y-axis (mm)	Distance in Z-axis (mm)	Rotation (Degrees)
Defect-1	50	137	-100	0
Defect-2	80.45	22	-76	130

From **Fig.3.13**, it can be observed that defect-1 is present on head region of test sample while defect-2 is present on the intersection of head and web region of test sample. These defects are present on opposite sides to each other.

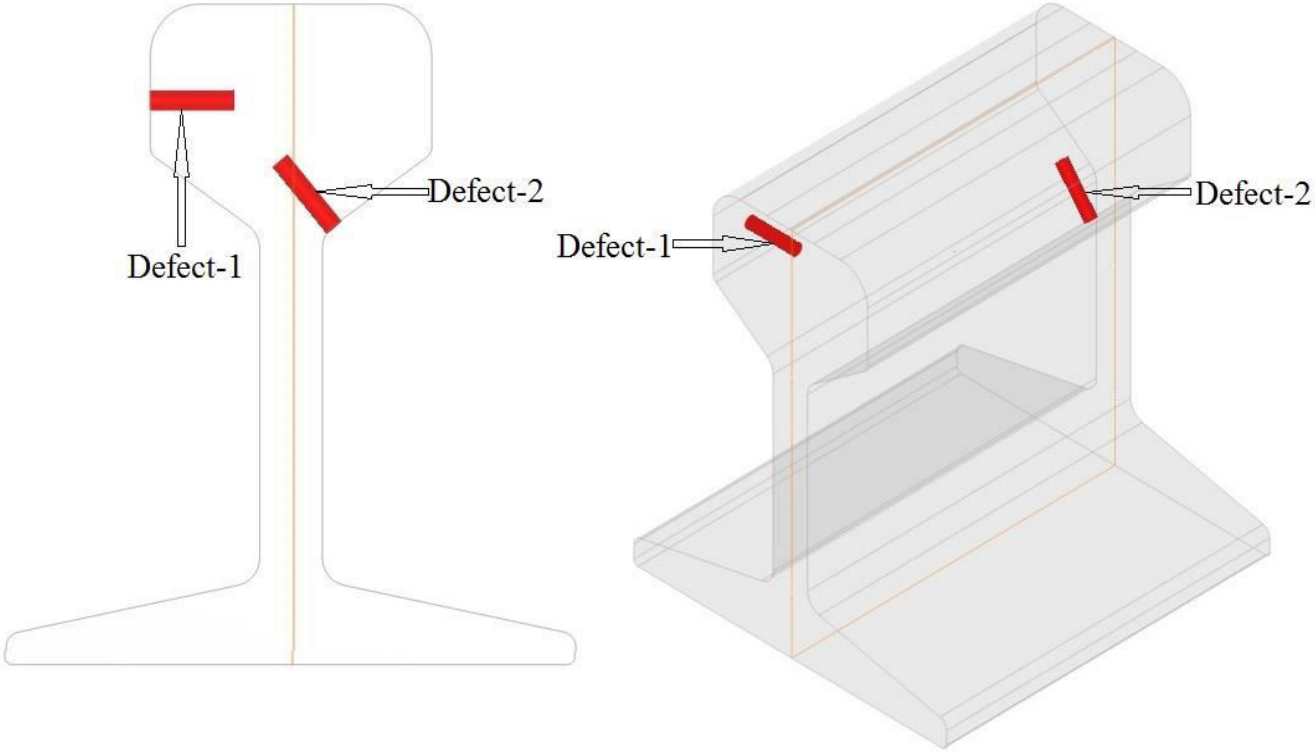

Fig.3.13. Front view and perspective view of defects in the test sample

3.2.1. Inspection of defects in the test sample using Phase Array-1 (PA1) (Sectorial scanning)

✓ Parameters:

All the parameters are same as the model used in "Beam computation" module. Here, we use shear waves with nominal refracted beam angle of 45° and 30° to 70° as the sweep. The additional parameters include positioning the wedge; selection of "UNISEQUENTIAL" mode as the scanning method with number of steps as 40 which means scanning is done for every one degree; selection of side and bottom specimen echoes in the interaction part of simulation settings and specification of the sensitivity zone. The parameters of sensitivity zone are given in **Table.3.5.**

To maintain the wedges at centre in vertical direction and at the corners in horizontal direction, Offset-X is chosen as 77 mm and Offset-Y is chosen as 15 mm in case of defect-1 inspection and as 77 mm and 140 mm in case of defect-2 inspection under the inspection settings with wedge centre as the reference point. Direction of scanning is chosen as positive for inspecting defect-1 and negative for inspecting defect-2.

Table.3.5. Parameters of sensitivity zone

X-zone	155 mm
Y-zone	151 mm
Z-zone	171.83 mm
Local Cartesian coordinates (X)	63 mm
Local Cartesian coordinates (Z)	86 mm

✓ Model:

PA1 is mounted on the left and right corners of the specimen to perform inspection of defect-1 and defect-2 respectively that is shown in **Fig.3.14 (a)** and **Fig.3.14 (b)**. The transmitted and reflected/scattered ultrasonic waves can be seen. The region covering the test sample as a rectangular box is referred to as sensitivity zone.

Attenuation is a phenomenon in which the signal intensity of transmitted ultrasonic waves decreases gradually as they go deeper into an object. It might be caused due to various reasons like absorption, scattering, diffraction etc. High frequency leads to high attenuation and vice versa. We shall consider attenuation since real ultrasonic waves get attenuated as they travel in any test sample. So, for this, choose "Power attenuation law" in transversal wave attenuation section in specimen settings.

The formula of power attenuation law is:

$$\alpha(f) = \alpha_0 \left(\frac{f}{f_0} \right)^p \quad \textbf{(3.1)}$$

From the formula **(3.1)**, wave attenuation (α) is 0.25 dB/mm; power of the attenuation rate (p) is 4; wave frequency (f) is 5 MHz. These parameters remain same for both longitudinal and transversal wave attenuation.

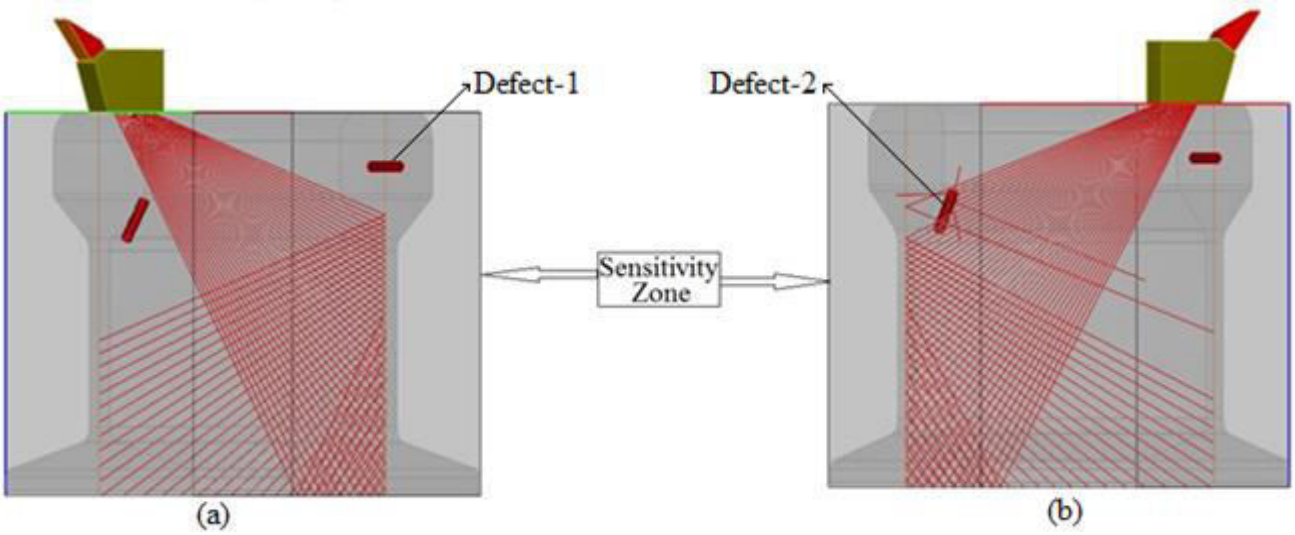

Fig.3.14. Wedge position for inspecting **(a)** defect-1 using PA1 **(b)** defect-2 using PA1

✓ Results:

From **Fig.3.15 (a)**, it is clearly visible that during the inspection of defect-1, both the defects are identified whereas from **Fig.3.15 (b),** it can be noticed that during the inspection of defect-2, only defect-2 is identified. We can further analyse these defects using S-scan and A-scan results.

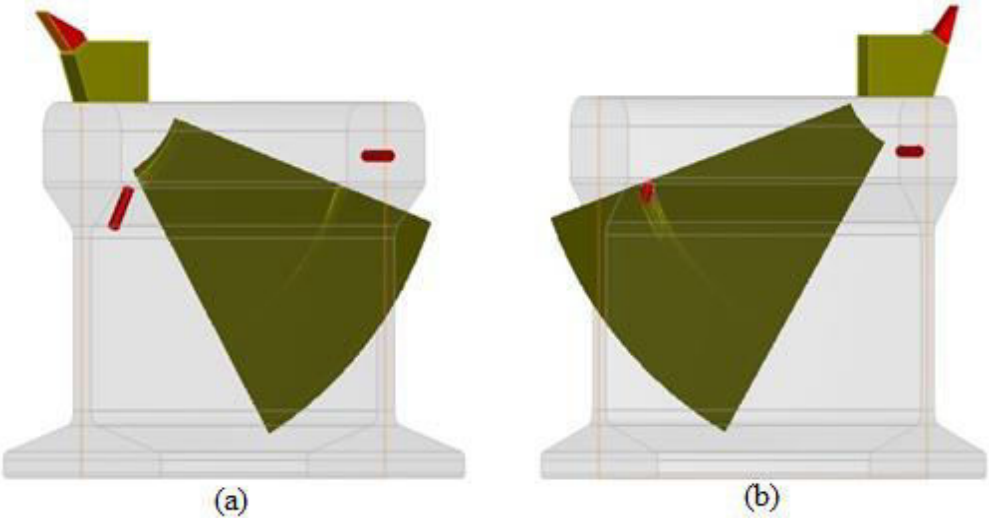

Fig.3.15. 3D image view of the test sample while inspecting **(a)** defect-1 using PA1 **(b)** defect-2 using PA1

The resultant S-scans and corresponding A-scans while inspecting defect-1 using PA1 is shown in **Fig.3.16**. Both the defects are identified in this case. An echo with moderate amplitude indicates defect-1 that is identified at 70° while another echo with high amplitude indicates defect-2 that is identified at 30°.

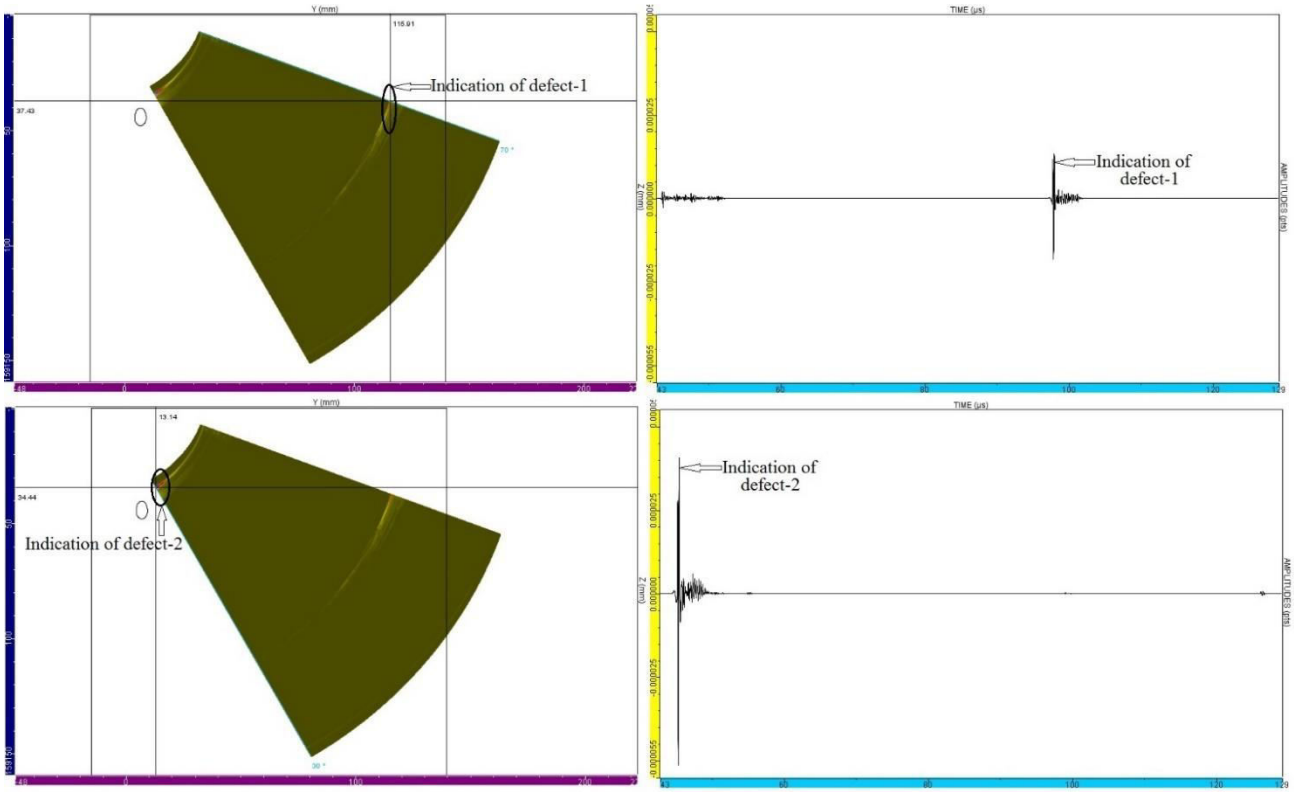

Fig.3.16. S-scan and corresponding A-scan results while inspecting defect-1 using PA1

The resultant S-scan and corresponding A-scan while inspecting defect-2 using PA1 is shown in **Fig.3.17**. Only defect-2 is identified here at 69° which is an echo with very high amplitude.

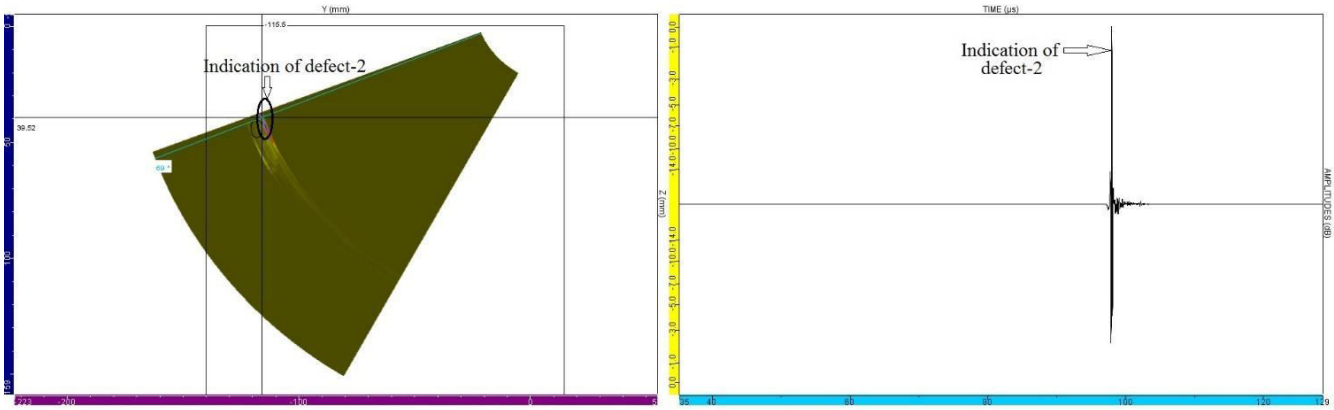

Fig.3.17. S-scan and corresponding A-scan results while inspecting defect-2 using PA1

3.2.2. Inspection of defects in test sample using Phase Array-2 (PA2) (Sectorial scanning)

- Wedge-1:

✓ Parameters:

All the parameters are same as the model used in "Beam computation" module. Here, we use longitudinal waves with nominal refracted beam angle of 0° and -30° to +30° as the sweep. The additional parameters include positioning the wedge; selection of "UNISEQUENTIAL" mode as the scanning method with number of steps as 60 which means scanning is done for every one degree; selection of side and bottom specimen echoes in the interaction part of simulation settings and specification of the sensitivity zone which is given in **Table.3.6** and **Table.3.7**.

To maintain the wedges at centre and exactly above the defects, Offset-X is chosen as 76.3 mm and Offset-Y is chosen as 137 mm in case of defect-1 inspection and as 76.3 mm and 22 mm in case of defect-2 inspection under the inspection settings with wedge centre as the reference point.

Table.3.6. Parameters of sensitivity zone for the inspection of defect-1

X-zone	74.4 mm
Y-zone	155 mm
Z-zone	171.83 mm
Local Cartesian coordinates (X)	0 mm
Local Cartesian coordinates (Y)	-59.5 mm
Local Cartesian coordinates (Z)	86 mm

Table.3.7. Parameters of sensitivity zone for the inspection of defect-2

X-zone	74.4 mm
Y-zone	155 mm
Z-zone	171.83 mm
Local Cartesian coordinates (X)	0 mm
Local Cartesian coordinates (Y)	55 mm
Local Cartesian coordinates (Z)	86 mm

✓ Model:

PA2 (Wedge-1) is mounted exactly above defect-1 and defect-2 respectively that is shown in **Fig.3.18 (a)** and **Fig.3.18 (b)**. The region covering the test sample as a rectangular box is referred to

as sensitivity zone. We shall consider attenuation since real ultrasonic waves get attenuated as they travel in any test sample. So, for this, choose "Power attenuation law" in longitudinal wave attenuation section in specimen settings.

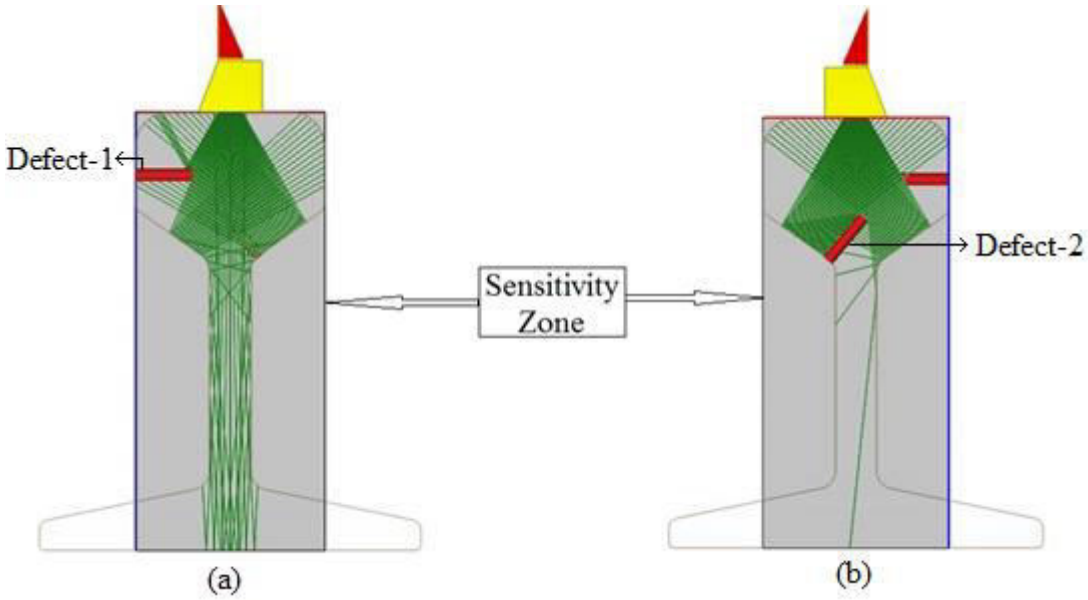

Fig.3.18. Wedge position for inspecting **(a)** defect-1 using PA2 (Wedge-1)
(b) defect-2 using PA2 (Wedge-1)

✓ Results:

From **Fig.3.19 (a)**, defect-1 is identified whereas from **Fig.3.19 (b),** defect-2 is identified. Also, there are side and bottom reflections in both the cases. Further analysis of these defects can be done using S-scan and A-scan results.

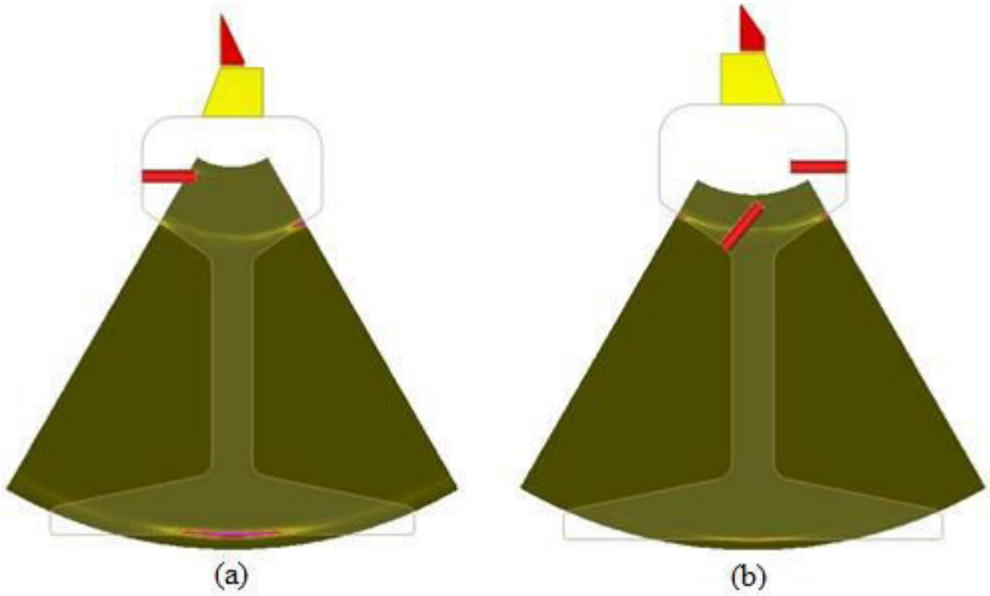

Fig.3.19. 3D image view of the test sample while inspecting **(a)** defect-1 using PA2 (Wedge-1)
(b) defect-2 using PA2 (Wedge-1)

The resultant S-scans and corresponding A-scans while inspecting defect-1 using PA2 (Wedge-1) is shown in **Fig.3.20**. Here, defect-1 is identified at -27° which is an echo with very small amplitude.

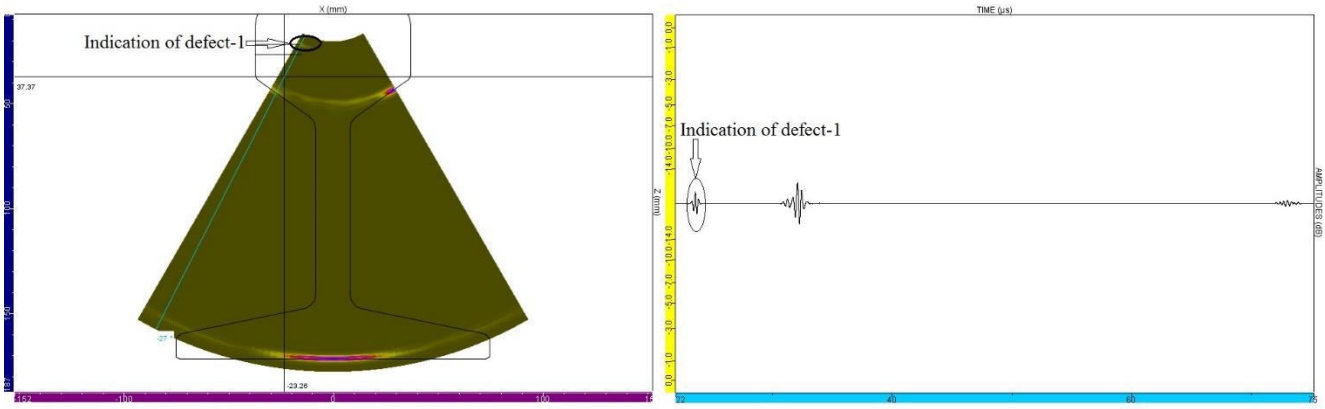

Fig.3.20. S-scan and corresponding A-scan results while inspecting defect-1 using PA2 (Wedge-1)

The resultant S-scans and corresponding A-scans while inspecting defect-1 using PA2 (Wedge-1) is shown in **Fig.3.21**. Here, defect-2 is identified at -1° which is an echo with very small amplitude.

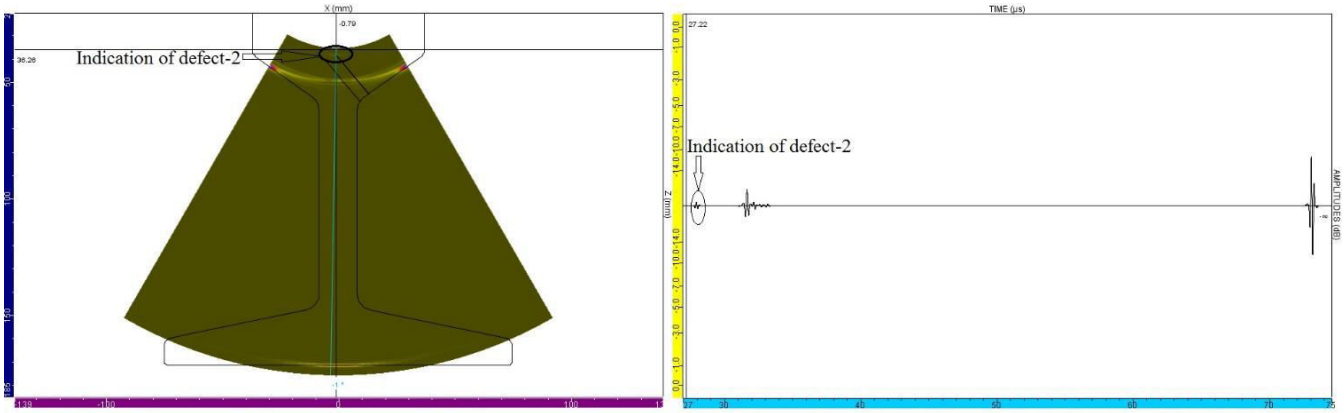

Fig.3.21. S-scan and corresponding A-scan results while inspecting defect-2 using PA2 (Wedge-1)

- Wedge-2:

✓ Parameters:

All the parameters are same as the model used in "Beam computation" module. Here, we use shear waves with nominal refracted beam angle of 55° and 30° to 70° as the sweep.

The additional parameters include positioning the wedge; selection of "UNISEQUENTIAL" mode as the scanning method with number of steps as 40 which means scanning is done for every one degree; selection of side and bottom specimen echoes in the interaction part of simulation settings and specification of the sensitivity zone given in **Table.3.8**.

To maintain the wedges at centre in vertical direction and at the corners in horizontal direction, Offset-X is chosen as 77 mm and Offset-Y is chosen as 11.5 mm in case of defect-1 inspection and as 77 mm and 143.5 mm in case of defect-2 inspection under the inspection settings with wedge

centre as the reference point. Direction of scanning is chosen as positive for inspecting defect-1 and negative for inspecting defect-2.

Table.3.8. Parameters of sensitivity zone

X-zone	155 mm
Y-zone	151 mm
Z-zone	171.83 mm
Local Cartesian coordinates (X)	66 mm
Local Cartesian coordinates (Z)	86 mm

✓ Model:

PA2 (Wedge-2) is mounted on the left and right corners of the specimen to perform inspection of defect-1 and defect-2 respectively that is shown in **Fig.3.22 (a)** and **Fig.3.22 (b)**. The transmitted and reflected/scattered ultrasonic waves can be seen. The region covering the test sample as a rectangular box is referred to as sensitivity zone. We shall consider attenuation since real ultrasonic waves get attenuated as they travel in any test sample. So, for this, choose "Power attenuation law" in transversal wave attenuation section in specimen settings.

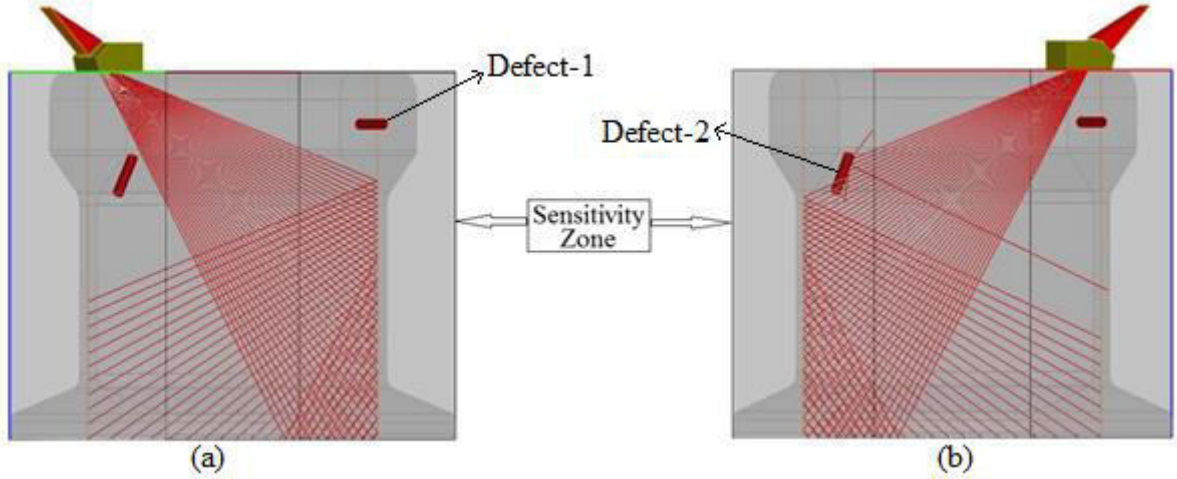

Fig.3.22. Wedge position for inspecting **(a)** defect-1 using PA2 (Wedge-2)
(b) defect-2 using PA2 (Wedge-2)

✓ Results:

From **Fig.3.23 (a)**, it is clearly visible that during the inspection of defect-1, both the defects are identified whereas from **Fig.3.23 (b),** it can be noticed that during the inspection of defect-2, only defect-2 is identified. We can further analyse these defects using S-scan and A-scan results.

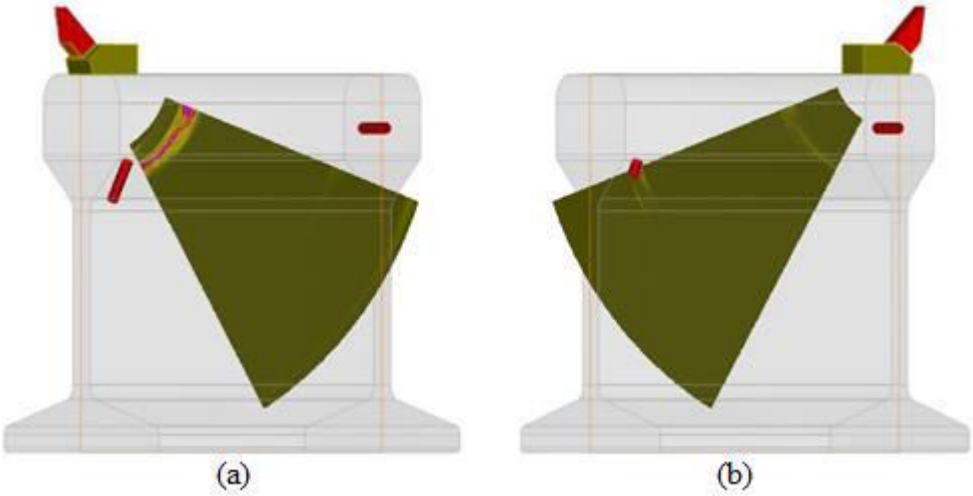

Fig.3.23. 3D image view of the test sample while inspecting **(a)** defect-1 using PA2 (Wedge-2) **(b)** defect-2 using PA2 (Wedge-2)

The resultant S-scans and corresponding A-scans while inspecting defect-1 PA2 (Wedge-2) is shown in **Fig.3.24**. Both the defects are identified here. An echo with very small amplitude indicates defect-1 that is identified at 70° while another echo with moderate amplitude indicates defect-2 that is identified at 30°.

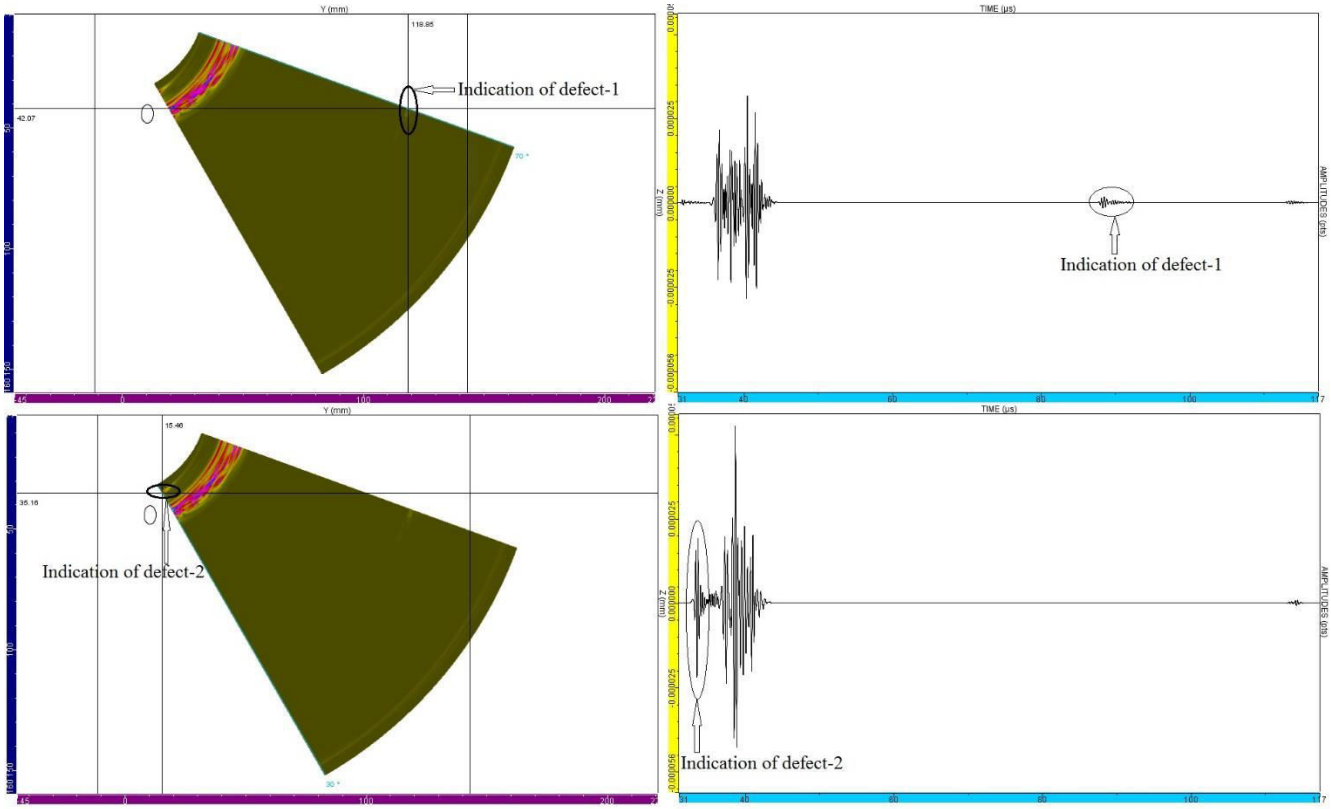

Fig.3.24. S-scan and corresponding A-scan results while inspecting defect-1 using PA2 (Wedge-2)

The resultant S-scan and corresponding A-scan while inspecting defect-2 PA2 (Wedge-2) is shown in **Fig.3.25**. Only defect-2 is identified here at 70° which is an echo with very high amplitude.

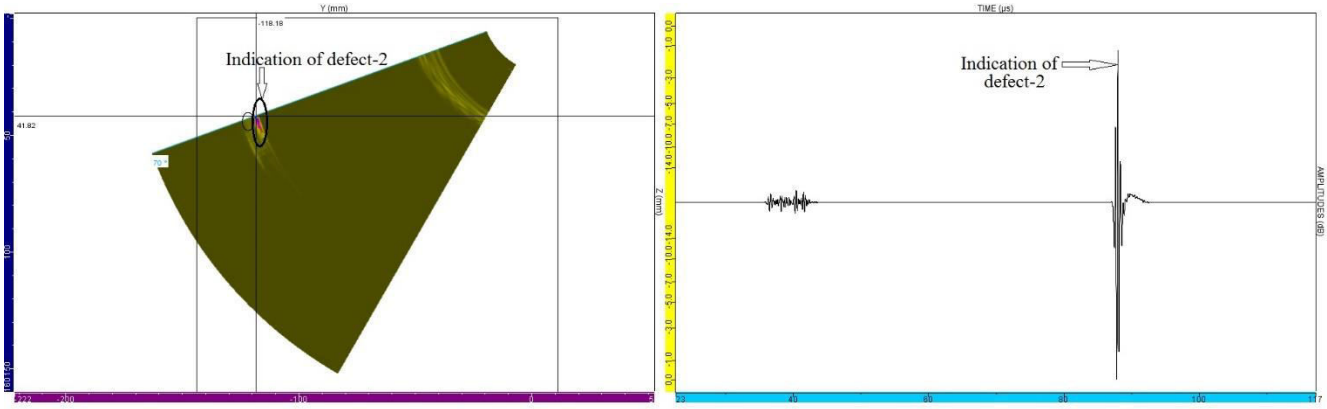

Fig.3.25. S-scan and corresponding A-scan results while inspecting defect-2 using PA2 (Wedge-2)

- Wedge-3:

✓ Parameters:

All the parameters are same as the model used in "Beam computation" module. Here, we use longitudinal waves with nominal refracted beam angle of 60° and 30° to 70° as the sweep. The additional parameters include positioning the wedge; selection of "UNISEQUENTIAL" mode as the scanning method with number of steps as 40 which means scanning is done for every one degree; selection of side and bottom specimen echoes in the interaction part of simulation settings and specification of the sensitivity zone given in **Table.3.9**.

To maintain the wedges at centre in vertical direction and at the corners in horizontal direction, Offset-X is chosen as 77 mm and Offset-Y is chosen as 13 mm in case of defect-1 inspection and as 77 mm and 142 mm in case of defect-2 inspection under the inspection settings with wedge centre as the reference point. Direction of scanning is chosen as positive for inspecting defect-1 and negative for inspecting defect-2.

Table.3.9. Parameters of sensitivity zone

X-zone	155 mm
Y-zone	151 mm
Z-zone	171.83 mm
Local Cartesian coordinates (X)	64.5 mm
Local Cartesian coordinates (Z)	86 mm

✓ Model:

PA2 (Wedge-3) is mounted on the left and right corners of the specimen to perform inspection of defect-1 and defect-2 respectively that is shown in **Fig.3.26 (a)** and **Fig.3.26 (b)**. The transmitted and reflected/scattered ultrasonic waves can be seen. The region covering the test sample as a rectangular box is referred to as sensitivity zone. We shall consider attenuation since real ultrasonic waves get attenuated as they travel in any test sample. So, for this, choose "Power attenuation law" in transversal wave attenuation section in specimen settings.

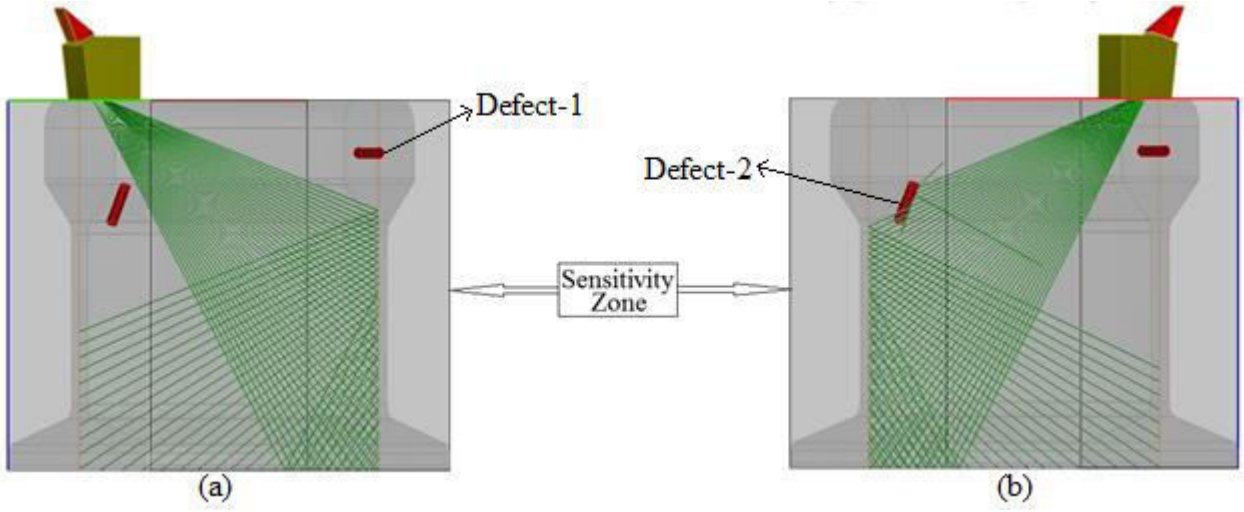

Fig.3.26. Wedge position for inspecting **(a)** defect-1 using PA2 (Wedge-3)
(b) defect-2 using PA2 (Wedge-3)

✓ Results:

From **Fig.3.27 (a)**, it is clearly visible that during the inspection of defect-1, both the defects are identified whereas from **Fig.3.27 (b),** it can be noticed that during the inspection of defect-2, only defect-2 is identified. We can further analyse these defects using S-scan and A-scan results.

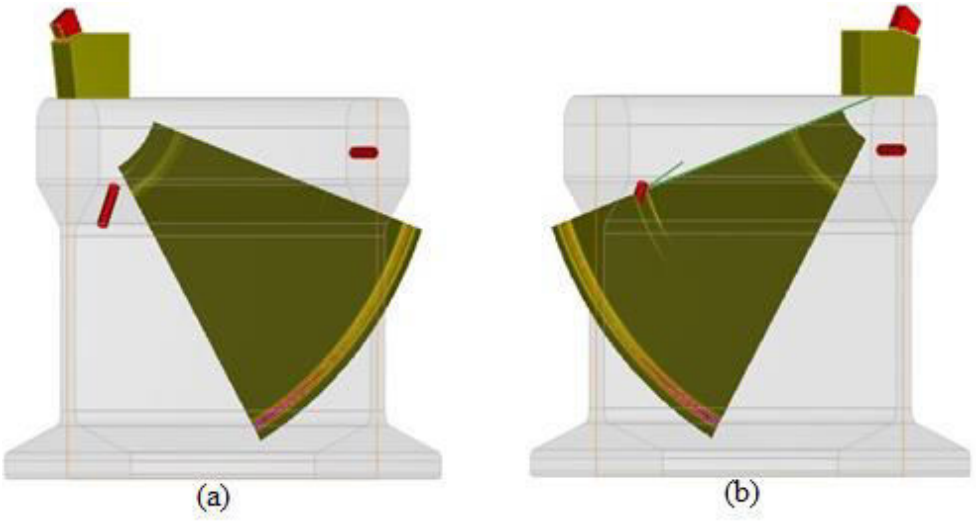

Fig.3.27. 3D image view of the test sample while inspecting **(a)** defect-1 using PA2 (Wedge-3)
(b) defect-2 using PA2 (Wedge-3)

The resultant S-scans and corresponding A-scans while inspecting defect-1 using PA1 is shown in **Fig.3.28**. Both the defects are identified in this case. An echo with very small amplitude indicates defect-1 that is identified at 70° while another echo with moderate amplitude indicates defect-2 that is identified at 30°.

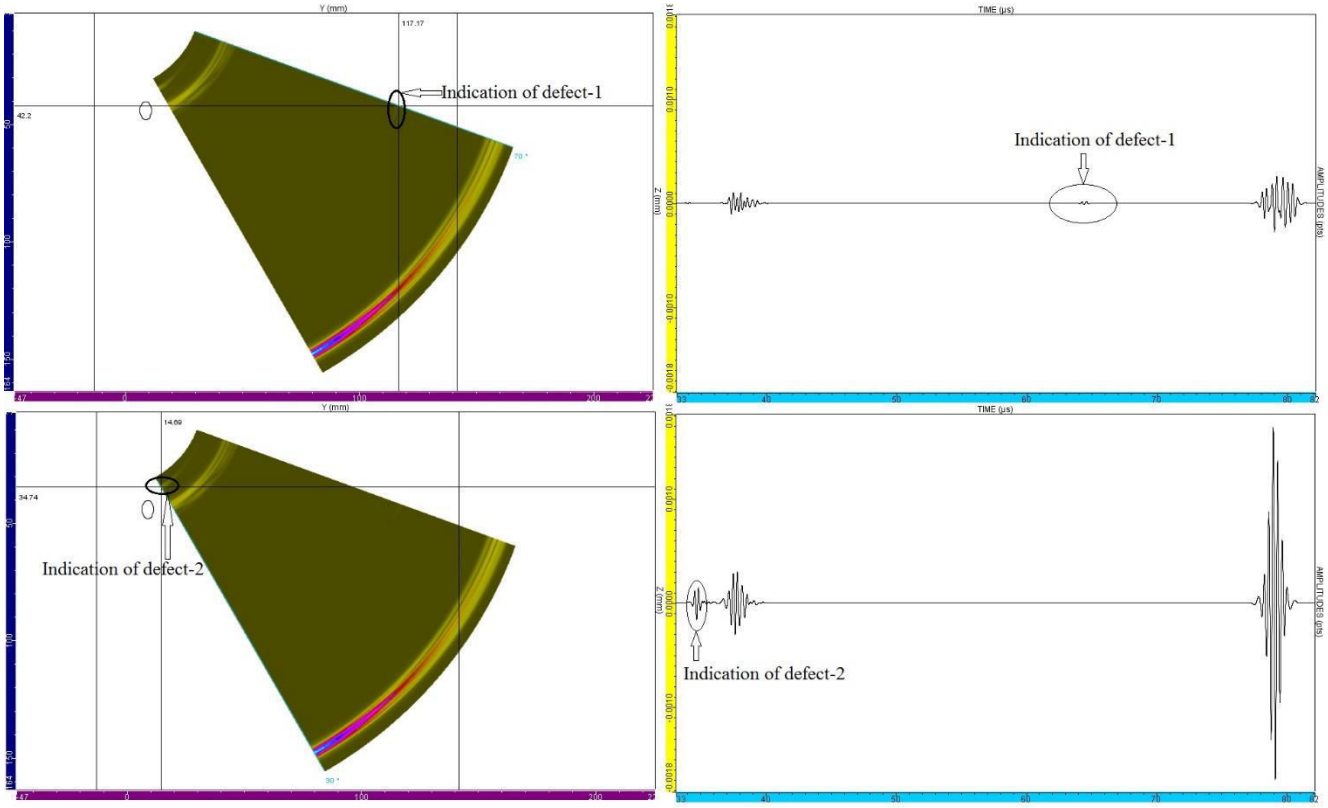

Fig3.28. S-scan and corresponding A-scan results while inspecting defect-1 using PA2 (Wedge-3)

The resultant S-scan and corresponding A-scan while inspecting defect-2 using PA2 (Wedge-3) is shown in **Fig.3.29**. Only defect-2 is identified here at 70° which is an echo with high amplitude.

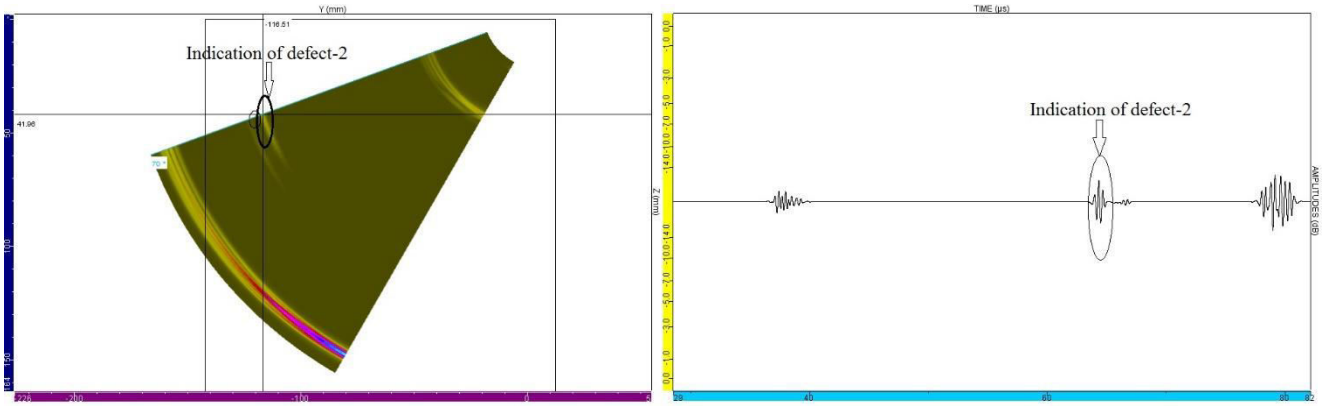

Fig.3.29. S-scan and corresponding A-scan results while inspecting defect-2 using PA2 (Wedge-3)

3.2.3. Calibration of results (Sectorial scanning)

The calibration tab allows us to compare the simulation results with a reference calibration. Here, we shall calibrate the results obtained from inspection of defect-1 and inspection of defect-2 separately. For this purpose, we shall not consider the side and bottom echoes to get clear view of reflections from the defects. Also, sensitivity zone is limited to the respective defect in each case.

- Calibration of results from inspection of defect-1:

PA2 (Wedge-1) configuration that performs inspection along the profile is neglected as it is a totally different case. So, other three cases are considered for calibration that include PA1, PA2 (Wedge-2) and PA2 (Wedge-3) configurations for inspecting defect-1. Choose "Manual" mode in the calibration section of simulation settings. PA1 wedge position has highest amplitude of 0 dB (18.346E-6 points) compared to other two while inspecting defect-1. Hence, the results are calibrated with respect to this amplitude. Models after limiting the sensitivity zone to defect-1 is shown in **Fig.3.30**.

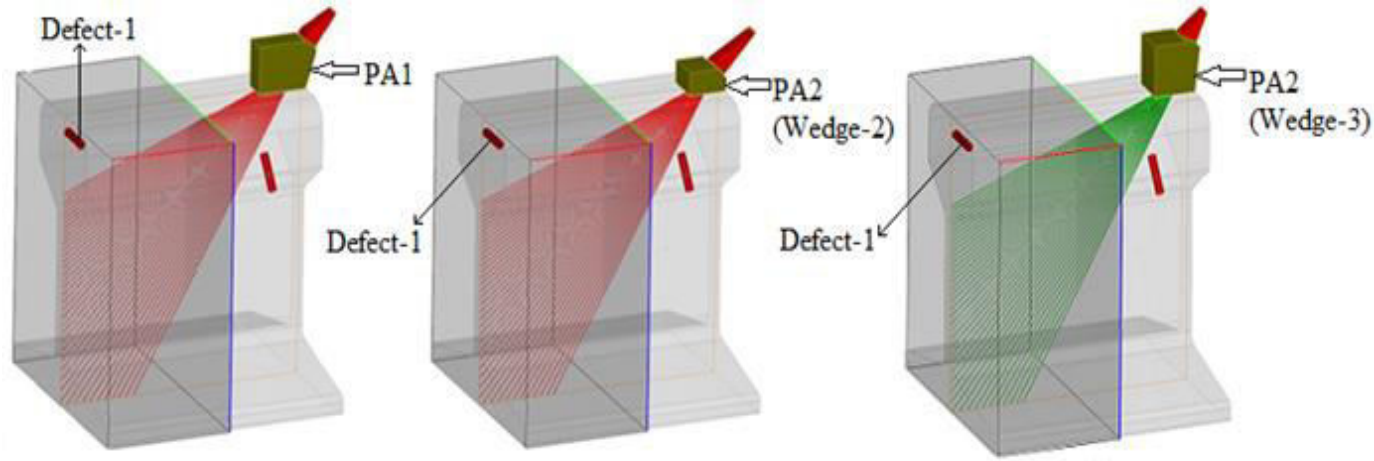

Fig.3.30. Models after limiting sensitivity zone to defect-1 for calibration

The calibrated S-scan and A-scan results while inspecting defect-1 can be seen in **Fig.3.31** where we can observe that PA1 has obtained the highest reflection from defect-1, PA2 (Wedge-2) configuration has obtained quite moderate reflection from defect-1. PA2 (wedge-3) configuration also got reflection which is almost invisible in S-scan but a slight variation can be seen in A-scan that indicates the presence of defect-1 in the test sample.

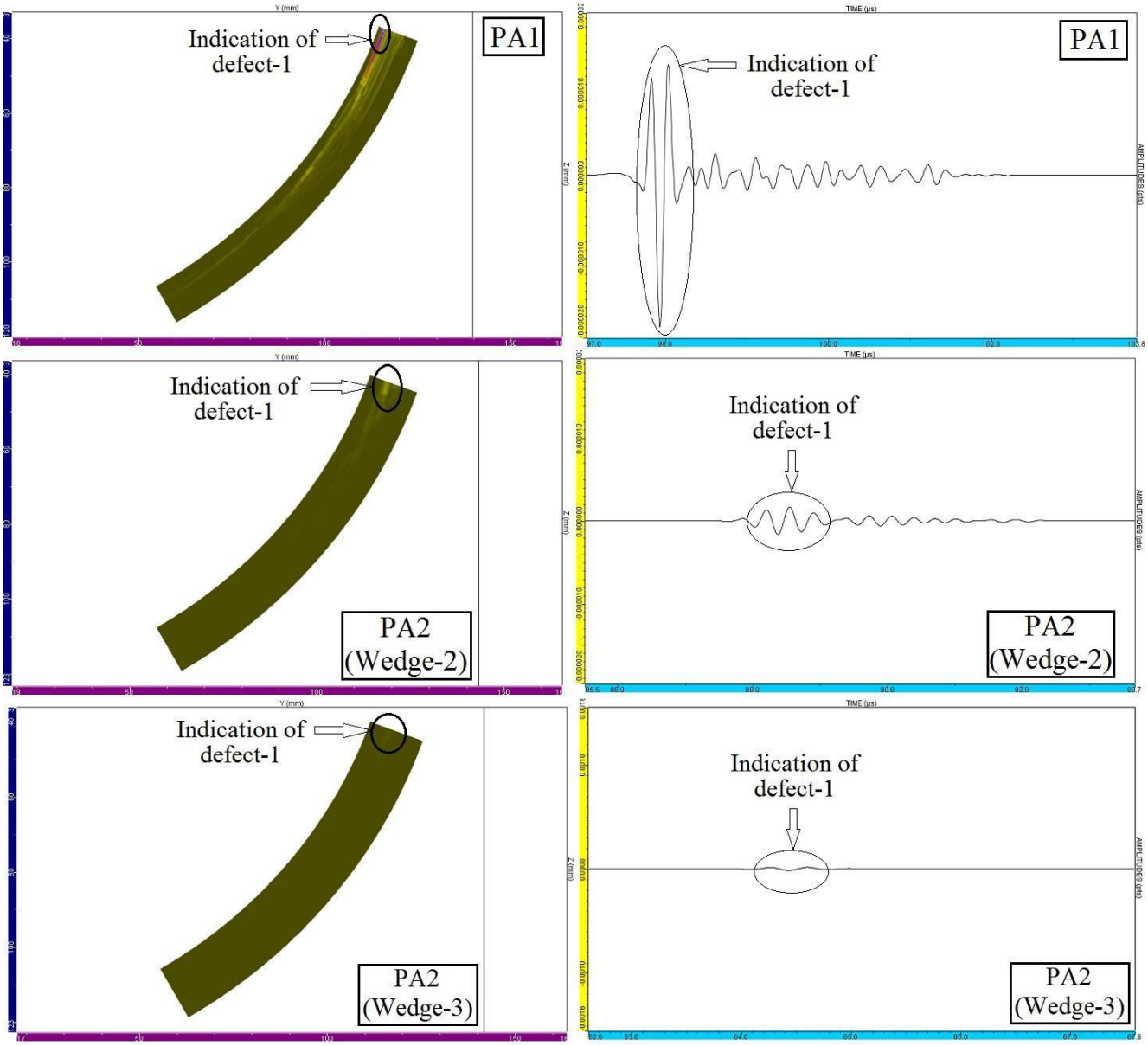

Fig.3.31. Calibrated results for inspection of defect-1

- Calibration of results from inspection of defect-2:

PA2 (Wedge-1) configuration that performs inspection along the profile is neglected as it is a totally different case. So, other three cases are considered for calibration that include PA1, PA2 (Wedge-2) and PA2 (Wedge-3) configurations for inspecting defect-2. Choose "Manual" mode in the calibration section of simulation settings. PA1 wedge position has highest amplitude of 0 dB (1.6936E-3 points) compared to other two while inspecting defect-2. Hence, the results are calibrated with respect to this amplitude. Models after limiting the sensitivity zone to defect-2 is shown in **Fig.3.32**. The calibrated S-scan and A-scan results while inspecting defect-2 can be seen in **Fig.3.33** where we can observe that PA1 has obtained the highest reflection from defect-2, PA2 (Wedge-2) configuration has obtained moderate reflection from defect-2 and PA2 (Wedge-2) configuration has obtained lowest reflection from defect-2.

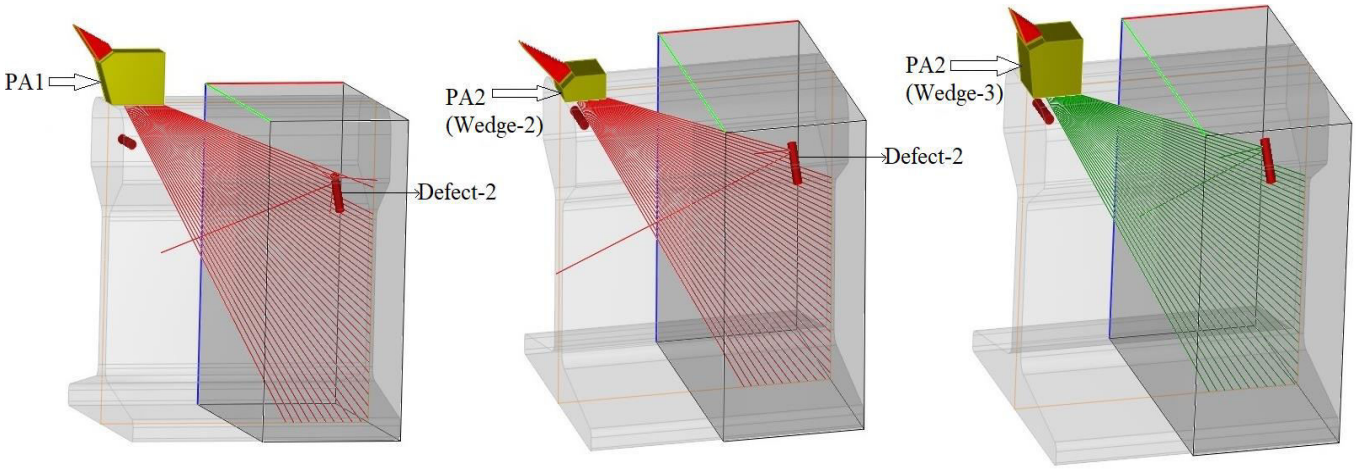

Fig.3.32. Models after limiting the sensitivity zone to defect-2 for calibration

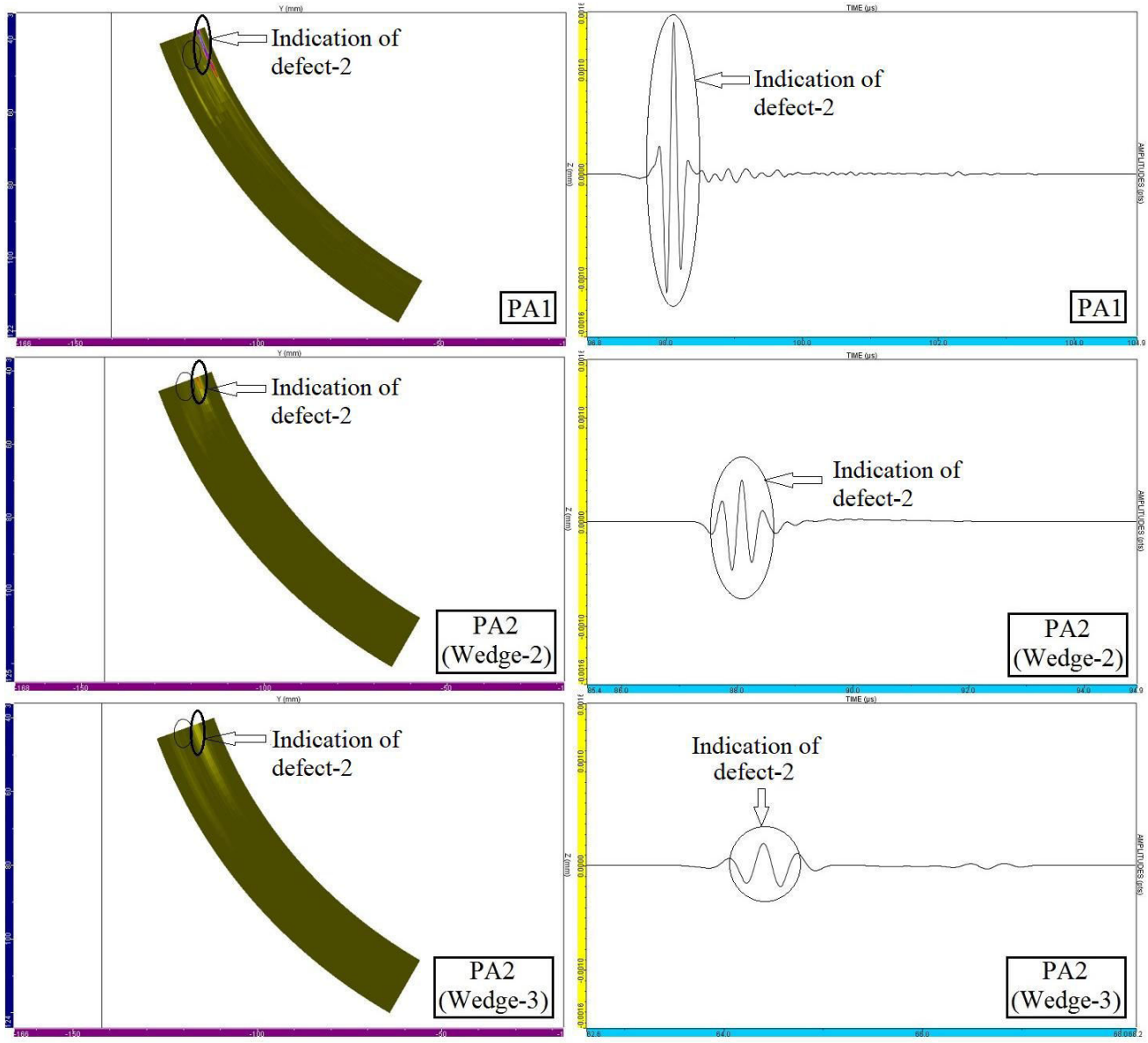

Fig.3.33. Calibrated results for inspection of defect-2

3.3.Inspection of defects in the test sample using Multi-point focusing

Here, we shall implement "Multi-point focusing" as the transmission technique and move the wedge near each one of the defect accordingly.

3.3.1. Inspection of defect-1 in the test sample using PA1 (Multi-point focusing)

Table.3.10 gives multi-point focusing settings for inspecting defect-1 where extremity number-1 refers to the first point's position along X-axis and Z-axis; extremity number-2 refers to the last point's position along X-axis and Z-axis; number of steps indicates the total number of points in an aligned manner. Apart from these settings, the wedge parameter (offset Y) and the sensitivity zone parameters must be changed as per the desired wedge position.

Table.3.10. Multi-point focusing settings for inspecting defect-1

Points	Aligned
Extremity Number-1	X: Varies as per the wedge position Z: 10 mm
Extremity Number-2	X: Varies as per the wedge position Z: 50 mm
Number of steps	40

PA1 which uses shear waves at a refracted angle of 45° operating at frequency of 5 MHz showed better results compared to the PA2. So, we shall consider PA1 for further inspection of defect-1. For this, six different wedge positions are considered which starts from the corner and moves towards the defect. The positions of the wedge for inspecting defect-1 are given in **Table.3.11**.

Table.3.11. Wedge positions for inspecting defect-1

Position Number	**Distance moved**	**Extremity-1&2 (X)**	**Abs. Max. Amplitude**
1	0 mm (Initial)	122	-20.5 dB (3.370E-6 points)
2	30 mm	92	-13.5 dB (7.478E-6 points)
3	50 mm	72	-8.8 dB (13.378E-6 points)
4	70 mm	52	-3.2 dB (24.421E-6 points)
5	90 mm	32	0 dB (35.234E-6 points)
6	100 mm	22	-0.6 dB (32.813E-6 points)

Various positions of PA1 used for inspecting defect-1 is shown in **Fig.3.34** where the multiple points can be seen as blue dots and seems to be a straight line as the points are aligned.

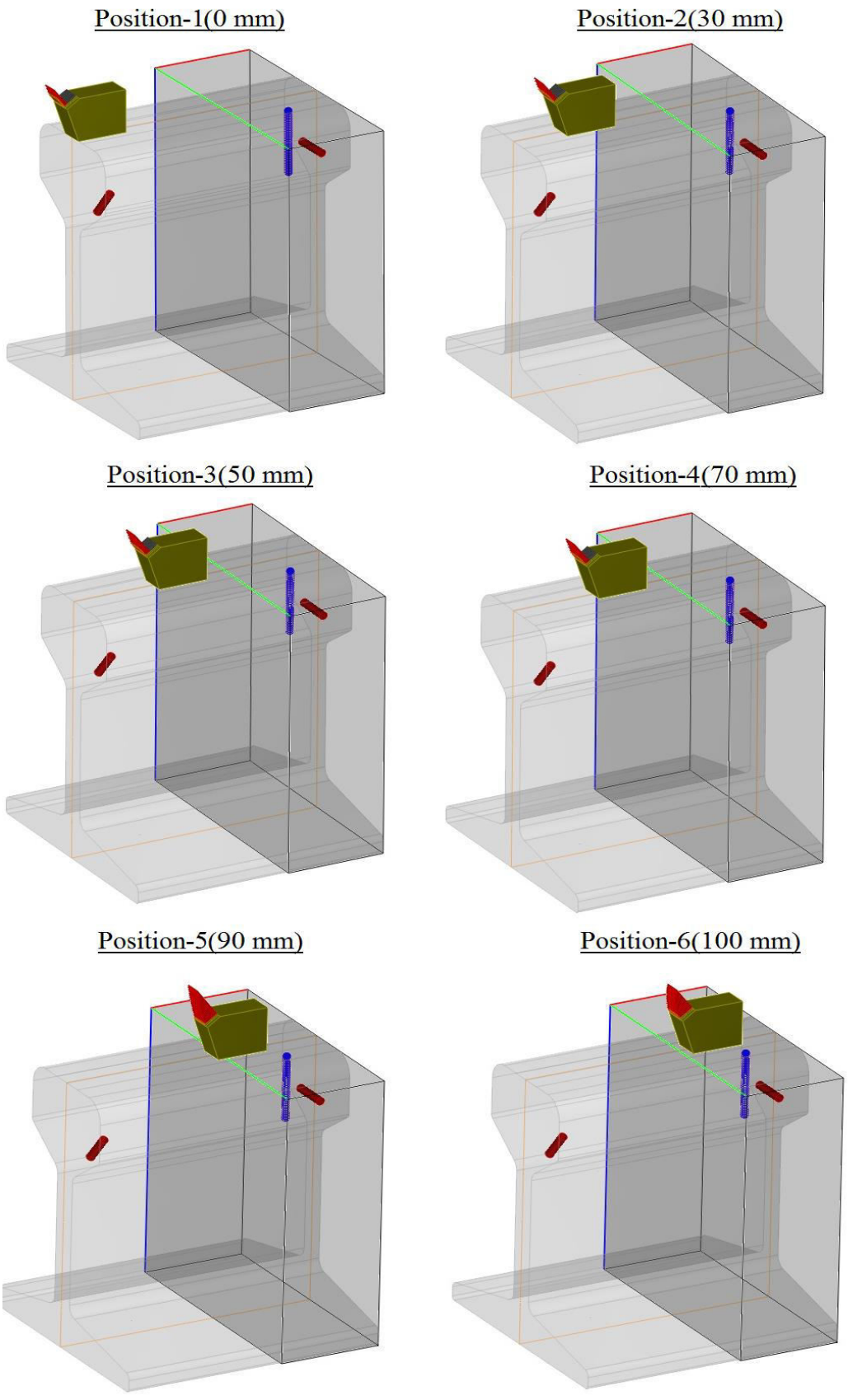

Fig.3.34. Various positions of PA1 used for inspecting defect-1

From **Fig.3.35**, we can observe that as the wedge is moved towards the defect-1, the amplitude of reflections from defect-1 kept increased. At wedge position-5 i.e. 90 mm from the left corner, the maximum amplitude is obtained. Later, at position-6 i.e. 100 mm from the left corner, slight reduction in amplitude can be observed.

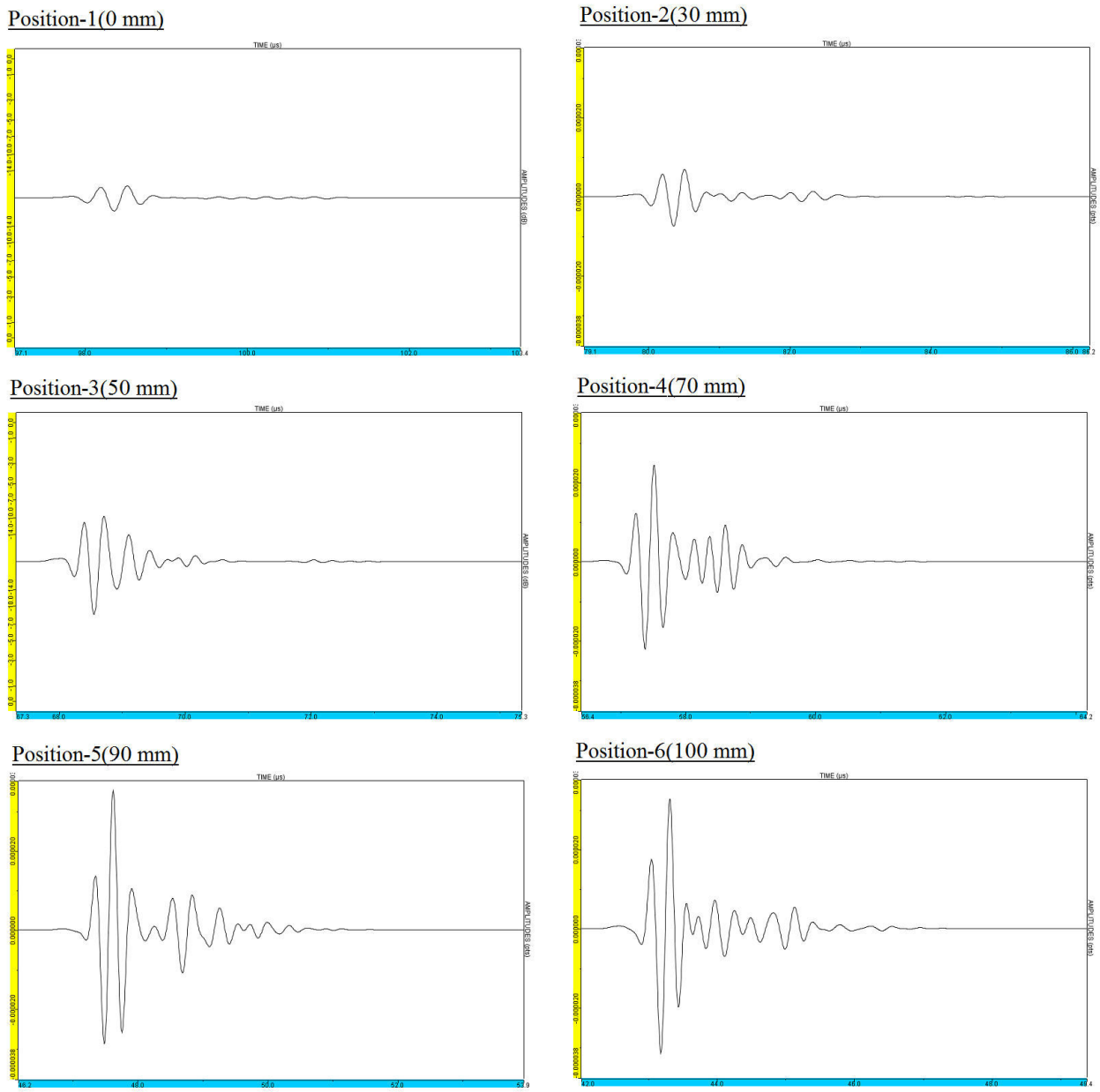

Fig.3.35. Calibrated A-scan results at each wedge position when inspecting defect-1

From **Fig.3.36**, we can observe that as the wedge is moved towards the defect-1, the indications of reflections from defect-1 kept increased. At wedge position-5 i.e. 90 mm from the left corner, the brightest indication is obtained. Later, at position-6 i.e. 100 mm from the left corner, brightness of the indication can be seen reduced a little.

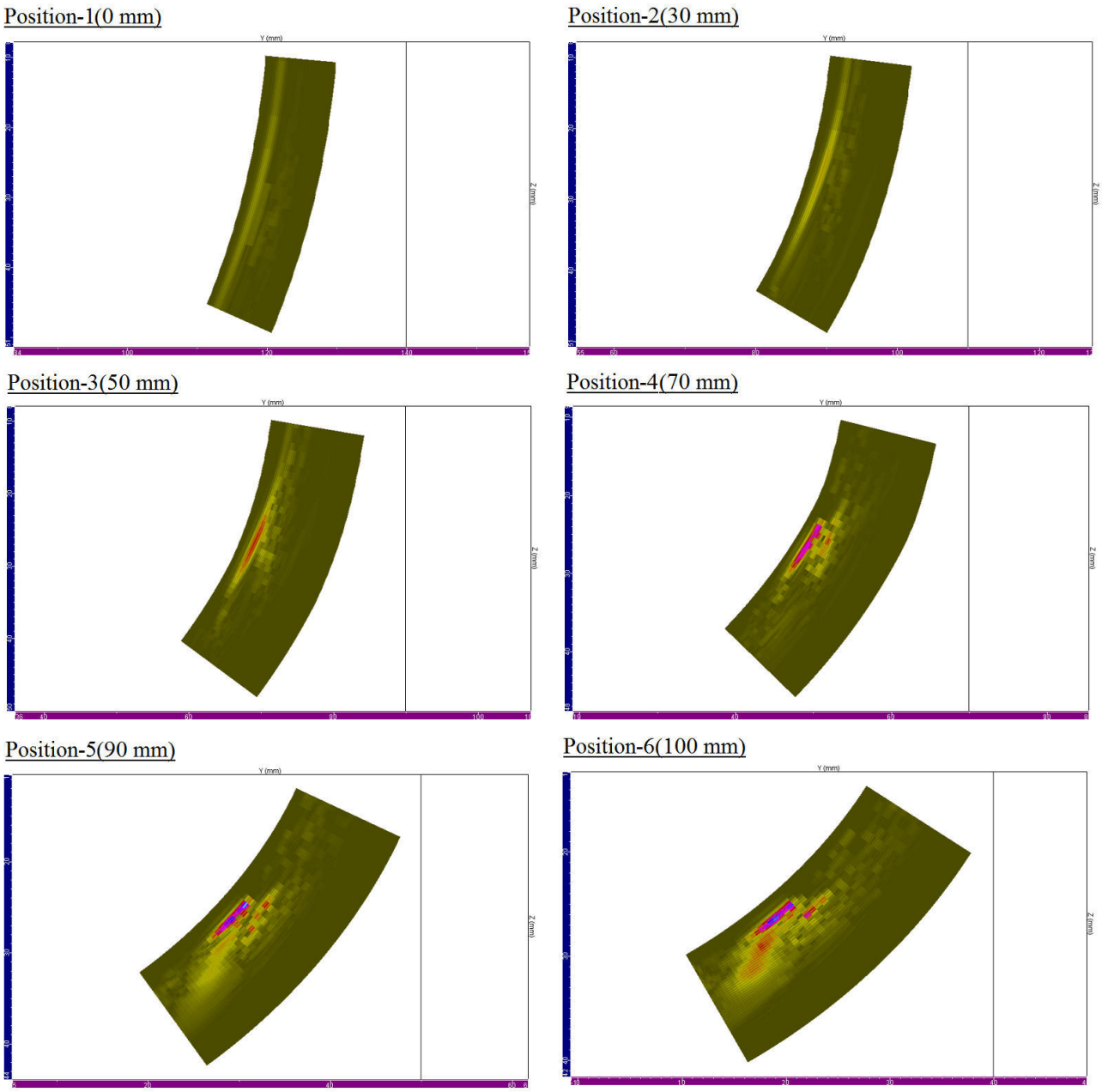

Fig.3.36. Calibrated S-scan results at each wedge position when inspecting defect-1

3.3.2. Inspection of defect-2 in the test sample using PA1 (Multi-point focusing)

Table.3.12 gives multi-point focusing settings for inspecting defect-2 where extremity number-1 refers to the first point's position along X-axis and Z-axis; extremity number-2 refers to the last point's position along X-axis and Z-axis; number of steps indicates the total number of points in an aligned manner.

Table.3.12. Multi-point focusing settings for inspecting defect-2

Points	Aligned
Extremity Number-1	X: Varies as per the wedge position Z: 30 mm
Extremity Number-2	X: Varies as per the wedge position Z: 70 mm
Number of steps	40

Apart from these settings, the wedge parameter (offset Y) and the sensitivity zone parameters must be changed as per the desired wedge position. PA1 which uses shear waves at a refracted angle of 45° operating at frequency of 5 MHz showed better results compared to the other Phased Array i.e. PA2. So, we shall consider PA1 for further inspection of defect-2. For this, six different wedge positions are considered which starts from the corner and moves towards the defect. The positions of the wedge for inspecting defect-2 are given in **Table.3.13**.

Table.3.13. Wedge positions for inspecting defect-2

Position Number	**Distance moved**	**Extremity-1&2 (X)**	**Abs. Max. Amplitude**
1	0 mm (Initial)	118	-13.4 dB (1.4613E-3 points)
2	20 mm	98	-7.3 dB (2.9552E-3 points)
3	40 mm	78	-3.3 dB (4.6851E-3 points)
4	60 mm	58	-1.9 dB (5.5321E-3 points)
5	80 mm	38	0 dB (6.8598E-3 points)
6	90 mm	28	-0.3 dB (6.6600E-3 points)

Various positions of PA1 used for inspecting defect-2 is shown in **Fig.3.37** where the multiple points can be seen as blue dots and seems to be a straight line as the points are aligned.

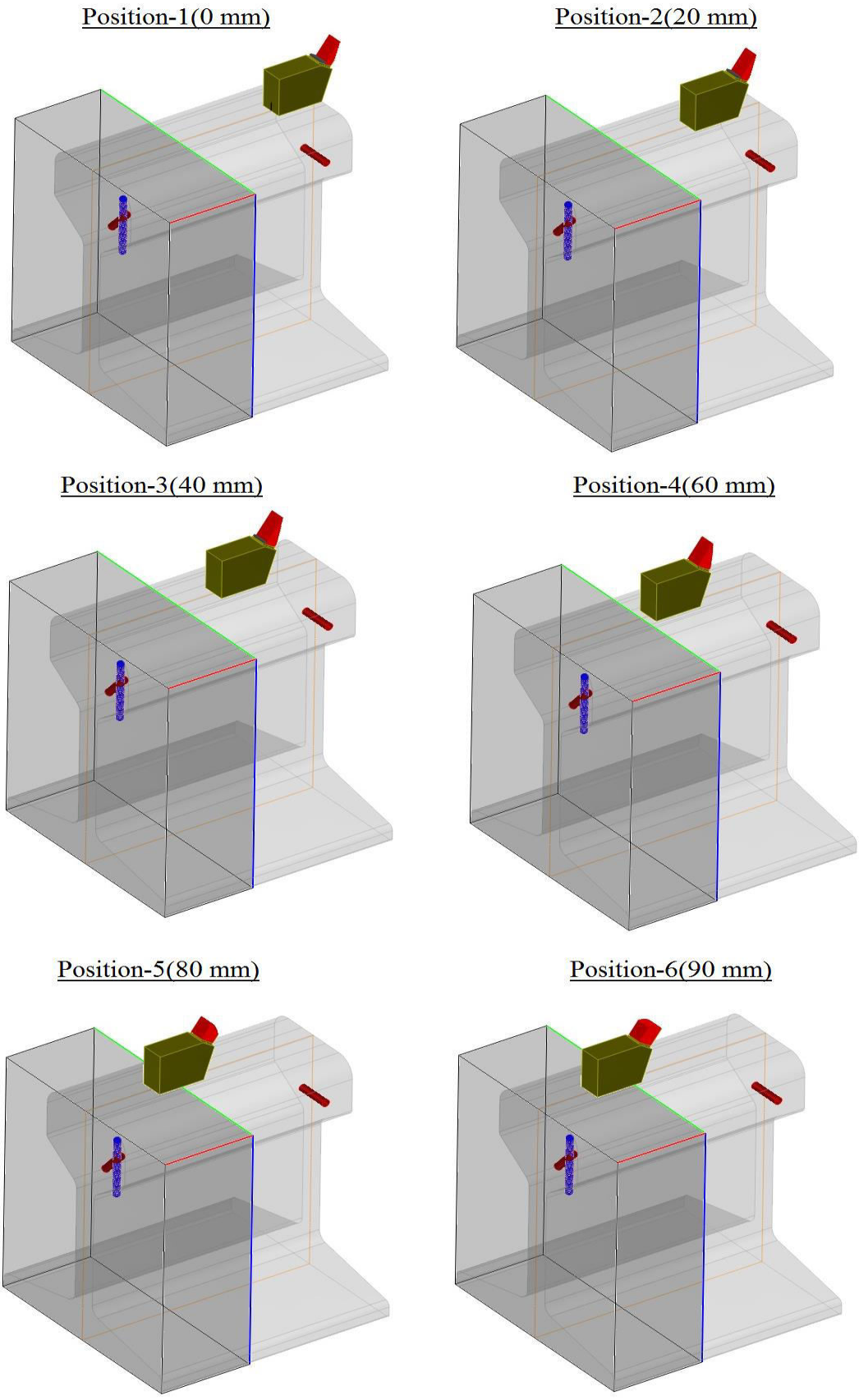

Fig.3.37. Various wedge positions used for inspecting defect-2

From **Fig.3.38**, we can observe that as the wedge is moved towards the defect-2, the amplitude of reflections from defect-2 kept increased. At wedge position-5 i.e. 80 mm from the left corner, the maximum amplitude is obtained. Later, at position-6 i.e. 90 mm from the left corner, the amplitude can be seen reduced a little.

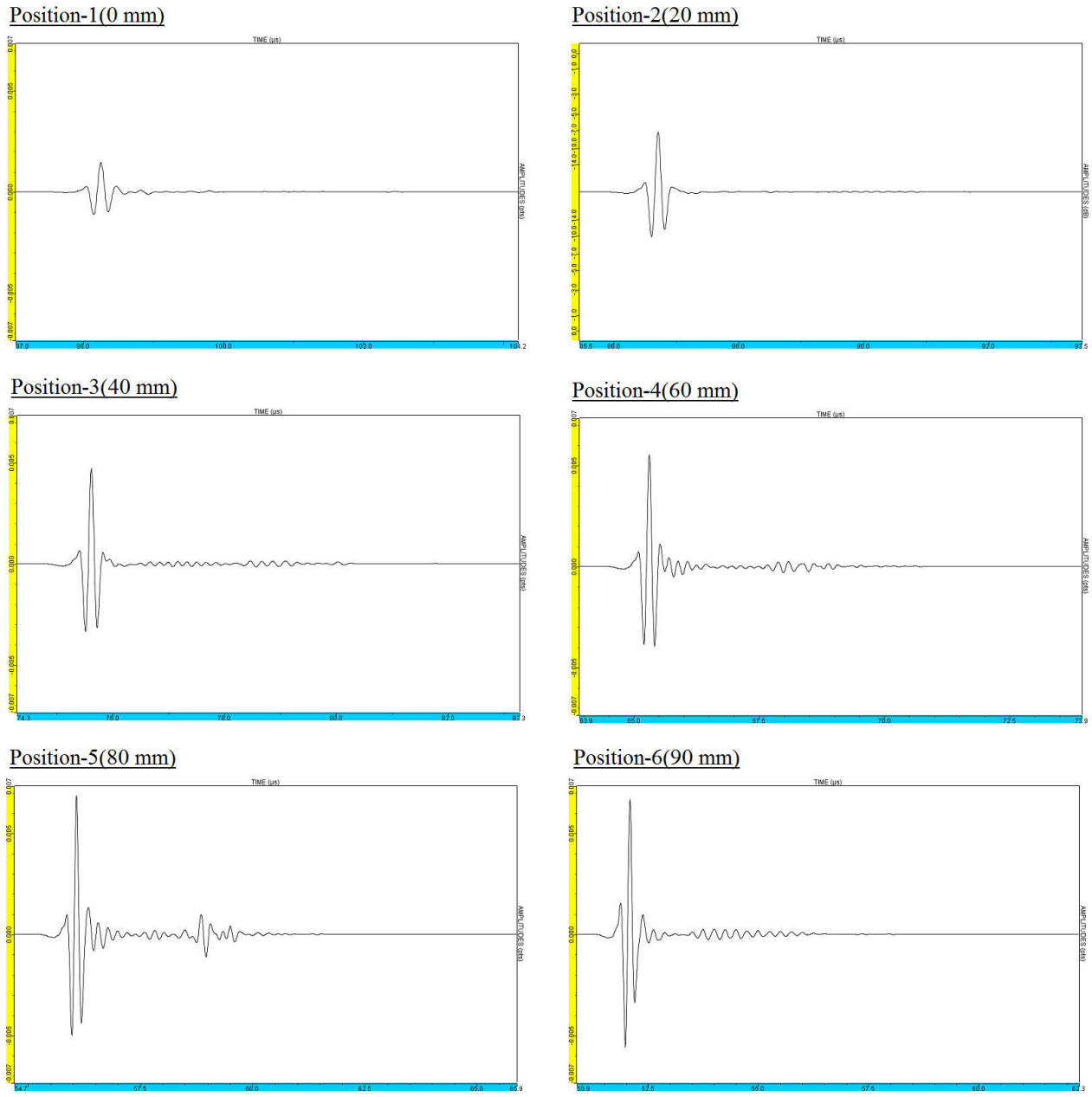

Fig.3.38. Calibrated A-scan results at each wedge position when inspecting defect-2

From **Fig.3.39**, we can observe that as the wedge is moved towards the defect-2, the indications of reflections from defect-2 kept increased. At wedge position-5 i.e. 80 mm from the left corner, the brightest indication is obtained. Later, at position-6 i.e. 90 mm from the left corner, brightness of the indication can be seen reduced a little.

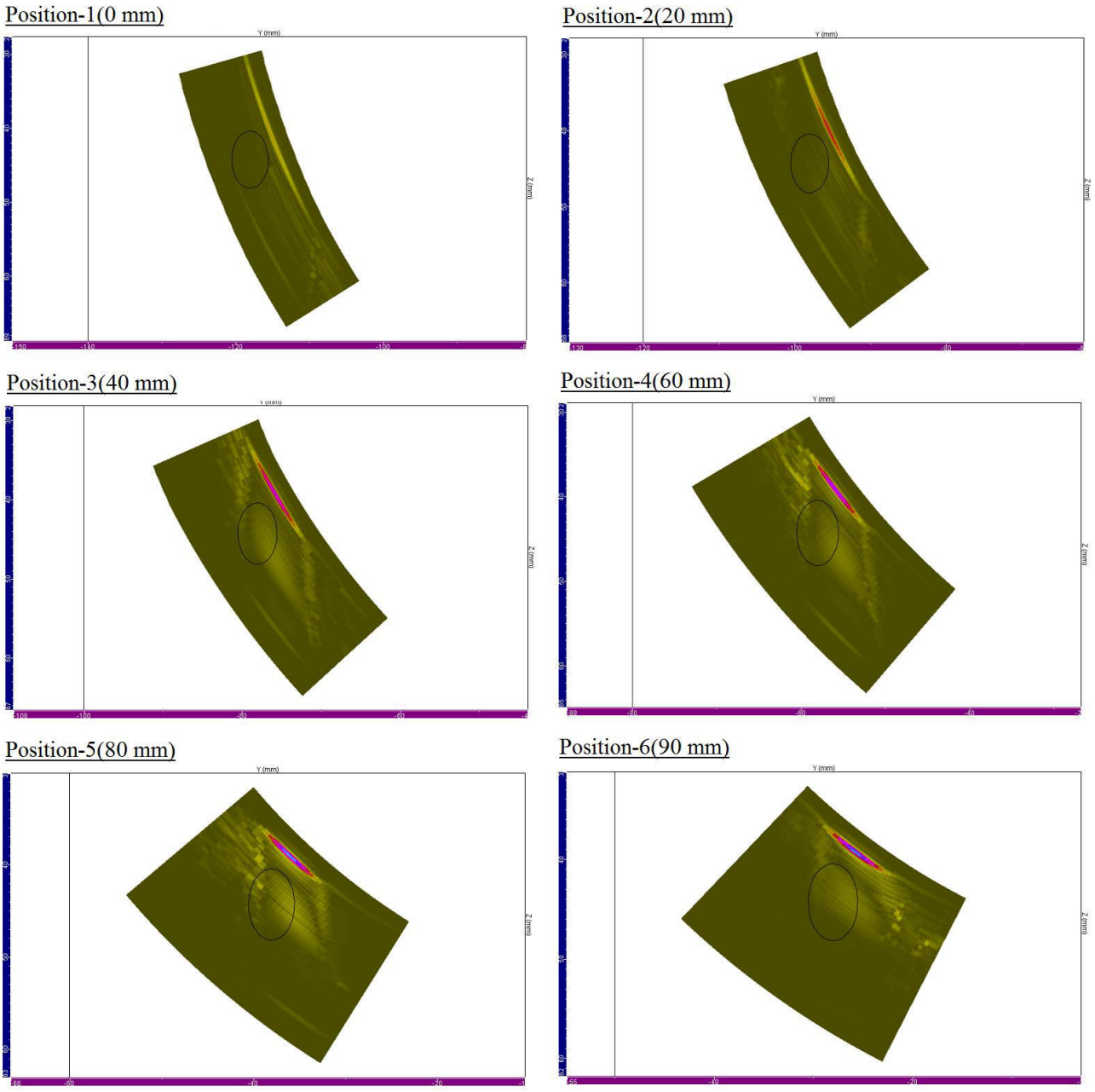

Fig.3.39. Calibrated S-scan results at each wedge position when inspecting defect-2

3.4.Conclusions

Here by I conclude that the ultrasonic beams were modelled with the given two types of phased arrays i.e. PA1 and PA2. PA2 (Wedge-1) configuration showed a steady beam intensity both in the near field and far field compared to other phased array configurations. Coming to the inspection part, PA2 (Wedge-1) configuration has detected both the defects when it was positioned right above the defects. From the calibrated results, we can say that PA1 which used shear waves at a refracted angle of 45° has a highest amplitude of 0 dB compared to PA2 (Wedge-2&3) configurations that had negative amplitudes. Up on observing the results of multi-point focusing, we can say that both the defects were identified when PA1 was positioned close to them. In case of inspecting defect-1, the optimal position was 90 mm towards it with highest amplitude of 0 dB and for inspecting defect-2, the optimal position was 80 mm towards it with highest amplitude of 0 dB as well. When PA1 was moved further beyond the optimal positions, it resulted in negative amplitude.

4. Experimental Analysis

Here, we shall analyse the two Phased Arrays i.e. PA1 and PA2 that were used for computer modelling (CIVA software). For this purpose, OMNISCAN^{MX} manufactured by OLYMPUS is used. The dimensions of test sample and the location of defects in it were already discussed in section 2. The parameters for inspecting both the defects experimentally are given in **Table.4.1**.

Table.4.1. Important parameters for inspection of defects using different phased arrays

Phased Array	Ultrasonic wave type	Velocity (m/s)	Minimum angle (degrees)	Maximum angle (degrees)
PA1	SW	3240	30	70
PA2 (Wedge-1)	LW	5890	-30	+30
PA2 (Wedge-1)	SW	3240	30	70
PA2 (Wedge-3)	LW	5890	30	70

4.1.Inspection of defects in the test sample using Phased Array-1 (PA1)

PA1 uses shear waves at a refracted angle of 45° and operates at a frequency of 5 MHz. The probe number given by OLYMPUS is "5L16-9.6x10-45SW-P-2.5-HY" which contains an integrated wedge with it. Hence, there is no need to use an external wedge.

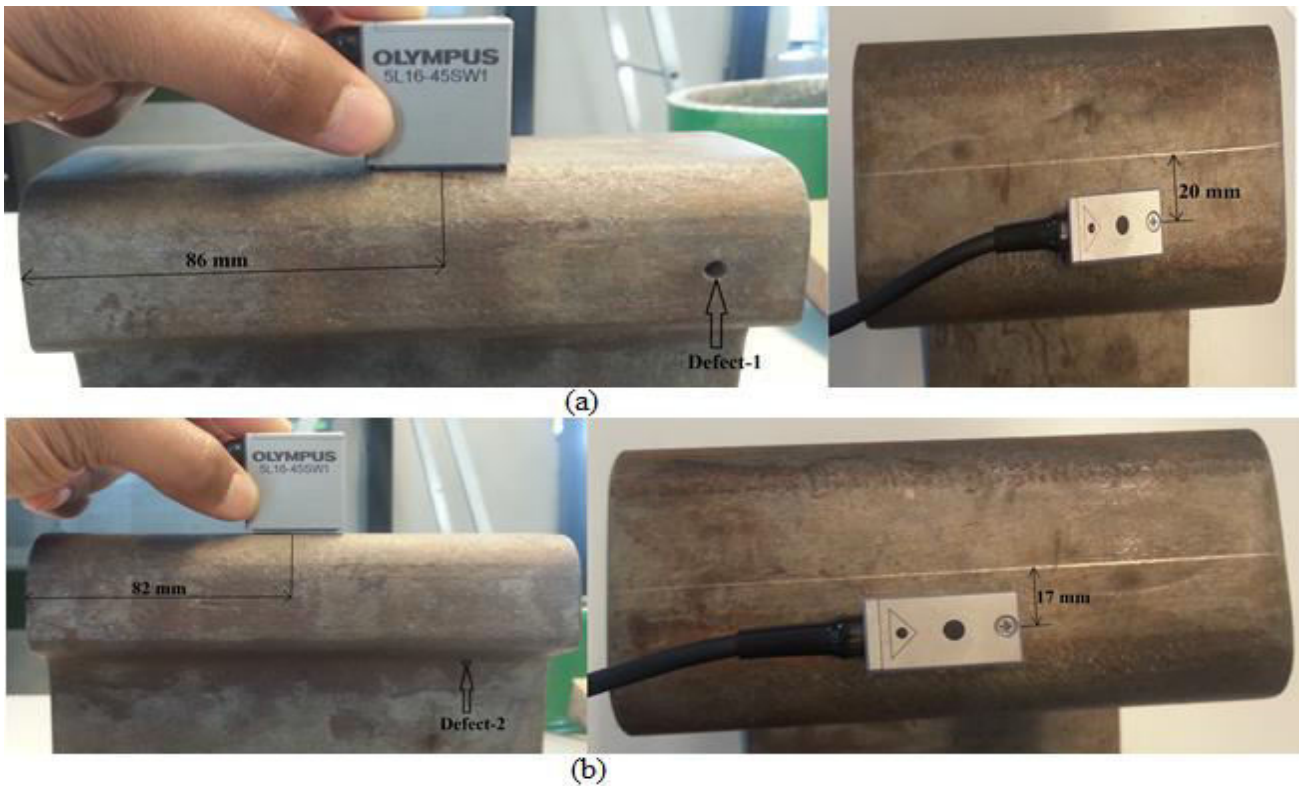

Fig.4.1. Position of PA1 on the test sample **(a)** for inspecting defect-1 **(b)** for inspecting defect-2

From **Fig.4.1 (a)**, it is clearly shown that the wedge is placed 86 mm towards the defect-1 from left corner and it is positioned 20 mm away from the center for the inspection of defect-1. Similarly, wedge is placed 82 mm towards the defect-2 from left corner and it is positioned 17 mm away from the center for the inspection of defect-2 which is shown in **Fig.4.1 (b)**.

From **Fig.4.2**, the indication of defect-1 is clearly visible at 66°. Similarly, from **Fig.4.3**, the indication of defect-2 is clearly visible at 51°. Other echoes might be resulting from front, side or back walls of the test sample.

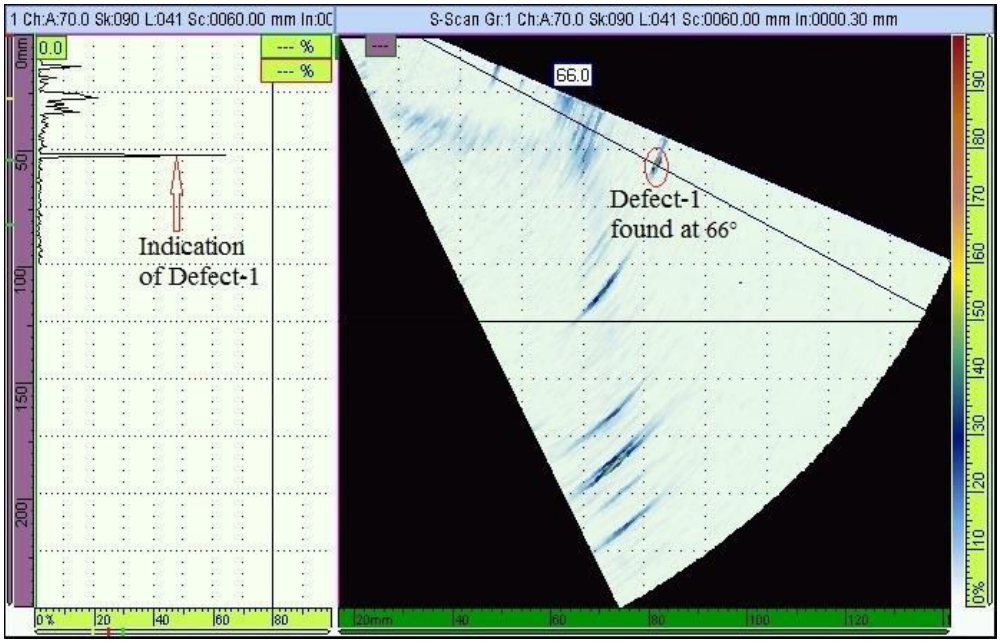

Fig.4.2. S-scan image for inspection of defect-1 using PA1

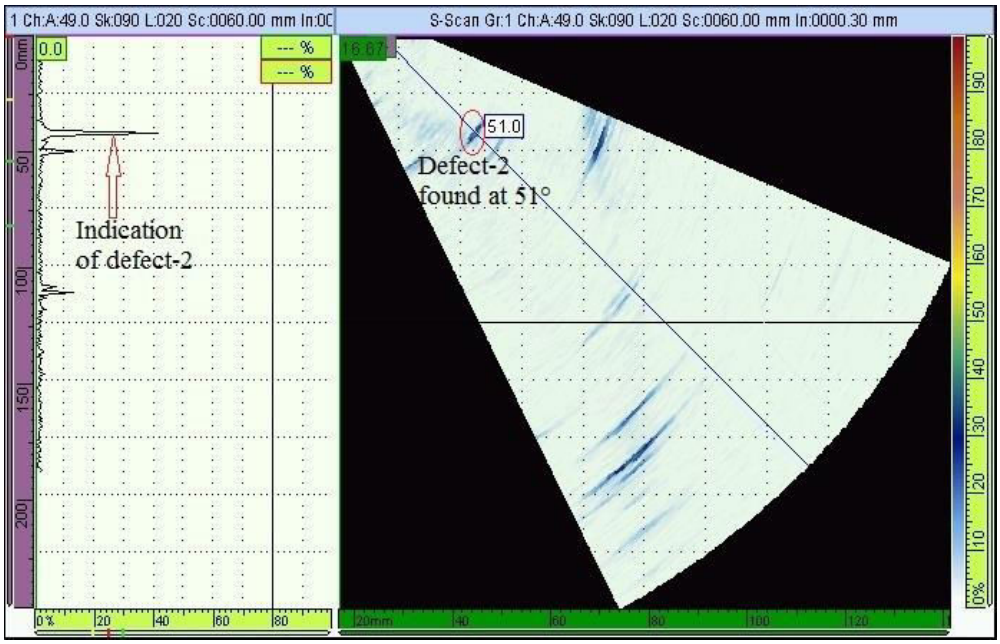

Fig.4.3. S-scan image for inspection of defect-2 using PA1

4.2.Inspection of defects in the test sample using Phased Array-2 (PA2)

- Wedge-1:

PA2 (wedge-1) uses longitudinal waves at a refracted angle of 0° and operates at a frequency of 5 MHz. The probe number given by OLYMPUS is "5L16-9.6x10-A10-P-2.5-HY" and the wedge number is "SA10-0L".

From **Fig.4.4 (a)**, it is clearly shown that the wedge is placed 138 mm towards the defect-1 from left corner and it is positioned 14 mm away from the center for the inspection of defect-1. Similarly, wedge is placed 130 mm towards the defect-2 from left corner and it is positioned at the center for the inspection of defect-2 which is shown in **Fig.4.4 (b)**.

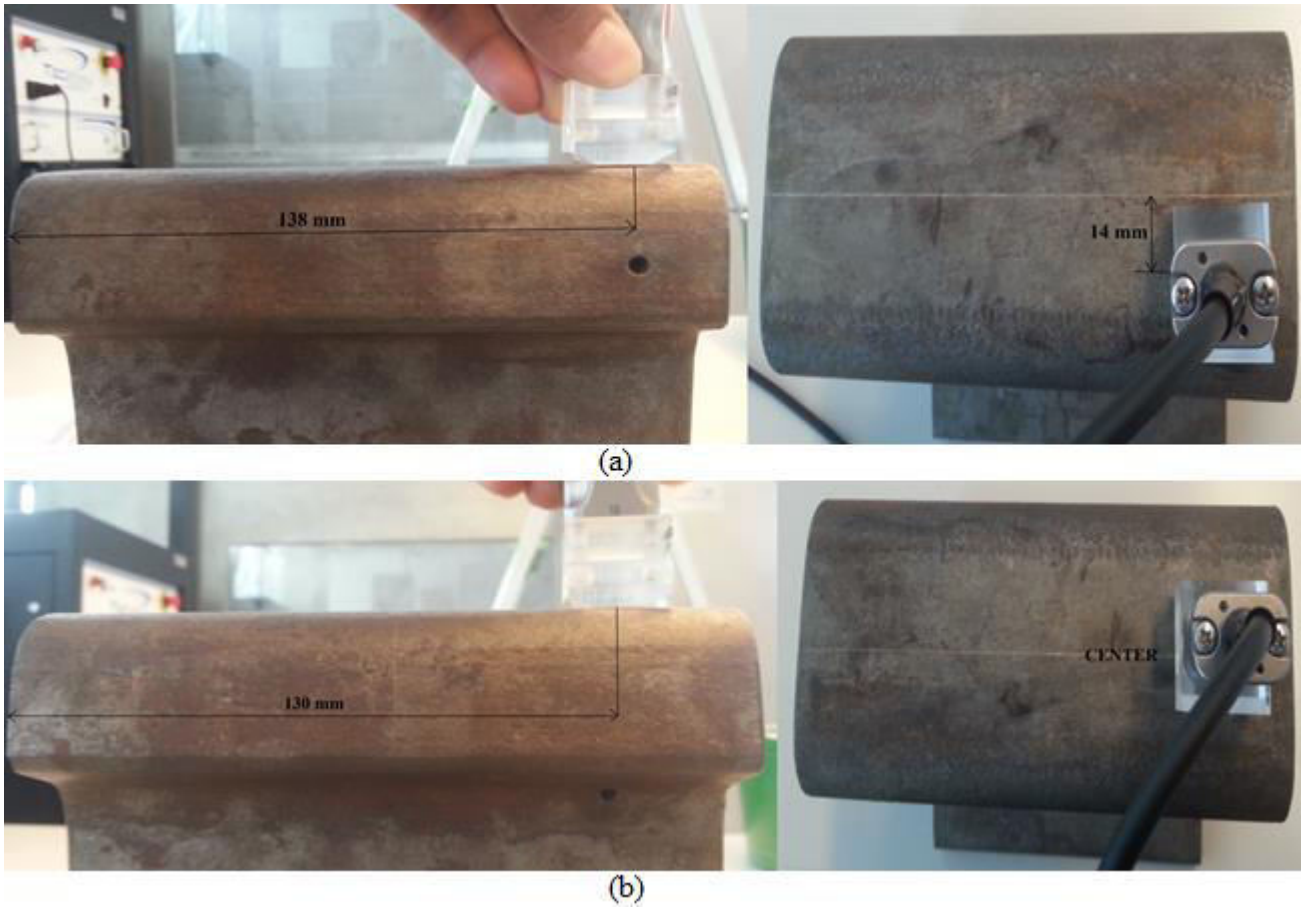

Fig.4.4. Position of PA2 (Wedge-1) on the test sample **(a)** for inspecting defect-1 **(b)** for inspecting defect-2

From **Fig.4.5**, the indication of defect-1 is clearly visible at 4°. Similarly, from **Fig.4.6**, the indication of defect-2 is clearly visible at -1°. Other echoes might be resulting from front, side or back walls of the test sample.

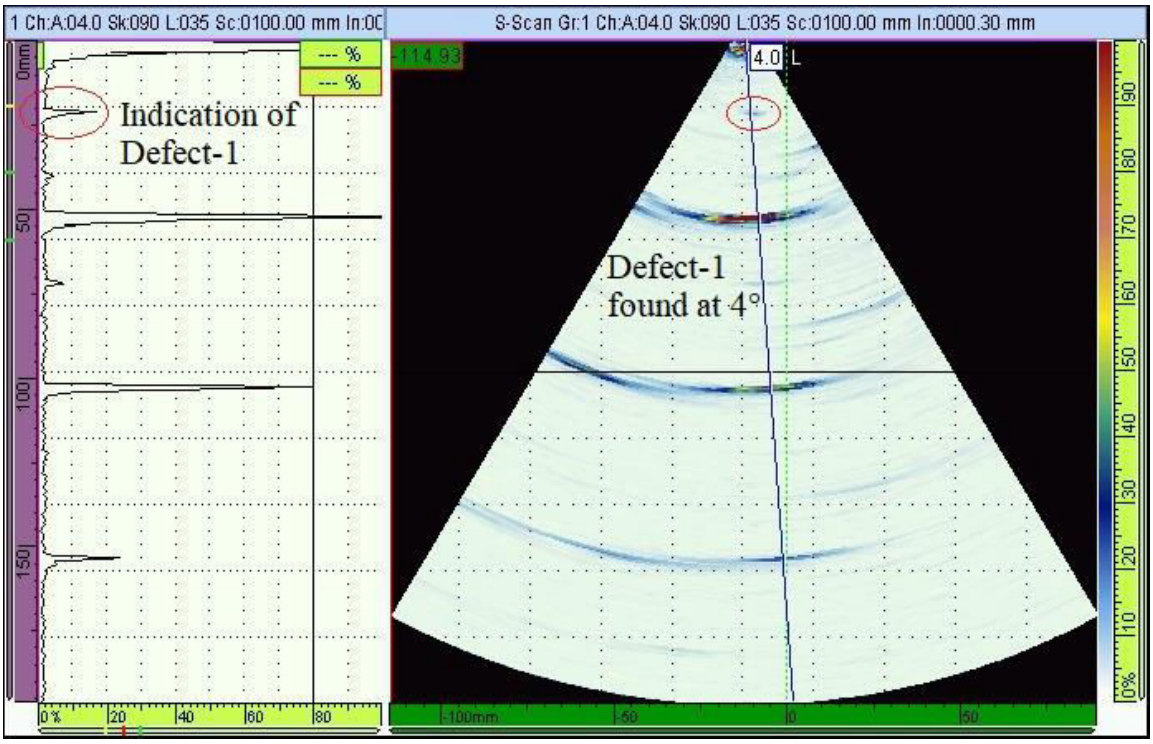

Fig.4.5. S-scan image for inspection of defect-1 using PA2 (Wedge-1)

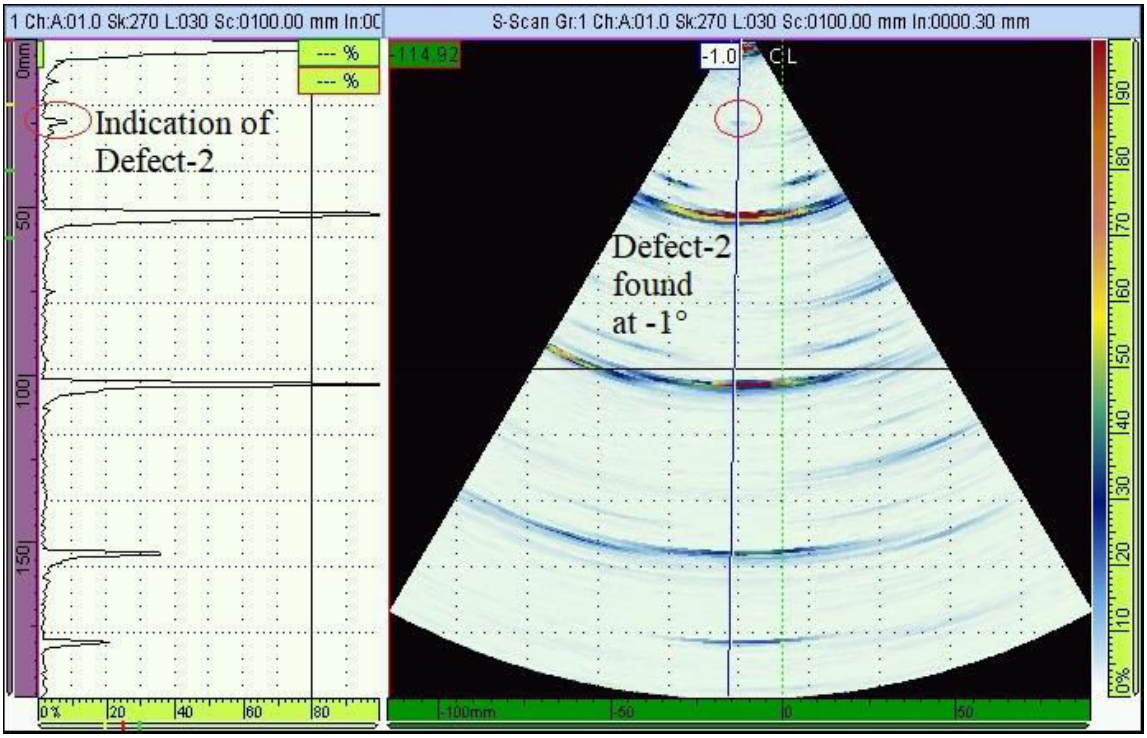

Fig.4.6. S-scan image for inspection of defect-2 using PA2 (Wedge-1)

- Wedge-2:

PA2 (wedge-2) uses shear waves at a refracted angle of 55° and operates at a frequency of 5 MHz. The probe number given by OLYMPUS is "5L16-9.6x10-A10-P-2.5-HY" and the wedge number is "SA10-N55S".

From **Fig.4.7 (a)**, it is clearly shown that the wedge is placed 51 mm towards the defect-1 from left corner and it is positioned 20 mm away from the center for the inspection of defect-1. Similarly, wedge is placed 63 mm towards the defect-2 from left corner and it is positioned 17 mm away from the center for the inspection of defect-2 which is shown in **Fig.4.7 (b)**.

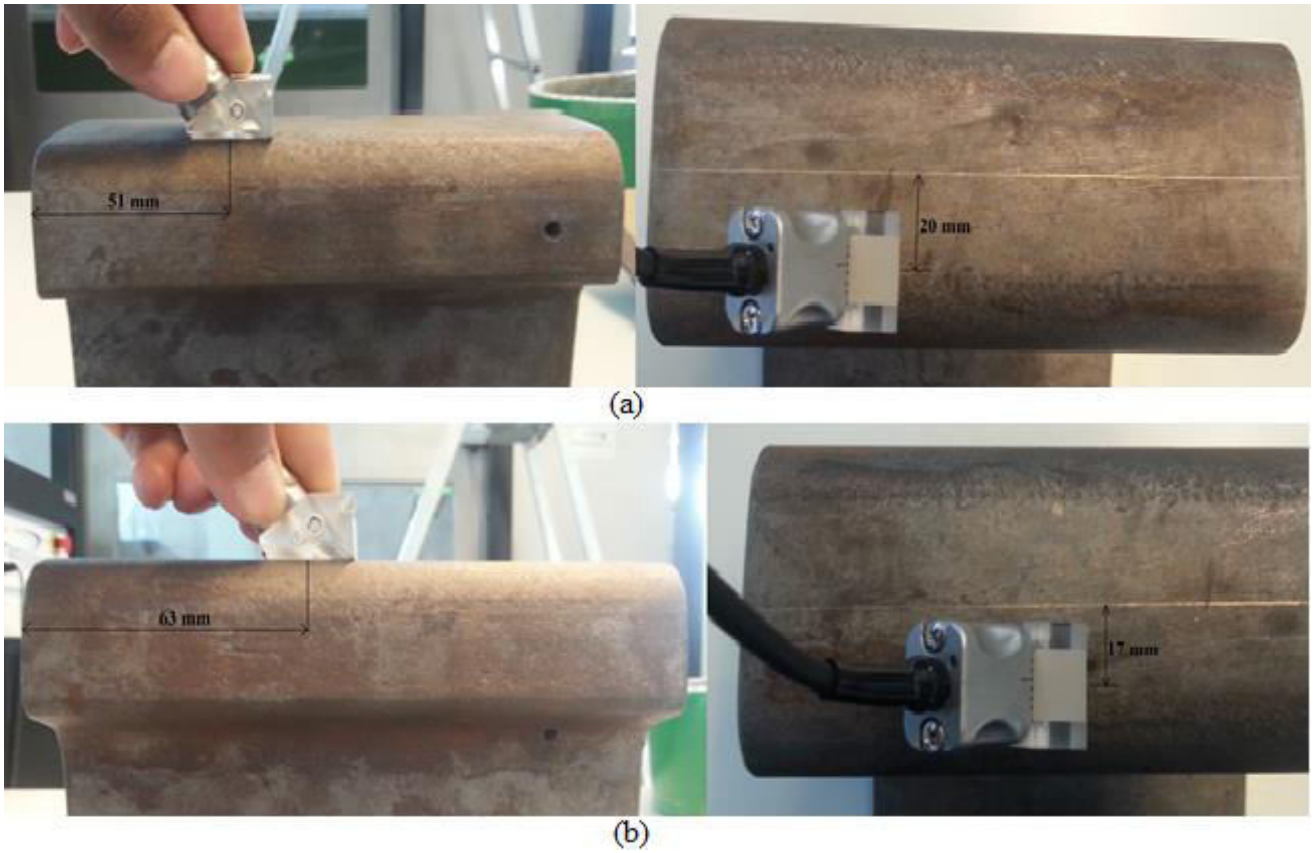

Fig.4.7. Position of PA2 (Wedge-2) on the test sample **(a)** for inspecting defect-1 **(b)** for inspecting defect-2

From **Fig.4.8**, the indication of defect-1 is clearly visible at 70°. Similarly, from **Fig.4.9**, the indication of defect-2 is clearly visible at 69°. Other echoes might be resulting from front, side or back walls of the test sample.

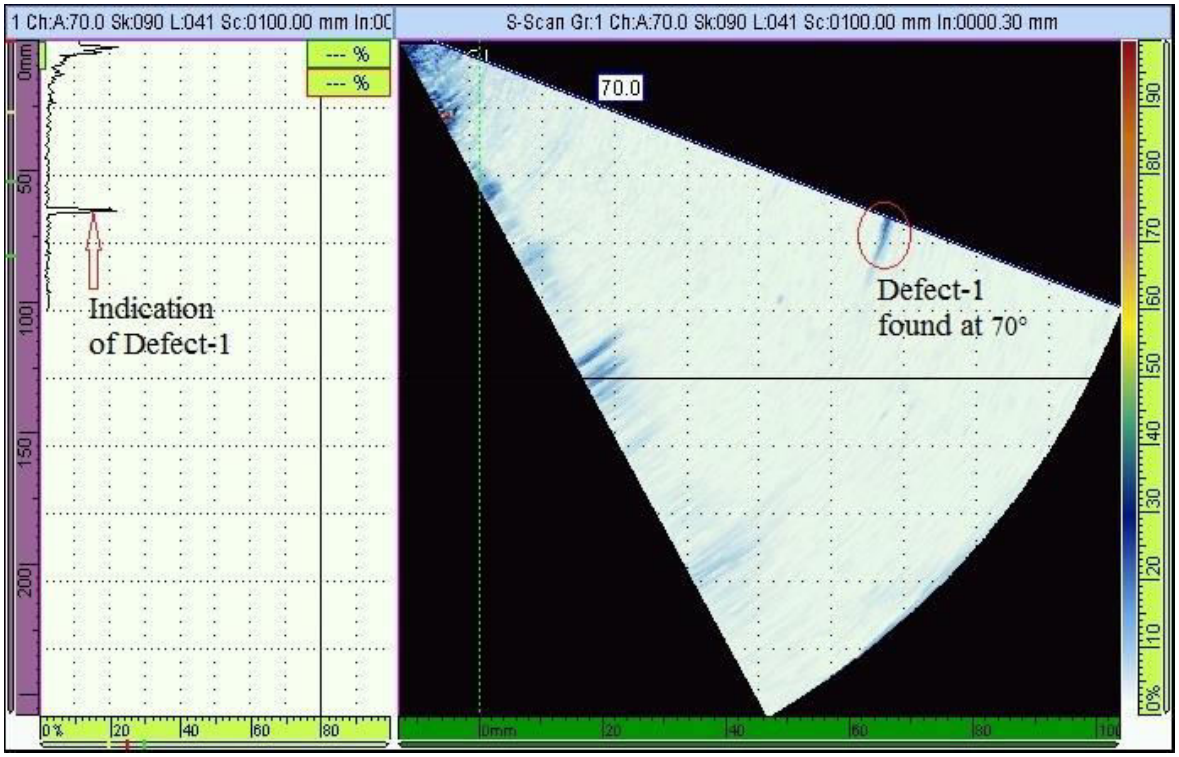

Fig.4.8. S-scan image for inspection of defect-1 using PA2 (Wedge-2)

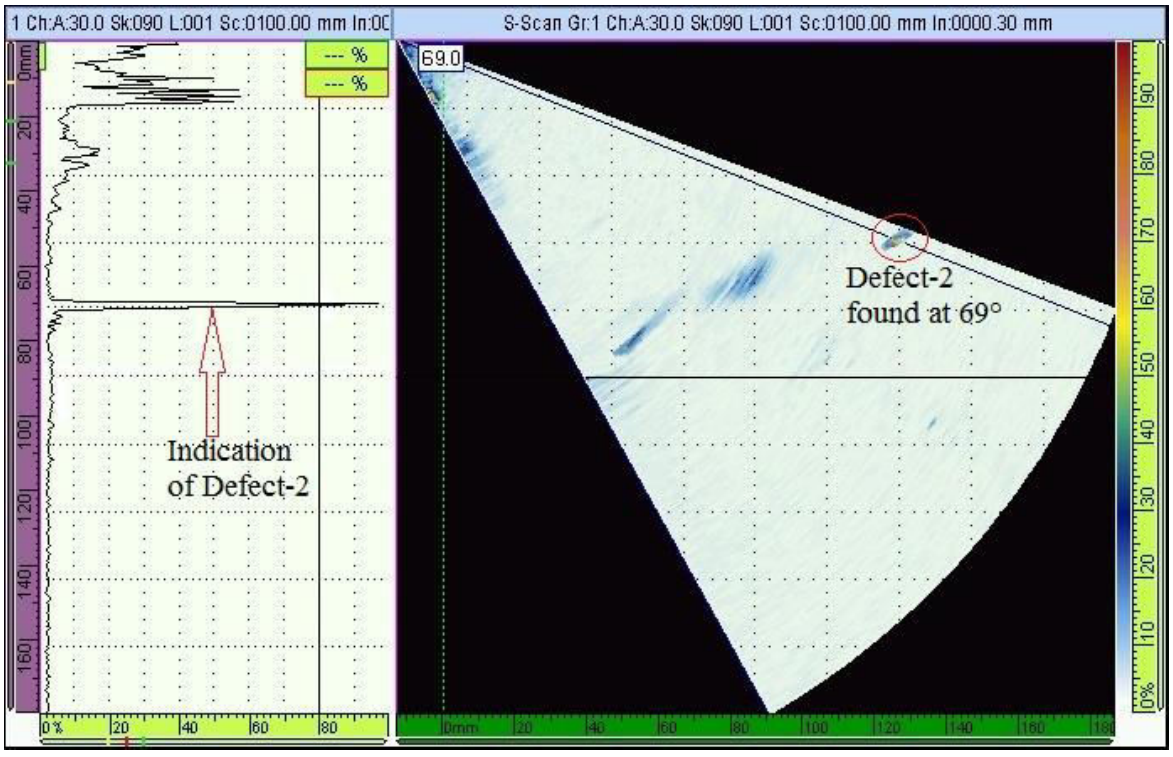

Fig.4.9. S-scan image for inspection of defect-2 using PA2 (Wedge-2)

- Wedge-3:

PA2 (wedge-3) uses longitudinal waves at a refracted angle of 60° and operates at a frequency of 5 MHz. The probe number given by OLYMPUS is “5L16-9.6x10-A10-P-2.5-HY” and the wedge number is “SA10-N60L”.

From **Fig.4.10 (a)**, it is clearly shown that the wedge is placed 110 mm towards the defect-1 from left corner and it is positioned 20 mm away from the center for the inspection of defect-1. Similarly, wedge is placed 117 mm towards the defect-2 from left corner and it is positioned 17 mm away from the center for the inspection of defect-2 which is shown in **Fig.4.10 (b)**.

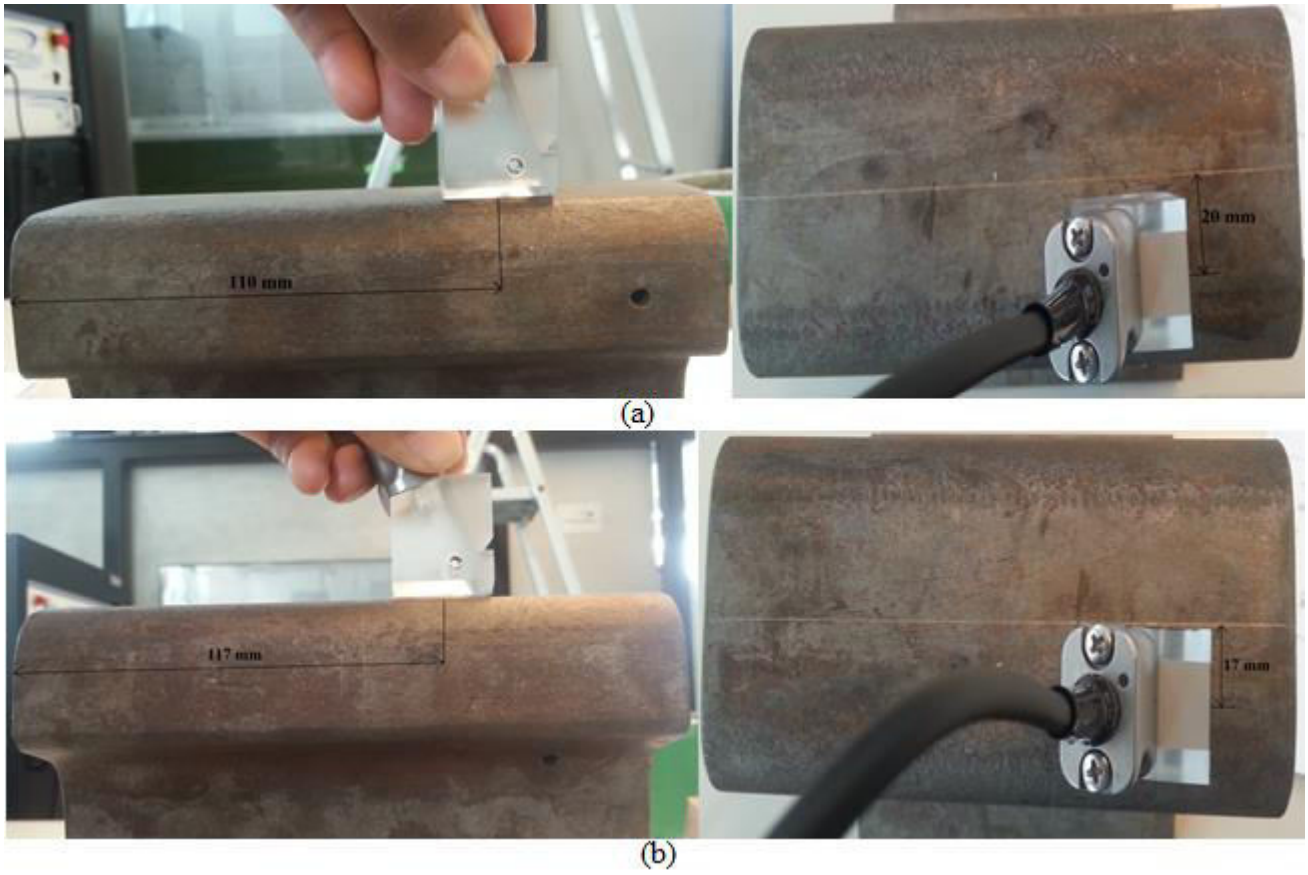

Fig.4.10. Position of PA2 (Wedge-3) on the test sample **(a)** for inspecting defect-1
(b) for inspecting defect-2

From **Fig.4.11**, the indication of defect-1 is clearly visible at 50°. Similarly, from **Fig.4.12**, the indication of defect-2 is clearly visible at 30°. Other echoes might be resulting from front, side or back walls of the test sample.

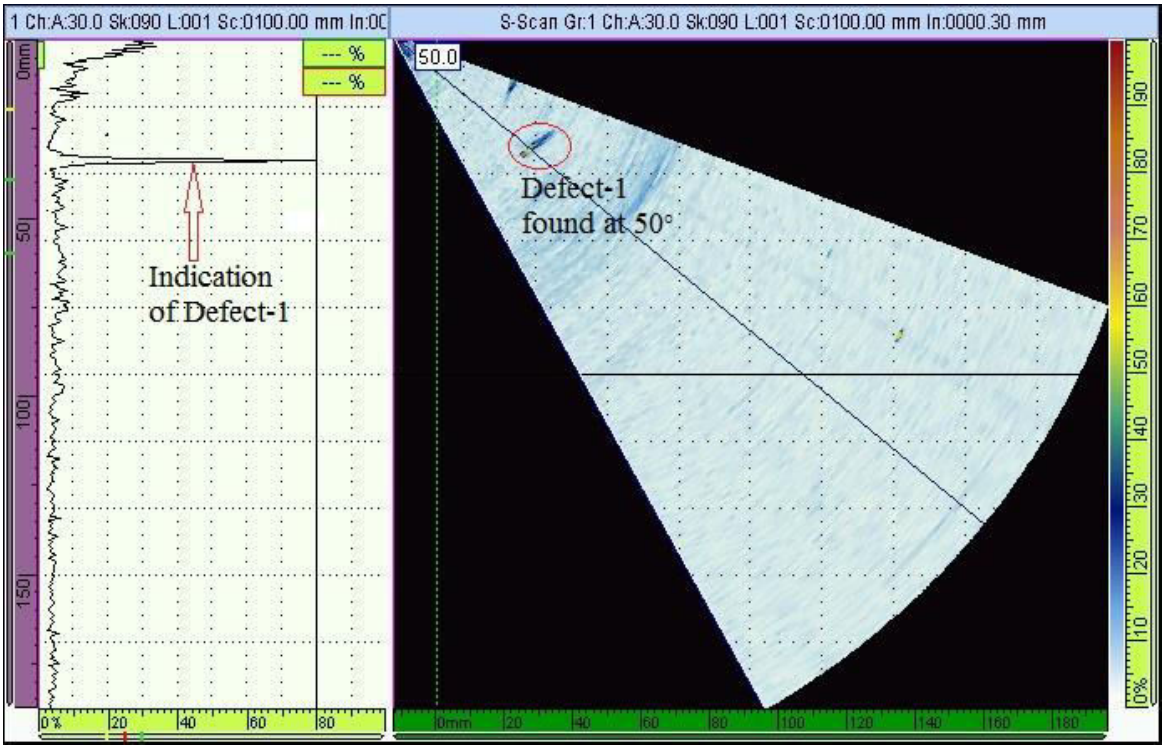

Fig.4.11. S-scan image for inspection of defect-1 using PA2 (Wedge-3)

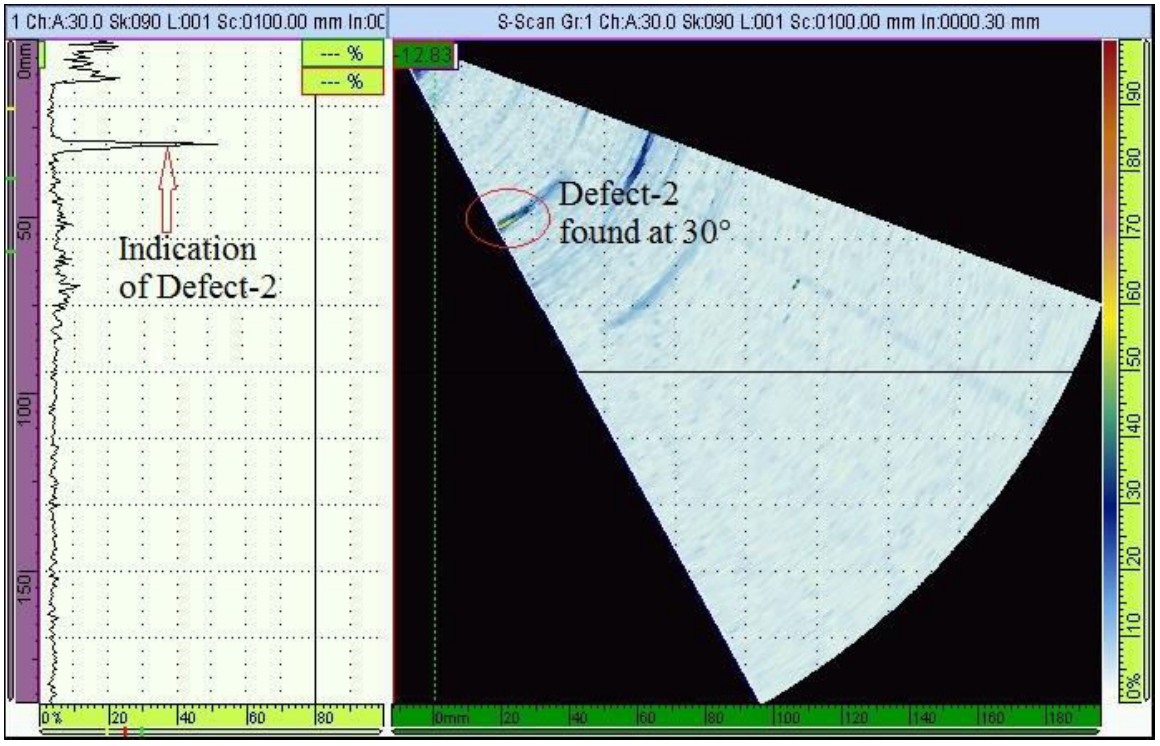

Fig.4.12. S-scan image for inspection of defect-2 using PA2 (Wedge-3)

4.3.Conclusions

From the experimental analysis, we can say that the given phased arrays identified both the defects when they were appropriately positioned on the test sample. PA2 (Wedge-1) configuration which used longitudinal waves with refracted angle of 0° identified both the defects well compared to other phased array configurations as the scanning was performed along the profile of test sample. As the wedge was positioned above the defects, the distance travelled by the wave to reach the defect is comparatively less. Hence, PA2 (Wedge-1) configuration can be used to inspect defects that are present in head and head-web interface of the rails.

5. Determination of position of defects in the test sample

In this section, we shall determine the position of defects in the test sample using the results obtained from inspection of defects using different phased arrays from CIVA software as well as experimental analysis. Theoretical calculations are performed in order to know the true positions of the defects in the test sample. Also, up on comparing the results of theoretical calculations with the ones obtained from CIVA software & experimental analysis, it is possible to determine the uncertainty which is discussed in section 6.

5.1. Formulas used for the calculations

1. Snell's Law:

$$\frac{Sin\,\alpha_i}{V_1} = \frac{Sin\,\alpha_r}{V_2} \quad \textbf{(5.1)}$$

Where,

α_i – Angle of incidence

α_r – Angle of refraction

V_1 – Ultrasonic wave velocity in the wedge

V_2 – Ultrasonic wave velocity in the test sample

2. Angle at which ultrasonic waves enter the wedge, $\alpha_L = 90° - \alpha_i$ **(5.2)**

3. From Pythagorean Theorem, $\text{Sin}\ \alpha_L = M / L$ **(5.3)**

Where,

M – Length of normal

L – Distance between source and surface of the test sample

4. Actual time taken for the wave to reach the defect, $t = t_2 - t_1$ **(5.4)**

Where,

t_1 – Time taken for ultrasonic waves to reach surface of the test sample from source

t_2 – Time taken for ultrasonic waves to reach the defect from surface of the test sample

5. Ultrasonic wave velocity, $V = 2 * L / t$ (or) $2 * Q / t$ **(5.5)**

Where.

L (or) Q – Distance between source and destination

t – Time taken for ultrasonic waves to reach destination from source

6. Successive angle, $\theta = 90° - \alpha_r$ **(5.6)**

7. Sin θ = R / Q **(5.7)**

   Where,

   R – Depth of defect from the surface of test sample

   Q – Distance between surface of test sample and defect

8. From Pythagorean Theorem, $P^2 + R^2 = Q^2$ **(5.8)**

5.2.Determination of position of defects in the test sample using computer modelling (CIVA)

Here, we shall determine the position of defect-1 and defect-2 from the CIVA results that were obtained from sectorial scanning. Pictorial representation of the phased array wedges help us to understand the important parameters and notations used for calculations.

5.2.1. Determination of position of defect-1 in the test sample

The arrangement of Phased Array wedges (PA1, PA2 (Wedge-2&3)) on test sample is shown in **Fig.5.1** while **Fig.5.2** shows the arrangement of PA2 (Wedge-1) on test sample for inspection of defect-1. From both the figures, 'A1' is the point at which beam enters wedge; "A" is the point at which beam enters the test sample and it creates an interface; "A2" is a point on the normal; 'B' is the point on test surface below which defect is found and 'C' is the point where highest reflection from defect-1 is obtained. A1–A–A2 and A–B–C forms two right-angled triangles which allow positioning the defect manually. 'Q' is the distance between wedge and the defect, 'P' is the distance between wedge and the point above the defect on the surface of test sample and 'R' is the depth of the defect from the surface of test sample where the maximum reflection is obtained. As we are interested in positioning the defect-1, only parameter 'R' is considered in all the calculations.

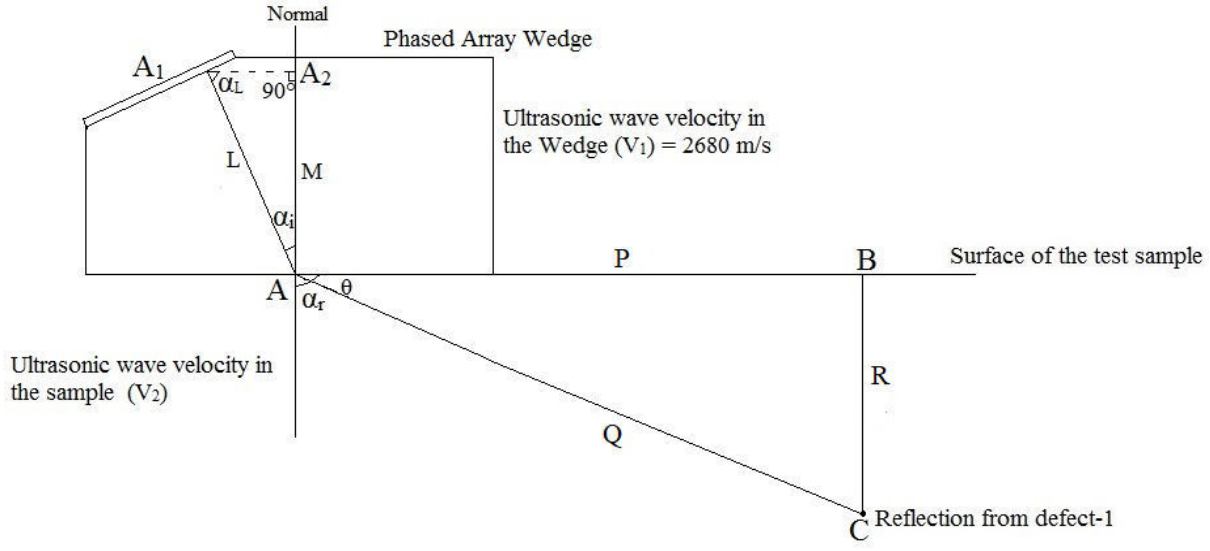

Fig.5.1. Inspection of defect-1 using PA1, PA2 (Wedge-2&3)

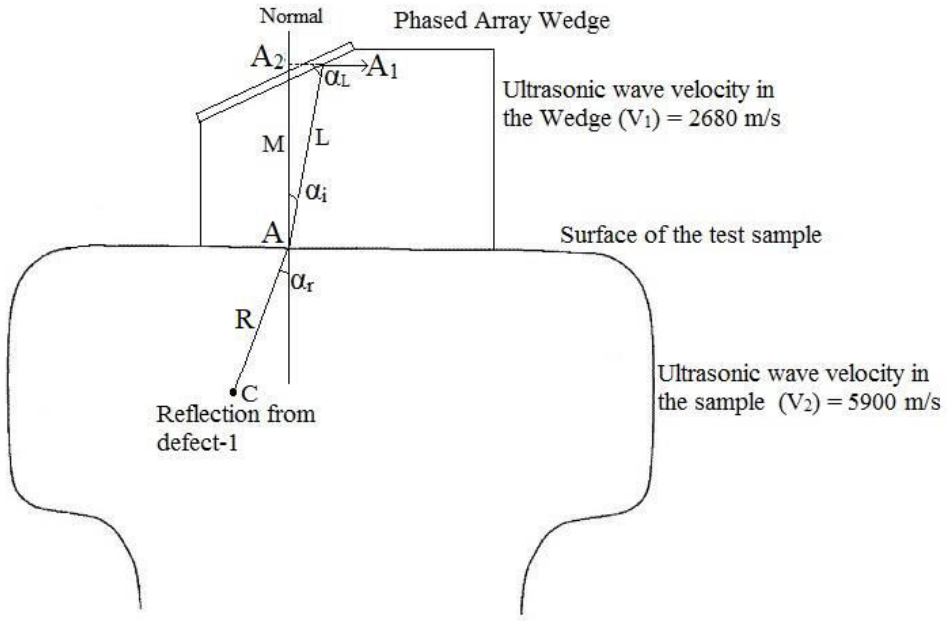

Fig.5.2. Inspection of defect-1 using PA2 (Wedge-1)

In CIVA, Z-coordinate denotes the depth and hence it remains same although the phased arrays vary for inspecting defect-1. Z-coordinates at point-B and point-C are given in **Table.5.1**.

Table.5.1. Z-coordinates at points B and C with respect to inspection of defect-1

Phased Array	Z (mm)	
	At point 'B'	At point 'C'
PA1; PA2 (Wedge-2); PA2 (Wedge-3)	-124.44	-86.28
PA2 (Wedge-1)	-124.44	-101.86

To calculate R, we must subtract Z coordinates at point B and point C.

=> R = B – C = 124.44 – 86.28 = 38.16 mm (for three cases)

=> R = 124.44 – 101.86 = 22.58 (for one case)

As defect-1 is not present in the central axis of the rail, we may not get the exact defect location when scanning is done normal to profile with 30° to 70° sector. So, the value of 'R' remains same in three cases i.e. PA1, PA2 (Wedge-2&3) configurations as scanning is performed normal to profile of the test sample. The one case which gives exact defect location is PA2 (Wedge-1) configuration as the scanning is done along the profile of the test sample.

✓ Results:

Fig.5.3 clearly gives A-scan and S-scan results showing indication of defect-1 in the test sample in which A-scans indicate time taken by the signal to reach the defect from the entrance point and S-scans indicate the angle at which maximum reflection from defect-1 is obtained.

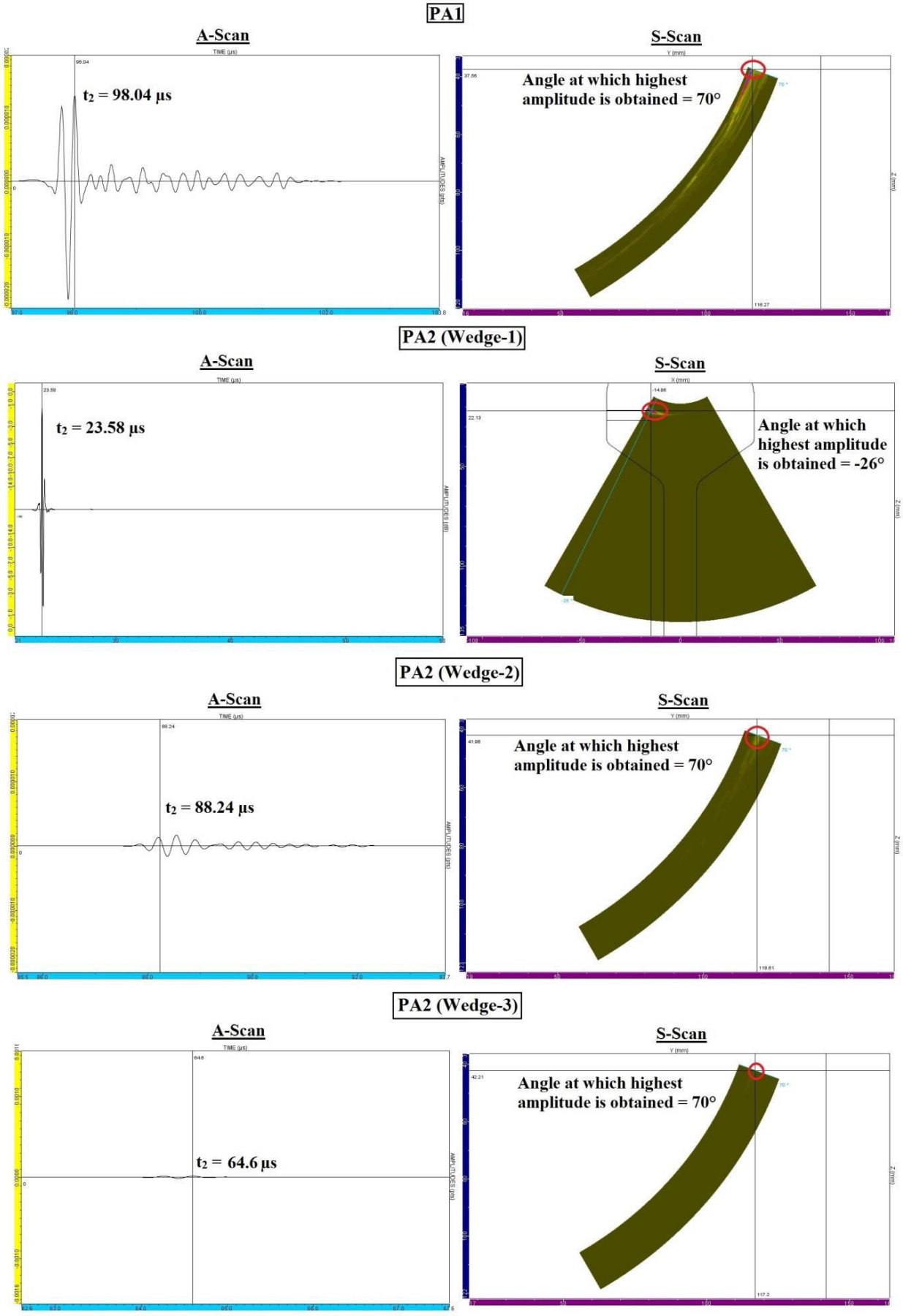

Fig.5.3. A-scan and S-scan results showing reflection from defect-1 in the test sample

✓ Estimation of time taken for the ultrasonic wave to reach the surface of test sample (t_1):

To determine the time taken for the ultrasonic wave to reach the surface of test sample, we must calculate the angle of incidence (α_i) for a refractive angle at which highest reflection from defect-1 is obtained. After finding the angle of incidence (α_i), we shall determine the distance between wave entrance and surface of test sample (L) of wedge since it changes for each angle.

Now, consider PA1.

✓ Initial parameters to determine 'M':

Distance between source and surface of test sample (L) = 31 mm; $\alpha_r = 45°$; $\alpha_i = 35.923°$.

Using formula (5.2), $\alpha_L = 54.077°$

Using formula (5.3), M = 25.1 mm → (Eq.1)

✓ Actual parameters where defect is identified:

$V_1 = 2680$ m/s; $V_2 = 3230$ m/s (Shear wave) and $\alpha_r = 70°$

Using formula (5.1), $\alpha_i = 51.23°$ and using formula (2), $\alpha_L = 38.76°$

Now, M = 25.1 mm (from Eq.1)

So, using formula (5.3), L = 40.1 mm

Using formula (5.5), $t_1 = 29.92$ µs

From **Fig.5.3**, t_2 is 98.04 µs for PA1. Hence, using formula (5.4), t = 68.12 µs;

Using formula (5.5), Q = 110.01 mm

Using formula (5.6), θ = 20°

Now, using formula (5.7), R = 37.62 mm

Table.5.2. Initial and actual parameters of different wedges of PA2 for inspecting defect-1

PA2 (Wedge-1)	Initial parameters: $\alpha_r = 0°$; $\alpha_i = 0°$; L = 20 mm Actual parameters: $\alpha_r = -26°$; $t_2 = 23.58$ µs; $V_1 = 2680$ m/s; $V_2 = 5900$ m/s
PA2 (Wedge-2)	Initial parameters: $\alpha_r = 55°$; $\alpha_i = 42.818°$; L = 19 mm Actual parameters: $\alpha_r = 70°$; $t_2 = 88.24$ µs; $V_1 = 2680$ m/s; $V_2 = 3230$ m/s
PA2 (Wedge-3)	Initial parameters: $\alpha_r = 60°$; $\alpha_i = 23.165°$; L = 23 mm Actual parameters: $\alpha_r = 70°$; $t_2 = 64.6$ µs; $V_1 = 2680$ m/s; $V_2 = 5900$ m/s

Similarly, up on substituting respective parameters given in **Table.5.2** and repeating the above calculations, we can determine the value of R in the case of different PA2 wedges. These resultant values of R are referred as CIVA values with respect to defect-1. The theoretical and CIVA values of R with respect to defect-1 are given in **Table.5.3**.

Table.5.3. Theoretical and CIVA values of R with respect to defect-1

Phased Array	R (mm)	
	Theoretical value	CIVA value
PA1	38.18	37.49
PA2 (Wedge-1)	22.58	23.16
PA2 (Wedge-2)	38.18	39.41
PA2 (Wedge-3)	38.18	39.14

5.2.2. Determination of position of defect-2 in the test sample

The arrangement of Phased Array wedges (PA1, PA2 (Wedge-2&3)) on test sample is shown in **Fig.5.4** while **Fig.5.5** shows the arrangement of PA2 (Wedge-1) on test sample for inspection of defect-2. From both the figures, 'A1' is the point at which beam enters wedge; "A" is the point at which beam enters the test sample and it creates an interface; "A2" is a point on the normal; 'B' is the point on test surface below which defect is found and 'C' is the point where highest reflection from defect-2 is obtained. A1–A–A2 and A–B–C forms two right-angled triangles which allow positioning the defect manually. 'Q' is the distance between wedge and the defect, 'P' is the distance between wedge and the point above the defect on the surface of test sample and 'R' is the depth of the defect from the surface of test sample where the maximum reflection is obtained. As we are interested in positioning the defect-2, only parameter 'R' is considered in all the calculations.

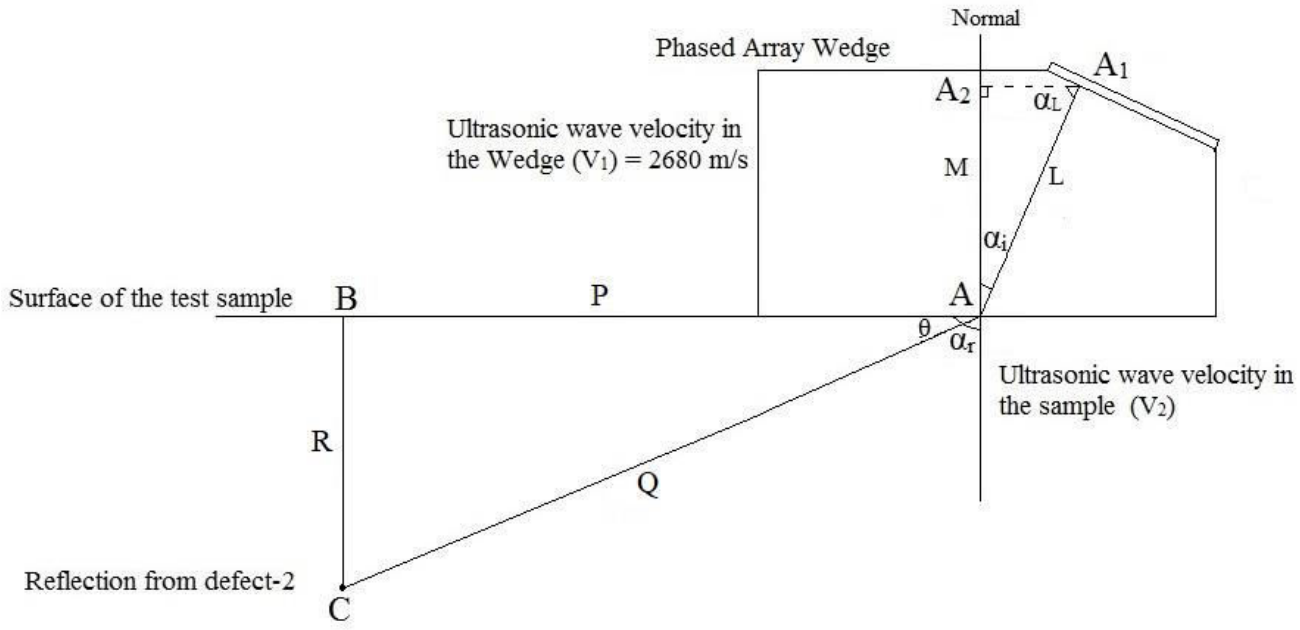

Fig.5.4. Inspection of defect-2 using PA1, PA2 (Wedge-2&3)

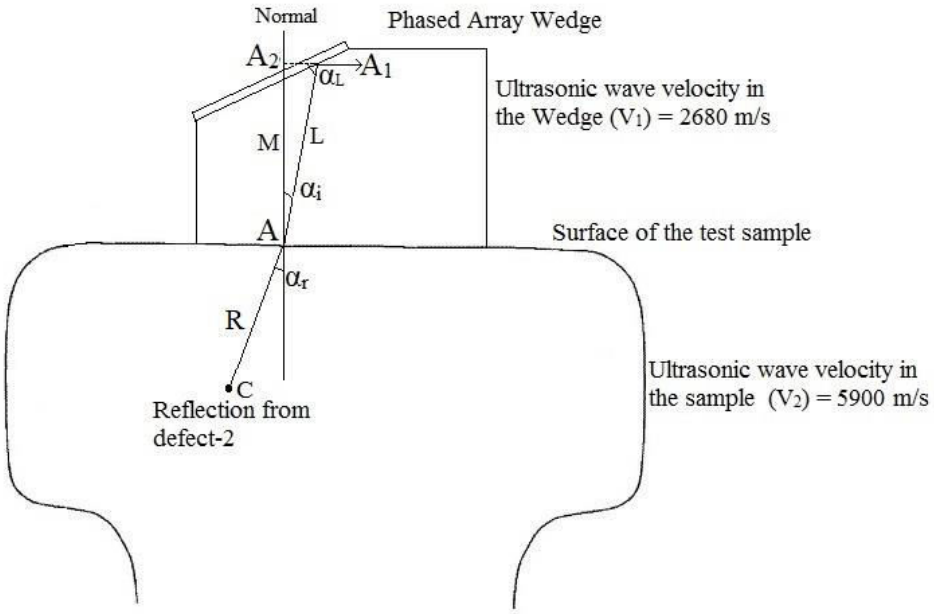

Fig.5.5. Inspection of defect-2 using PA2 (Wedge-1)

In CIVA, Z-coordinate denotes the depth and hence it remains same although the phased arrays vary for inspecting defect-2. Z-coordinates at point-B and point-C are given in **Table.5.4**.

Table.5.4. Z-coordinates at points B and C with respect to inspection of defect-2

Phased Array	Z (mm)	
	At point 'B'	At point 'C'
PA1; PA2 (Wedge-2); PA2 (Wedge-1); PA2 (Wedge-3)	-124.44	-85.83

To calculate R, we must subtract Z coordinates at point B and point C.

=> R = B – C = 124.44 – 85.83 = 38.61 mm

As defect-2 is present in the central axis of the rail, we get the exact defect location even though the scanning is done normal to profile with 30° to 70° sector. So, the value of 'R' remains same in all the cases.

✓ Results:

Fig.5.6 clearly gives A-scan and S-scan results showing indication of defect-2 in the test sample in which A-scans indicate time taken by the signal to reach the defect from the entrance point and S-scans indicate the angle at which maximum reflection from defect-2 is obtained.

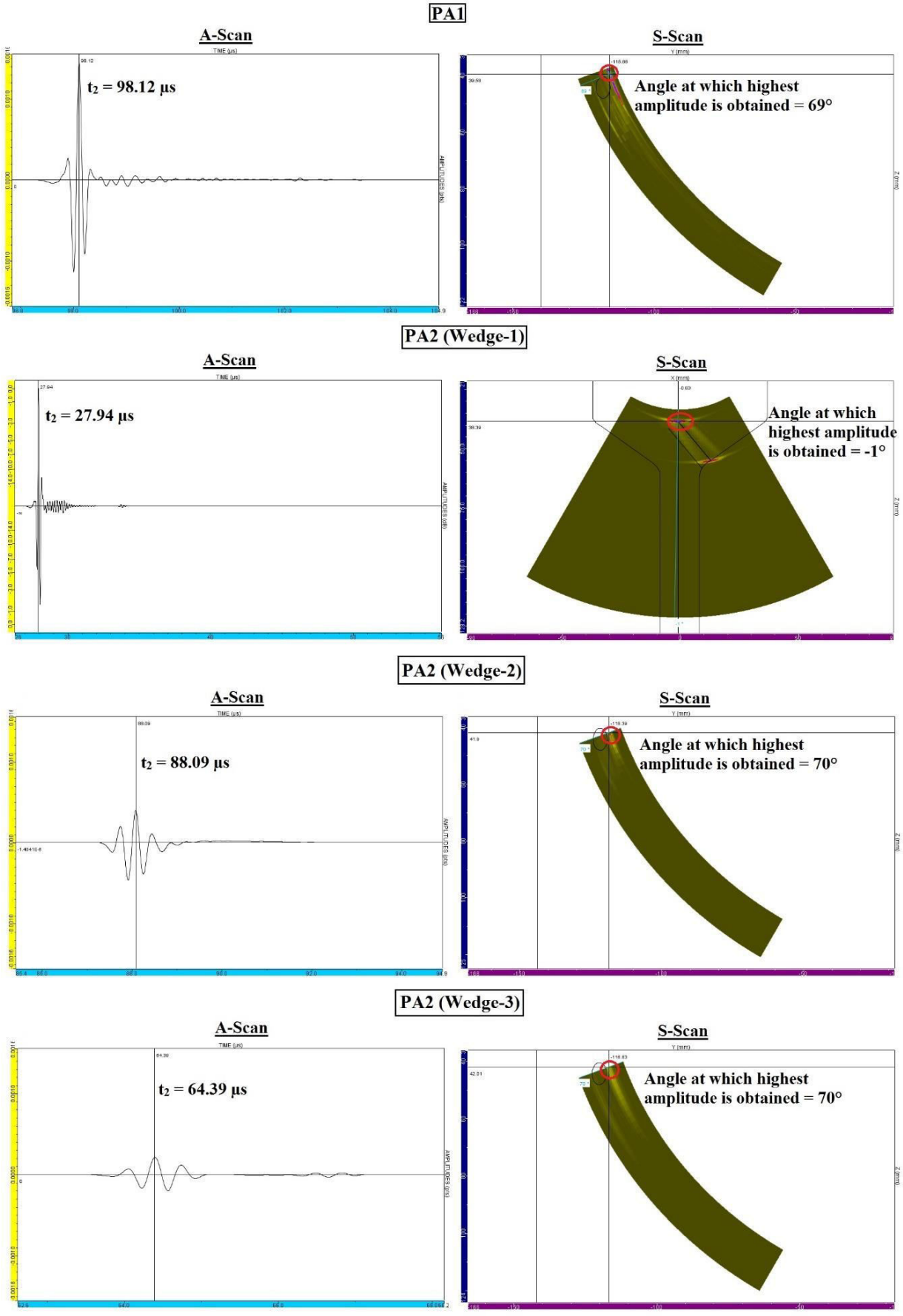

Fig.5.6. A-scan and S-scan results showing reflection from defect-2 in the test sample

✓ Estimation of time taken for the ultrasonic wave to reach the surface of test sample (t_1):

To determine the time taken for the ultrasonic wave to reach the surface of test sample, we must calculate the angle of incidence (α_i) for a refractive angle at which highest reflection from defect-2 is obtained. After finding the angle of incidence (α_i), we shall determine the distance between wave entrance and surface of test sample (L) of wedge since it changes for each angle.

Now, consider PA1.

✓ Initial parameters to determine 'M':

Distance between source and surface of test sample (L) = 31 mm; $\alpha_r = 45°$; $\alpha_i = 35.923°$.

Using formula (5.2), $\alpha_L = 54.077°$

Using formula (5.3), M = 25.1 mm → (Eq.2)

✓ Actual parameters where defect is identified:

$V_1 = 2680$ m/s; $V_2 = 3230$ m/s (Shear wave) and $\alpha_r = 69°$

Using formula (5.1), $\alpha_i = 50.70°$ and using formula (2), $\alpha_L = 39.30°$

Now, M = 25.1 mm (from Eq.2)

So, using formula (5.3), L = 39.62 mm

Using formula (5.5), $t_1 = 29.56$ µs

From **Fig.5.6**, t_2 is 98.12 µs for PA1. Hence, using formula (5.4), t = 68.56 µs;

Using formula (5.5), X = 110.72 mm

Using formula (5.6), $\theta = 21°$

Now, using formula (5.7), Z = 39.67 mm

Table.5.5. Initial and actual parameters of the different wedges of PA2 for inspecting defect-2

PA2 (Wedge-1)	Initial parameters: $\alpha_r = 0°$; $\alpha_i = 0°$; L = 20 mm Actual parameters: $\alpha_i = -1°$; $t_2 = 27.94$ µs; $V_1 = 2680$ m/s; $V_2 = 5900$ m/s
PA2 (Wedge-2)	Initial parameters: $\alpha_r = 55°$; $\alpha_i = 42.818°$; L = 19 mm Actual parameters: $\alpha_r = 70°$; $t_2 = 88.09$ µs; $V_1 = 2680$ m/s; $V_2 = 3230$ m/s
PA2 (Wedge-3)	Initial parameters: $\alpha_r = 60°$; $\alpha_i = 23.165°$; L = 23 mm Actual parameters: $\alpha_r = 70°$; $t_2 = 64.41$ µs; $V_1 = 2680$ m/s; $V_2 = 5900$ m/s

Similarly, up on substituting respective parameters given in **Table.5.5** and repeating the above calculations, we can determine the value of R in the case of different PA2 wedges. These resultant values of R are referred as CIVA values with respect to defect-2. The theoretical and CIVA values of R with respect to defect-2 are given in **Table.5.6**.

Table.5.6. Theoretical and CIVA values of R with respect to defect-2

Phased Array	R (mm)	
	Theoretical value	CIVA value
PA1	38.61	39.67
PA2 (Wedge-1)	38.61	38.40
PA2 (Wedge-2)	38.61	39.98
PA2 (Wedge-3)	38.61	39.83

5.3.Determination of position of defects in the test sample using experimental analysis

Here, we shall determine the position of defect-1 and defect-2 from the experimental results that were obtained from sectorial scanning. Pictorial representation of the phased array wedges help us to understand the important parameters and notations used for calculations.

5.3.1. Determination of position of defect-1 in the test sample

The arrangement of different Phased Array wedges (PA1, PA2 (Wedge-1, 2&3)) on the test sample for inspection of defect-1 is shown in **Fig.5.7**. These wedges are positioned in such a way that highest reflections from the defect-1 are obtained. Here, "A" is the point at which beam enters the test sample; 'B' is the point on test surface below which defect is found and 'C' is the point where highest reflection from defect-1 is obtained. A–B–C forms a right-angled triangle which allows positioning the defect manually. 'Q' is the distance between wedge and the defect, 'P' is the distance between wedge and the point above the defect on the surface of test sample and 'R' is the depth of the defect from the surface of test sample. In case of PA2 (Wedge-1), R can be directly determined since inspection is done along the profile of test sample. "α_r" is the angle of refraction at which highest reflection from the defect is obtained and "θ" is the successive angle.

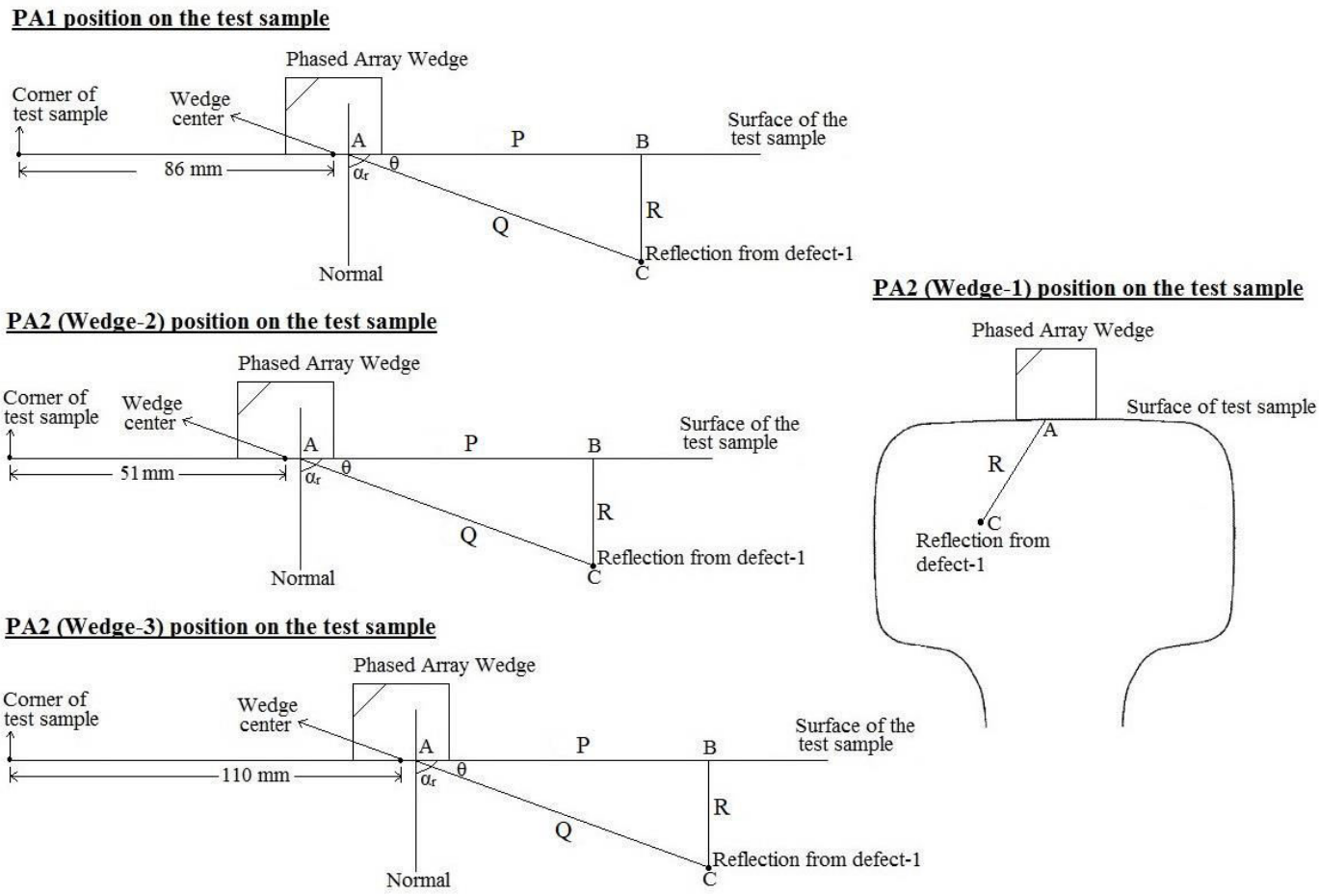

Fig.5.7. Arrangement of different Phased Array wedges for the inspection of defect-1

Table.5.7 gives the positions of different phased array wedges and their parameters that are obtained during the inspection of defect-1. R = Q in case of PA2 (Wedge-1) as the inspection is done along the profile of test sample.

Table.5.7. Positions and parameters of different phased array wedges while inspection of defect-1

Phased Array	Position on the test sample (mm)		Angle of refraction (α_r)	Distance between wedge and defect (Q or **R** in mm)
	From corner	From center		
PA1	86	20	66°	55
PA2 (Wedge-1)	138	14	4°	**22.6**
PA2 (Wedge-2)	51	20	70°	86
PA2 (Wedge-3)	110	20	50°	35

✓ Results:

Fig.5.8 shows the S-scans obtained using different Phased Array wedges from the inspection of defect-1. Two important parameters i.e. angle of refraction (α_r) and distance between wedge and defect (Q) are known from the S-scan.

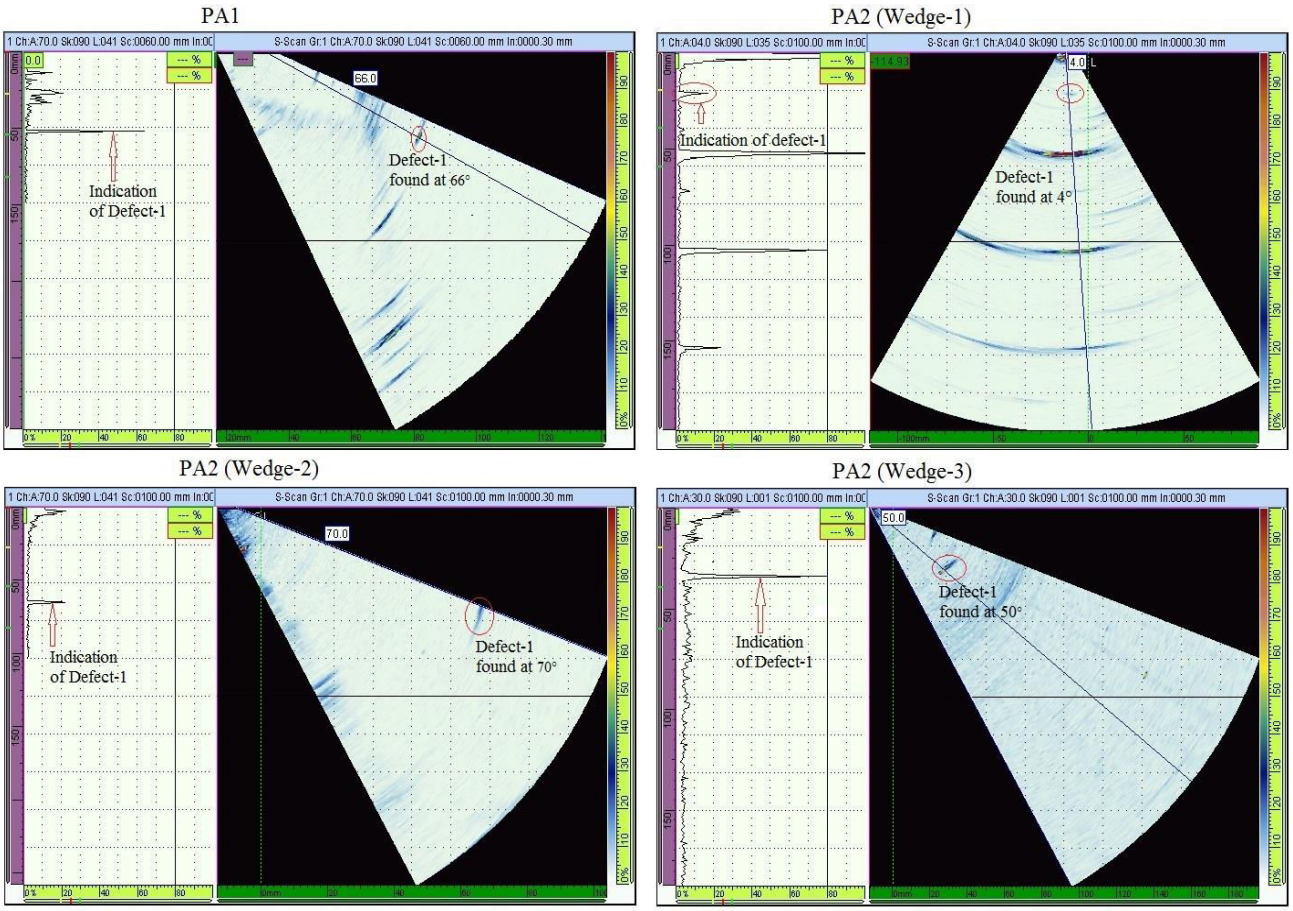

Fig.5.8. S-scans obtained using different Phased Array Wedges from inspection of defect-1

Theoretically, from the original test sample, we can measure depth of the defect-1 from the surface of test sample (R) using the normal measuring scale as it is clearly visible to naked eye. Now, upon using the formulas (5.6 & 5.7), it is possible for us to calculate depth of the defect-1 from the surface of test sample (R). The theoretical and experimental values of R are given in **Table.5.8**.

Table.5.8. Theoretical and experimental values of R with respect to defect-1

Phased Array	R (mm)	
	Theoretical value	Experimental value
PA1	23	22.37
PA2 (Wedge-1)	23	22.60
PA2 (Wedge-2)	23	23.65
PA2 (Wedge-3)	23	22.49

5.3.2. Determination of position of defect-2 in the test sample

The arrangement of different Phased Array wedges (PA1, PA2 (Wedge-1,2&3)) on the test sample for inspection of defect-2 is shown in **Fig.5.9**. These wedges are positioned in such a way that highest reflections from the defect are obtained. Here, "A" is the point at which beam enters the test sample; 'B' is the point on test surface below which defect is found and 'C' is the point where highest reflection from defect-2 is obtained. A–B–C forms a right-angled triangle which allows positioning the defect manually. 'Q' is the distance between wedge and the defect, 'P' is the distance between wedge and the point above the defect on the surface of test sample and 'R' is the depth of the defect from the surface of test sample. In case of PA2 (Wedge-1), R can be directly determined since inspection is done along the profile of test sample. "α_r" is the angle of refraction at which highest reflection from the defect is obtained and "θ" is the successive angle.

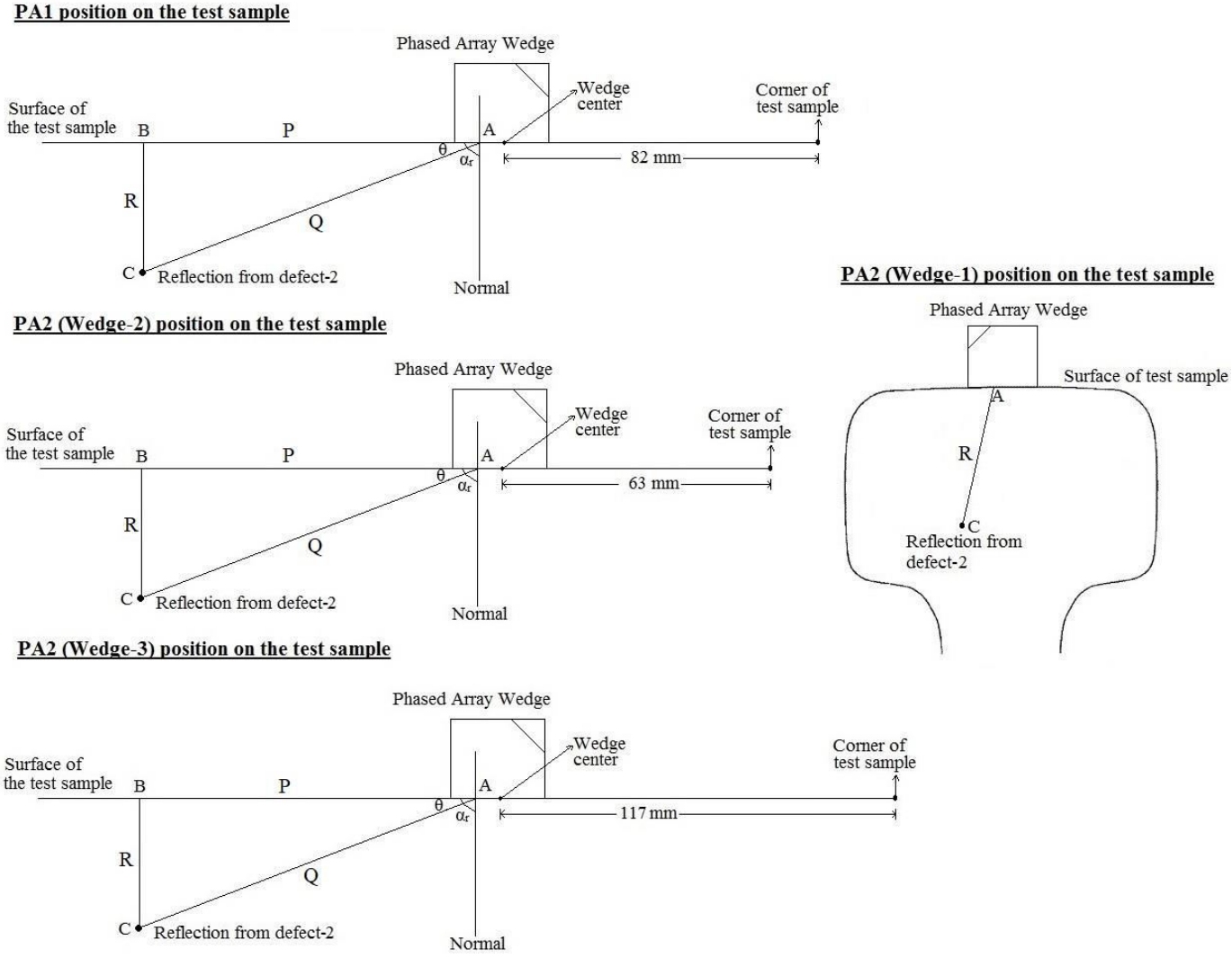

Fig.5.9. Arrangement of different Phased Array wedges for the inspection of defect-2

The calculations for determining depth of defect-2 (inner face) from the surface of test sample is shown in **Fig.5.10**. It is important since defect-2 is present with a rotation inside the test sample. By considering the angle of rotation to be 45°and performing the calculations shown in the figure, we can say that depth of defect-2 (inner face) from the surface of test sample is 25.61 mm. This value is constant for all the Phased Array Wedges since reflection is obtained from inner face of the defect-2.

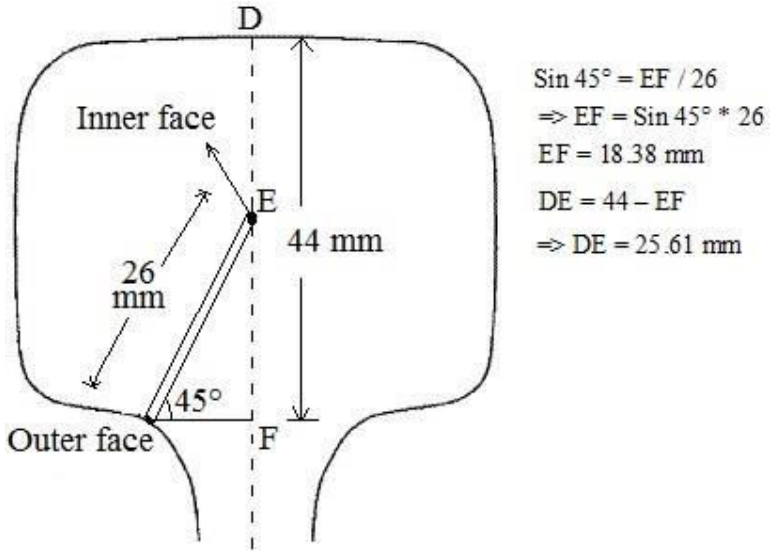

Fig.5.10. Calculation of depth of defect-2 (inner face) from the surface of test sample

The positions of different phased array wedges and their parameters that are obtained during the inspection of defect-2 are given in **Table.5.9**. R = Q in case of PA2 (Wedge-1) as the inspection is done along the profile of test sample.

Table.5.9. Positions and parameters of different phased array Wedges while inspection of defect-2

Phased Array	Position on the test sample (mm)		Angle of refraction (α_r)	Distance between wedge and defect (Q or **R**, in mm)
	From corner	From center		
PA1	82	17	51°	39
PA2 (Wedge-1)	130	0	-1°	**25**
PA2 (Wedge-2)	63	17	69°	70
PA2 (Wedge-3)	117	17	30°	30

✓ Results:

Fig.5.11 shows the S-scans obtained using different Phased Array wedges from the inspection of defect-2. Two important parameters i.e. angle of refraction (α_r) and distance between wedge and defect (Q) are known from the S-scan.

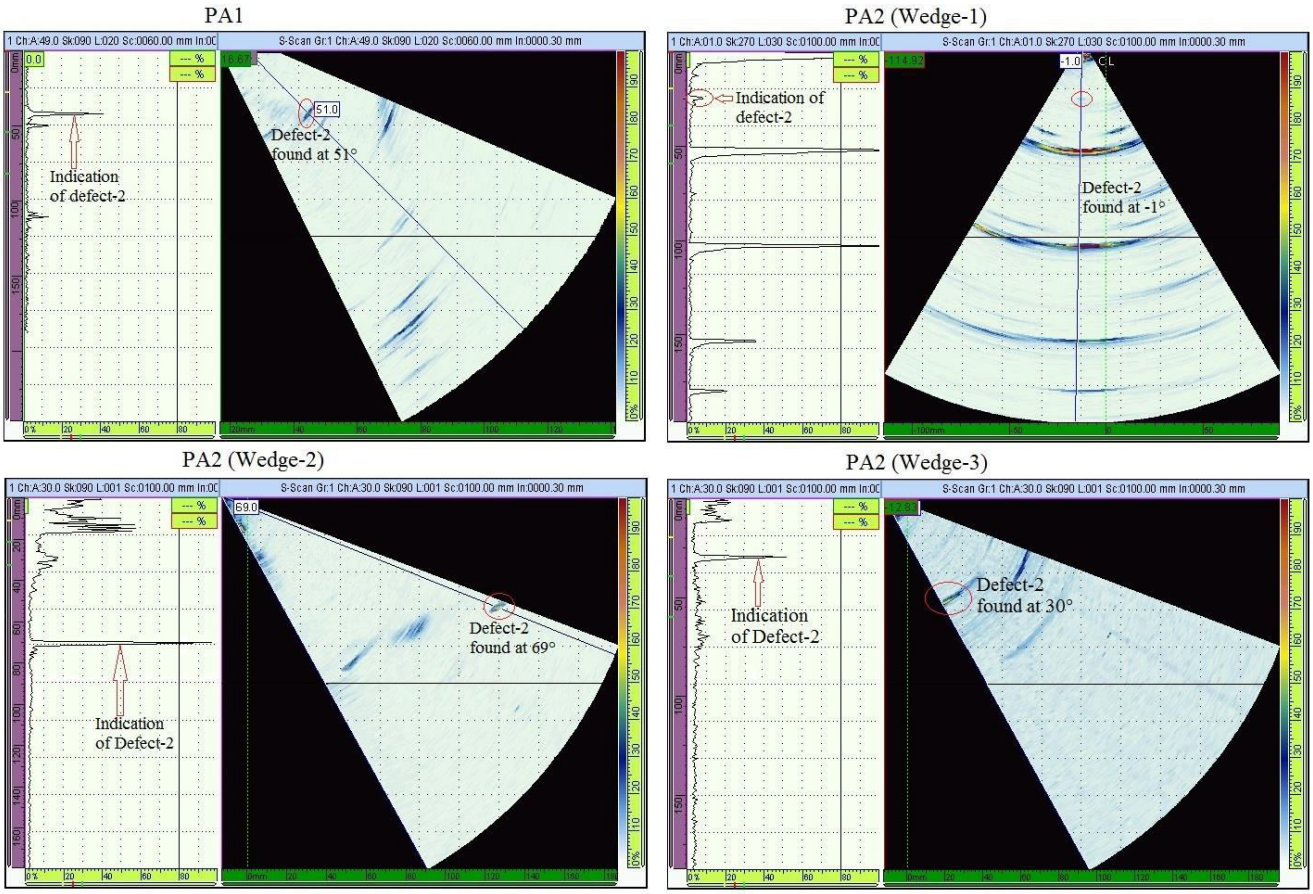

Fig.5.11. S-scans obtained using different Phased Array wedges from inspection of defect-2

Theoretically, from the original test sample, we can measure depth of the defect-2 (outer face) from the surface of test sample (R) using the normal measuring scale as it is clearly visible to naked eye. The calculations for determining depth of defect-2 (inner face) from the surface of test sample is already shown in **Fig.5.10**. Now, upon using the formulas (5.6 & 5.7), it is possible for us to calculate depth of the defect-2 from the surface of test sample (R). The theoretical and experimental values of R are given in **Table.5.10**.

Table.5.10. Theoretical and experimental values of R with respect to defect-1

Phased Array	R (mm)	
	Theoretical value	Experimental value
PA1	25.61	24.54
PA2 (Wedge-1)	25.61	25.10
PA2 (Wedge-2)	25.61	25.05
PA2 (Wedge-3)	25.61	26.19

5.4.Conclusions

Hence, the positions of the defects in the test sample were determined from the CIVA results as well as experimental results. In CIVA, theoretical values while positioning the defects were obtained using the coordinates at two points i.e. point above the defect on the test sample and point where highest reflection from the defects was obtained. In experimental part, theoretical values were obtained by measuring the depth of the defects manually using a measuring scale. Using the appropriate formulas, the depths of defect-1 and defect-2 were calculated with the help of results obtained from the inspection of the respective defects using CIVA and experimentally. The uncertainty in these theoretical and CIVA/experimental values are calculated in section-6.

6. Evaluation of uncertainties in determining the position of defects

Uncertainty is an important parameter in any measurement which measures the accuracy of a measurement result. Uncertainty may be expressed in many ways. In our case, there are only two measurement results to be compared i.e. experimental / CIVA results and theoretical results. Hence, percentage error representation is the best way to express the uncertainty in the measurement. The formula of percentage error is given as:

$$\% \text{ error} = \frac{|\text{Theoretical value} - \text{Measured value (CIVA/Experimental)}|}{\text{Theoretical value}} \text{ X } 100 \qquad \textbf{(6.1)}$$

6.1.Evaluation of uncertainties in determining the position of defects from CIVA results

To determine the uncertainty in positioning the defects, we shall use theoretical and CIVA values of R given in **Table.5.3** with respect to inspection of defect-1 and **Table.5.6** with respect to inspection of defect-1. The uncertainty in the measurement results of R in terms of percentage error can be calculated using formula (6.1) and given in **Table.6.1**.

Table.6.1. Determination of uncertainty in "R" while positioning defect-1 & defect-2 using CIVA

Phased Array	R (mm)					
	Defect-1			Defect-2		
	Theoretical value	CIVA value	Uncertainty (% error)	Theoretical value	CIVA value	Uncertainty (% error)
PA1	38.18	37.49	0.69%	38.61	39.67	1.06%
PA2 (Wedge-1)	22.58	23.16	0.58%	38.61	38.40	0.21%
PA2 (Wedge-2)	38.18	39.41	1.23%	38.61	39.98	1.37%
PA2 (Wedge-3)	38.18	39.14	0.96%	38.61	39.83	1.22%

6.2.Evaluation of uncertainties in determining the position of defects from experimental results

To determine the uncertainty in positioning the defects, we shall use theoretical and experimental values of R given in **Table.5.8** with respect to inspection of defect-1 and **Table.5.10** with respect to inspection of defect-1. The uncertainty in the measurement results of R in terms of percentage error can be calculated using formula (6.1) and given in **Table.6.2**.

Table.6.2. Determination of uncertainty in "R" while positioning defect-1 & defect-2 experimentally

Phased Array	R (mm)					
	Defect-1			Defect-2		
	Theoretical value	Exp. value	Uncertainty (% error)	Theoretical value	Exp. value	Uncertainty (% error)
PA1	23	22.37	0.63%	25.61	24.54	1.07%
PA2 (Wedge-1)	23	22.60	0.40%	25.61	25.10	0.51%
PA2 (Wedge-2)	23	23.65	0.65%	25.61	25.05	0.56%
PA2 (Wedge-3)	23	22.49	0.51%	25.61	26.19	0.58%

6.3.Possible sources of uncertainty in the measurement results

There are many sources of errors that lead to uncertainty in the measurement results. Hence, the possible sources of uncertainty in the measurement results can be viewed as [22], [23]:

- ✓ Skill of the operator
- ✓ Reading errors
- ✓ Environmental conditions such as temperature, humidity etc.
- ✓ Improper linkage between probe and measuring instrument
- ✓ Background noise (low S/N ratio)
- ✓ Response of the probe which leads to change in time intervals between source and target.
- ✓ Variation of Ultrasonic wave velocity in the test.

6.4.Evaluation of uncertainty due to variation of velocities in the test sample

Here, we shall consider that longitudinal wave velocity varies by 5900±100 m/s and shear wave velocity varies by 3230±50 m/s. Upon considering these conditions, individual calculations are performed for determining the positions of defect-1 and defect-2 seperately and hence the uncertainty in positioning of each defect is determined. The parameters that are required to determine the position of defects with variation in velocities are listed in **Table.6.3**.

Table.6.3. Parameters of different PAs to determine the position of defects with varying velocities

Phased Array	Defect-1	Defect-2
PA1	t = 68.12 μs; α_r = 70°	t = 68.56 μs; α_r = 69°
PA2 (Wedge-1)	t = 8.36 μs; α_r = -26°	t = 13.02 μs; α_r = -1°
PA2 (Wedge-2)	t = 71.34 μs; α_r = 70°	t = 72.37 μs; α_r = 70°
PA2 (Wedge-3)	t = 38.78 μs; α_r = 70°	t = 39.47 μs; α_r = 70°

Now, using formula (5.5), distance between wedge and defect i.e. 'Q' can be calculated. Using formula (5.6), successive angle 'θ' can be calculated using which it is possible to calculate depth of

the defect from surface of test sample i.e. 'R' from formula (5.7). The resultant values of 'R' for different ultrasonic wave velocities are calculated. Uncertainty in this case would be the average of error between the two calculated values of R as we know that true value of R lies between them. These calculated values of R and the resultant uncertainty from these values are given in **Table.6.4** with respect to defect-1 and in **Table.6.5** with respect to defect-2.

Table.6.4. Uncertainty in positioning defect-1 considering different ultrasonic wave velocities

Phased Array	R (mm)		
	For V = 3180 m/s (S.W) and 5800 m/s (L.W)	For V = 3280 m/s (S.W) and 6000 m/s (L.W)	Uncertainty
PA1	37.04	38.20	±0.58
PA2 (Wedge-1)	24.24	25.08	±0.42
PA2 (Wedge-2)	38.79	40.01	±0.61
PA2 (Wedge-3)	38.46	39.79	±0.67

Table.6.5. Uncertainty in positioning defect-2 considering different ultrasonic wave velocities

Phased Array	R (mm)		
	For V = 3180 m/s (S.W) and 5800 m/s (L.W)	For V = 3280 m/s (S.W) and 6000 m/s (L.W)	Uncertainty
PA1	39.06	40.29	±0.62
PA2 (Wedge-1)	37.75	38.56	±0.41
PA2 (Wedge-2)	39.35	40.59	±0.62
PA2 (Wedge-3)	39.14	40.49	±0.68

6.5.Conclusions

Uncertainty in the results were determined in terms of percentage error. Upon taking the difference between results from CIVA/experiments and results from theoretical calculations, it was possible to obtain uncertainty. Low uncertainty means good consistency in any measurement. PA2 (Wedge-1) configuration obtained lowest uncertainty while determing positions of defect-1 and defect-2 both with CIVA as well as experimentally. The possible sources of uncertainty in the measurement results were listed briefly. Taking one of the sources into the account i.e. variation of velocities in the test sample, uncertainty in positioning the defects was calculated. In this case also, PA2 (Wedge-1) configuration attained lowest uncertainty.

CONCLUSIONS AND SUGGESTIONS

From this thesis, we can say that position of defects in rail (test sample) was successfully determined using CIVA software as well as experimentally. While modelling the beams in CIVA, beam profile that includes intensity of beam in near field and far field of different phased arrays was studied. From the calibrated results, we can say that PA1 obtained highest amplitude compared to PA2 (Wedge-2&3) configurations that had negative amplitudes. From the experimental analysis, PA2 (Wedge-1) configuration identified both the defects well compared to other phased array configurations as the wedge was positioned above the defects and hence the distance travelled by the wave to reach the defect is comparatively less.

As we are interested in positioning the defects, only parameter 'R' i.e. depth of the defect-1 and defect-2 from the surface of test sample was taken into account. While positioning the defects using CIVA, PA2 (Wedge-1) configuration obtained lowest uncertainty of 0.58% and 0.21% during the positioning of defect-1 and defect-2 respectively. While positioning the defects experimentally, PA2 (Wedge-1) configuration stood out tall compared to PA1 and other PA2 configurations since an uncertainty of 0.40% and 0.51% was obtained during the positioning of defect-1 and defect-2 respectively. Possible sources of uncertainties were listed, out of which variation of velocities in the test sample was considered to check how it affects the positioning of defects. Hence, PA2 (Wedge-1) configuration has recorded a lowest uncertainty of ±0.42 mm in case of determining the position of defect-1 and ±0.41 mm in case of determining the position of defect-2.

The suggestions from this thesis are:

- Phased arrays that perform inspection along the profile of the rail (for example, with a coverage of -30° to +30° region) can be used to detect and position the defects that are present in the head region of the rail.
- Phased arrays that perform inspection normal to the profile of the rail (for example, with a coverage of 30° to 70° region) can be used to detect and position the defects that are present in the web region of the rail.

INFORMATION SOURCE LIST

1. D.F.Cannon, K.O.Edel, S.L.Grassie, and K.Sawley. Rail defects: an overview.Fatigue Fracture Engineering Material Structures, Chapter-26: 865–887, 2003.
2. U.Zerbst, K.Madler and H.Hintze. Fracture mechanics in railway applications – an overview. Engineering Fracture Mechanics, Chapter-72: 163–194, 2005.
3. M.L.Peterson, B.D.Jeffrey, and R.M.Gutkowski. Limitations in size and type of detectable defects in rail flaw inspection. Insight, Chapter-42: 306–311, 2000.
4. R.Pohl, A.Erhard, H.J.Montag, H.M.Thomas, and H.Wustenberg. NDT techniques for railroad wheel and gauge corner inspection, Chapter-37: 89–94, 2004.
5. R.A.Smith. The wheel-rail interface, some recent accidents. Fatigue Fracture Engineering Material Structures, Chapter-26: 901–907, 2003.
6. Manual for ultrasonic testing of rails and welds [Viewed on 18th November, 2015]- http://www.ecr.indianrailways.gov.in/uploads/files/1357555682170-usfd.pdf
7. Rail Inspection Technologies by INNOTRACK [Viewed on 15th November, 2015]- http://www.innotrack.net/IMG/pdf/d441.pdf
8. Flash butt welding (Google Images) [Viewed on 19th November, 2015]- http://3.imimg.com/data3/YF/NN/MY-3197693/butt-250x250.jpg
9. Alumino-Thermic(AT) welding (Google Images) [Viewed on 19th November, 2015]- http://www.gcegroup.com/files/images/Markets_images/Thermit.jpg
10. Ultrasonic arrays for non-destructive evaluation: A review by Bruce W. Drinkwater, Paul D. Wilcox, NDT & E International Journal-Volume 39, Pages 525–54, October 2006.
11. Development of Phased-Array Ultrasonic Testing Acceptability Criteria (Phase II) [Viewed on 05th December, 2015]- https://www.fhwa.dot.gov/publications/research/infrastructure/structures/bridge/14075/14075.pdf
12. Phased array ultrasonics- Wikipedia, the free Encyclopaedia [Viewed on 06th December, 2015]
13. NDT technical notes by Olympus NDT under the section “Intro to Ultrasonic Phased Array” [Viewed on 06th December, 2015]- http://www.olympus-ims.com/sv/ultrasonics/intro-to-pa/
14. Dr. Michael D. C. Moles, Colin R. Bird. Advances in Phased Array Ultrasonic Technology Applications by Olympus NDT- 2007.
15. Dr. Michael D. C. Moles, Colin R. Bird, Pamela Herzog. Introduction to Phased Array Ultrasonic Technology Applications by Olympus NDT- 2007.
16. Daniel Kass, Michael Moles PhD, Tom Nelligan. Phased Array Testing- Basic Theory for Industrial Applications by Olympus NDT- 2012.

17. Application of Ultrasonic Phased Arrays for Rail Flaw Inspection [Viewed on 27th December, 2015]- https://www.fra.dot.gov/Elib/Document/1195
18. High Speed Rail Testing with Phased Array Probes by R. Alaix, Speno International, Geneva, Switzerland [Viewed on 29th December, 2015]- http://www.uic.org/cdrom/2006/wcrr2006/pdf/242.pdf
19. Phase Array Principle [Viewed on 07th January, 2016]- http://www.imasonic.com/Industry/PA_principle.php
20. Fibre, Fuel, Phased Array and the Future- Transportation Technology Centre, Inc. (TTCI), a subsidiary of the Association of American Railroads [Viewed on 08th January, 2016]- http://www.aar.com/standards/2014%20DPFC%20-%20Orlando/Tuesday/DPLS%20Talk%20July%202015%20final_Stabler.pdf
21. Phased-array Ultrasonic Flaw Detector [Viewed on 08th January, 2016]- http://www.hitachi-power-solutions.com/en/products/product13/p029_02.html
22. A Beginner's Guide to Uncertainty of Measurement [Viewed on 15th May, 2017]- https://www.wmo.int/pages/prog/gcos/documents/gruanmanuals/UK_NPL/mgpg11.pdf
23. The calculating procedure for measurement uncertainty using ultrasound testing [Viewed on 15th May, 2017]- http://www.incdmtm.ro/editura/documente/pag.%207-11_THE%20CALCULATING%20PROCEDURE%20FOR%20MEASUREMENT.pdf